



**CAEN** Educational Handbook

2018

# Nuclear and Particle Physics Experiments

We proudly support the  
development of critical thinking



# **CAEN** Educational Handbook

**2018**



We are proud of the high quality of our products.

## ISO 9001

ISO 9001:2008 approved quality system ensures all our internal processes.

From R&D to the registration of the incoming purchase orders, through:

- Resource Planning
- Scheduling
- Production

Our quality system is responsible for the proper functioning of all our internal processes and is subject to regularly unannounced audits, carried out by the National Standards Authority.

From the initial product design and its development stages, till the delivery of the production batches, we follow documented procedures that cover every aspect of our business. The auditing of our procedures by an independent third party guaranties that our business runs smoothly and efficiently.

The quality of CAEN S.p.A. products is constantly monitored by the application of the UNI EN ISO 9001:2008 standard. CAEN S.p.A. is ISO 9001 certified since 1998.

ISO9001:2008  
certified Company



ISO 9001:2008  
cert. n. 9105.CAEN

Authorised  
research laboratory  
of the MIUR

## CAEN EDUCATIONAL

We proudly support the development of critical thinking

**CAEN enters the world of learning and training by providing modern physics experiments for University advanced labs based on the latest technologies and instrumentation.**

CAEN brings the experience acquired in more than 35 years of collaboration with the High Energy & Nuclear Physics community into the University educational laboratories. Thanks to the most advanced instrumentation developed by CAEN for the major experiments worldwide, together with the University teaching experience at the University of Insubria, a series of experiments covering several applications has been carried out and are presented in detailed Educational Notes.

The goal is to inspire students and guide them towards the analysis and comprehension of different physics phenomena with a series of experiments based on state-of-the art technologies, instruments and methods.

### CAEN Background

CAEN SpA is acknowledged as the only company in the world providing a complete range of High/Low Voltage Power Supply systems and Front-End/Data Acquisition modules which meet IEEE Standards for Nuclear and Particle Physics. Extensive Research and Development capabilities allowed CAEN SpA to play an important long term role in this field. CAEN activities have always been at the forefront of technology, thanks to years of intensive collaborations with the most important Research Centres of the world.

CAEN products appeal to a wide range of customers including engineers, scientists and technical professionals who all trust them to achieve their goals faster and more effectively.



In collaboration with University of Insubria, Como, Italy.

### Contacts:

#### CAEN S.p.A.

Via Vetràia 11  
55049 - Viareggio • Italy  
Phone +39.0584.388.398  
Fax +39.0584.388.959  
[educational@caen.it](mailto:educational@caen.it)  
[www.caen.it](http://www.caen.it)





# Website

More information including the complete experiment description is available on [www.caen.it/educational](http://www.caen.it/educational)

Home / Products / Educational


**Educational**

CAEN enters the world of learning and training by providing modern physics experiments for University advanced labs based on the latest technologies and instrumentation.

CAEN brings the experience acquired in more than 35 years of collaboration with the High Energy & Nuclear Physics community into the University educational laboratories.

The goal is to inspire students and guide them towards the analysis and comprehension of different physics phenomena with a series of experiments based on state-of-the-art technologies, instruments and methods.


**Educational Experiments**



A wide range of modern physics experiments for University advanced labs based on the latest technologies and instrumentation

[Learn More](#)


**Educational Kits**



A modern, digital and flexible platform developed by CAEN for teaching the fundamentals of Statistics & Nuclear and Modern Physics

[Show More](#)

**Educational Handbook**



[Download](#)

Use the Document library to download all experiment documentation. Note that each experiment is identified by **Experiment reference ID**.

The same ID is used on our web site to indicate:

- Short Experiment Guide
- University Level Experiment Guide

Some experiments are also provided with:  
*Secondary School Level Experiment Guide*

Find overview of all experiments

**NEW**

**Gamma Spectroscopy**

**Introduction**

In 1895 the radioactivity was discovered by H. Becquerel and in 1903 the Nobel Prize in Physics was assigned to Curie spouses for their studies on these phenomena. Radioactivity is around us and getting to know it experimentally is essential for physics students.

When an unstable nucleus decays in a cascade leading to a stable nucleus, it emits alpha or beta or gamma quanta or a combination of them. Gamma rays are high energy photons and the spectroscopy of the emitted  $\gamma$  rays is instrumental for understanding the mechanism of the interaction with matter, the fundamentals about detection and the underlying nuclear physics. Moreover, it is relevant in basic and applied fields of science and technology, from nuclear to medical physics, from archaeometry to homeland security.

The gamma spectroscopy experiments can be performed by using two different set-ups: The first one is the "Educational Gamma KIT", characterized by a modular structure that allows to execute all the applications. The alternative equipment is the "Emulation KIT" based on the CAEN Digital Detector Emulator (DT4800) together with Digital Multi-Channel Analyzer (DT5770). The latter allows to perform a series of lab experiments without using a radioactive source and a detector but simulating the signals produced by the interaction of particles with the detecting unit. The two set-ups are highly complementary.



**Experiments**

**SG6111 - Detected Gamma Radiation**

Gamma radioactivity detection by using a system composed of a scintillating crystal coupled to a photon detector.

**SG6112 - Poisson and Gaussian Distributions**

Study the statistical distribution of the counting rates of a gamma radioactive source. Comparison of the data to the Poisson distribution, fitting into a Gaussian as the mean number of counts grows. The study can be performed both experimentally, with the SPD kit or simulating it with the emulation kit.

**SG6113 - Energy Resolution**

The analysis of the spectrum of the deposited energy by a gamma ray in a detector discloses the essence of the interaction of high energy photons with matter and allows to learn by doing the detector related effects.

**SG6114 - System Calibration, Linearity and Resolution**

Recording and comparing the gamma energy spectra of several radioactive sources is the main goal of the experiment. The photo-peaks are used to calibrate the response of the system and to measure the energy resolution.

**SG6115 - A Combination of Different Scintillating Crystals: Light Yield, Scintillation Time and Resolution**

Compare the basic characteristics of different scintillating crystals, namely the light yield and the decay time of the scintillation light. Verify the effect on the energy resolution.

**SG6116 - Gamma Radiation Absorption**

The main goal of the experiment is the measurement of the gamma radiation absorption coefficient for different materials and different energies.

**SG6117 - Photoneuclear cross-section / Compton Scattering**

Determination of the ratio of the effective cross-sections due to Compton and Photoelectric effects as a function of photons energy.

**Equipment**

**SP5600C - Educational Gamma Kit**

Model	SP5600C	DT5720A	A355	SP5600C	SP5600C
Description	Power Supply & Amplification Unit	Desktop Digitizer 250MHz	Splitter	Mini Spectrometer	Absorption Tool

**SP5600EMJ - Emulation Kit**

Model	DT4800	DT5720
Description	Digital Detector Emulator	Desktop Multi-Channel Analyzer

**SP5600H1 - Educational KIT - Photonics Version**

Model	SP5600H1	DT5720A	A355	SP5600H1	SP5600H1	SP5600H1	SP5600H1	SP5600H1
Description	Power Supply & Amplification Unit	Desktop Digitizer 250MHz	Splitter	Mini Spectrometer	Absorption Tool	LED Driver	Sensor Holder for SPD600 with SPD kit	Scintillation Kit

**CAEN Electronic Instrumentation**

**Educational Physics Experiments**



**PARTICLE DETECTOR CHARACTERIZATION**

**Silicon Photomultiplier**

A state-of-the-art sensor to explore the quantum world

**NUCLEAR PHYSICS & RADIOACTIVITY**

**Gamma Spectroscopy**

Radioactivity is around us and getting to know it experimentally is essential for physics students.

**NUCLEAR PHYSICS & RADIOACTIVITY**

**Beta Spectroscopy**

Beta particles are electrons or positrons, resulting by nucleon decays in unstable nuclei.

**NUCLEAR PHYSICS & RADIOACTIVITY**

**Nuclear Imaging - PET**

Positron Emission Tomography (PET) scanner is the state-of-the-art medical imaging system.

**PARTICLE PHYSICS**

**Cosmic Rays**

The cosmic radiation, discovered by Victor Hess in 1912, includes all stable charged particles.

**PARTICLE PHYSICS**

**Photons**

The photon is the gauge boson for electromagnetism.

Find detailed informations on the educational kits on the dedicated web page.

Subscribe to our newsletter  
to be always updated on the  
new Applications!

# How to read this Handbook

Experiment name

Experiment reference ID

Experimental setup

Experiment task


Short description

A. Particle Detector Characterization - A.1 Silicon Photomultipliers

A.1.1

SiPM Characterization

SG6011



Related Experiment

A.1.2

C.2.1

D.1

Ordering Options

Code

Description

04060000AAAA

SP5600E - Educational Photon Kit

04060000AAAA

SP5600E - Educational Photon Kit

Purpose of the experiment

Characterization of a SiPM detector using an ultra-fast pulsed LED. Estimation of the main features of the detector at fixed bias voltage.

Fundamentals

Silicon Photomultipliers (SiPM) consist of a high-density (up to  $\sim 10^6/\text{mm}^2$ ) matrix of diodes connected in parallel on a common Si substrate. Each diode is an Avalanche Photo Diode (APD) operated in a limited Geiger-Müller regime connected in series with a quenching resistor, in order to achieve gain at level of  $\sim 10^6$ . As a consequence, these detectors are sensitive to single photons (even at room temperature). Features a dynamic range well above 100 photons/burst and have a high Photon Detection Efficiency (PDE) up to 50%. SiPM measures the light intensity simply by the number of fired cells. However, this information is affected and biased by stochastic effects characteristic of the sensor and occurring within the time window: spurious avalanches due to thermally generated carriers (a.k.a. Dark Counts), delayed avalanches associated to the release of carriers trapped in metastable states (a.k.a. Afterpulses) and an excess of fired cells due to photons produced in the primary avalanche, travelling in Silicon and triggering neighbouring cells (a phenomenon called Optical Cross Talk).

The typical SiPM response to a light pulse is characterized by multiple traces, each one corresponds to different numbers of fired cells, proportional to the number of impinging photons. Because of the high gain compared to the noise level, the traces are well separated, providing a photon number resolved detection of the light field.


Equipment

SP5600E - Educational Photon Kit

Model	SP5600	DT5720A	SP5601	SP5605C
Description	Power Supply and Amplification Unit	Desktop Digital 20MHz	LED Driver	Sensor Holder for SiPM

Currently the Silicon Photomultipliers are the new technology used in many important physics experiments. The Cherenkov Telescope Array (CTA) is one of these experiments. The CTA project is an initiative to build the next generation ground based very high energy gamma-ray instrument. It will serve as an open observatory to a wide astrophysics community and will provide a deep insight into the high-energy universe. The array of the CTA can be roughly grouped into three main themes, serving as key science drivers:

- Understanding the origin of cosmic rays and their role in the Universe
- Understanding the nature and variety of particle acceleration around black holes
- Searching for the ultimate nature of matter and physics beyond the Standard Model



Section & Subsection name

Related experiments

Ordering options

External reference

Equipment list

Requirements

Block diagram

Experimental results

A. Particle Detector Characterization - A.1 Silicon Photomultipliers

Requirements

No other tools are needed.

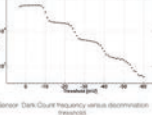
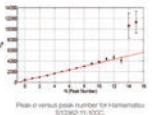
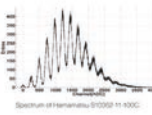
Carrying out the experiment

The light pulse from the SP5601 ultra-fast LED-Driver is driven through an optical clear fiber into the SP5605C SiPM holder housing the sensor under test and connected to the SP5600. The output signal from the SP5600 is connected to the input channel of the DT5720A Desktop Digitalizer equipped with the charge integration firmware, and triggered by the SP5601 LED-driver. The SP5600 and the DT5720A are connected to the PC through the USB. Use the default software values or optimize the bias voltage and discriminator threshold. The horizontal axis of the acquired spectrum is the ADC channels, therefore ADC-channel conversion ( $ADC_{ch}$ ) factor can be calculated to perform the experiment and determine the main features of the SiPM.

Results

The gain of the SiPM is evaluated from the output charge of the sensor. After the estimation of the ADC channel conversion factor ( $ADC_{ch}$ ) and the distance between adjacent peaks ( $\Delta PPADC_{ch}$ ), the SiPM gain can be calculated according to the following equation:
$$Gain = \frac{NPP_{ADC_{ch}}}{\Delta PP_{ADC_{ch}}} \cdot ADC_{ch}$$

The resolution power of the system can be evaluated plotting the  $\sigma$  of each peaks versus the number of peaks. The counts frequency, in absence of light, at 0.5 p.e. threshold represents the DCR. The ratio between the dark count at 1.5 p.e. threshold ( $DCR_{1.5}$ ) and the value at 0.5 p.e. threshold ( $DCR_{0.5}$ ) give the crosstalk estimation of the detector:



Spectrum of Hamamatsu S10592-11-100C

Peak  $\sigma$  versus peak number for Hamamatsu S10592-11-100C

Sensor Dark Count frequency versus discrimination threshold

Quick guide

Data plots

## Symbols Guide

Experiments with radioactive sources.

Data analysis code developed in MATLAB is available.

MATLAB® is a registered trademark of The MathWorks, Inc.

# Table of Contents

Introduction	pag 3
Website	pag 4
How to read this Handbook	pag 5

	pag
<b>A. Particle Detector Characterization</b>	<b>8</b>
<b>A.1 Silicon Photomultipliers (SiPM): a state-of-the art sensor to explore the quantum world</b>	<b>9</b>
A.1.1 SiPM Characterization	10
A.1.2 Dependence of the SiPM Properties on the Bias Voltage	12
A.1.3 Temperature Effects on SiPM Properties	14
<b>B. Nuclear Physics and Radioactivity</b>	<b>16</b>
<b>B.1 <math>\gamma</math> Spectroscopy</b>	<b>17</b>
B.1.1 Detecting $\gamma$ -Radiation	18
B.1.2 Poisson and Gaussian Distribution	20
B.1.3 Energy Resolution	22
B.1.4 System Calibration: Linearity and Resolution	24
B.1.5 A Comparison of Different Scintillating Crystals: Light Yield, Decay Time and Resolution	26
B.1.6 $\gamma$ -Radiation Absorption	28
B.1.7 Photonuclear cross-section/Compton Scattering cross-section	30
<b>B.2 <math>\beta</math> Spectroscopy</b>	<b>33</b>
B.2.1 Response of a Plastic Scintillating Tile	34
B.2.2 $\beta$ Spectroscopy	36
B.2.3 $\beta$ -Radiation: Transmission through Matter	38
B.2.4 $\beta$ -Radiation as a Method to Measure Paper Sheet Grammage and Thin Layer Thickness	40
<b>B.3 Nuclear Imaging - PET</b>	<b>43</b>
B.3.1 Basic Measurements: $\gamma$ Spectroscopy and System Linearity	44
B.3.2 Positron Annihilation Detection	46
B.3.3 Two-dimensional Reconstruction of a Radioactive Source	48
B.3.4 Spatial Resolution	50
<b>C. Particle Physics</b>	<b>52</b>
<b>C.1 Cosmic Rays</b>	<b>53</b>
C.1.1 Muons Detection	54
C.1.2 Muons Vertical Flux on Horizontal Detector	56
<b>C.2 Photons</b>	<b>59</b>
C.2.1 Quantum Nature of Light	60
C.2.2 Hands-on Photon Counting Statistics	62
<b>D. Advanced Statistics based on Silicon Photomultiplier Detectors</b>	<b>64</b>
D.1 An Educational Kit Based on a Modular SiPM System	66
D.2 A simple and robust method to study after-pulses in Silicon Photomultipliers	79
D.3 Background removal procedure based on the SNIP algorithm for $\gamma$ -ray spectroscopy	84

Products

89

Choose Your Educational Kit!

90

SP5600 - Power Supply and Amplification Unit	93
DT5720A - Desktop Digitizer	93
SP5601 - LED Driver	94
SP5650C - Sensor Holder with SiPM	94
SP5606 - Mini-Spectrometer	95
A315 - Splitter	95
SP5607 - Absorption Tool	96
SP5608 - Scintillating Tile	96
DT4800 - Digital Detector Emulator (micro-DDE)	97
DT5770 - Digital Multi-Channel Analyzer	97
SP5700 - EasyPET	98

Sales Network

pag 100



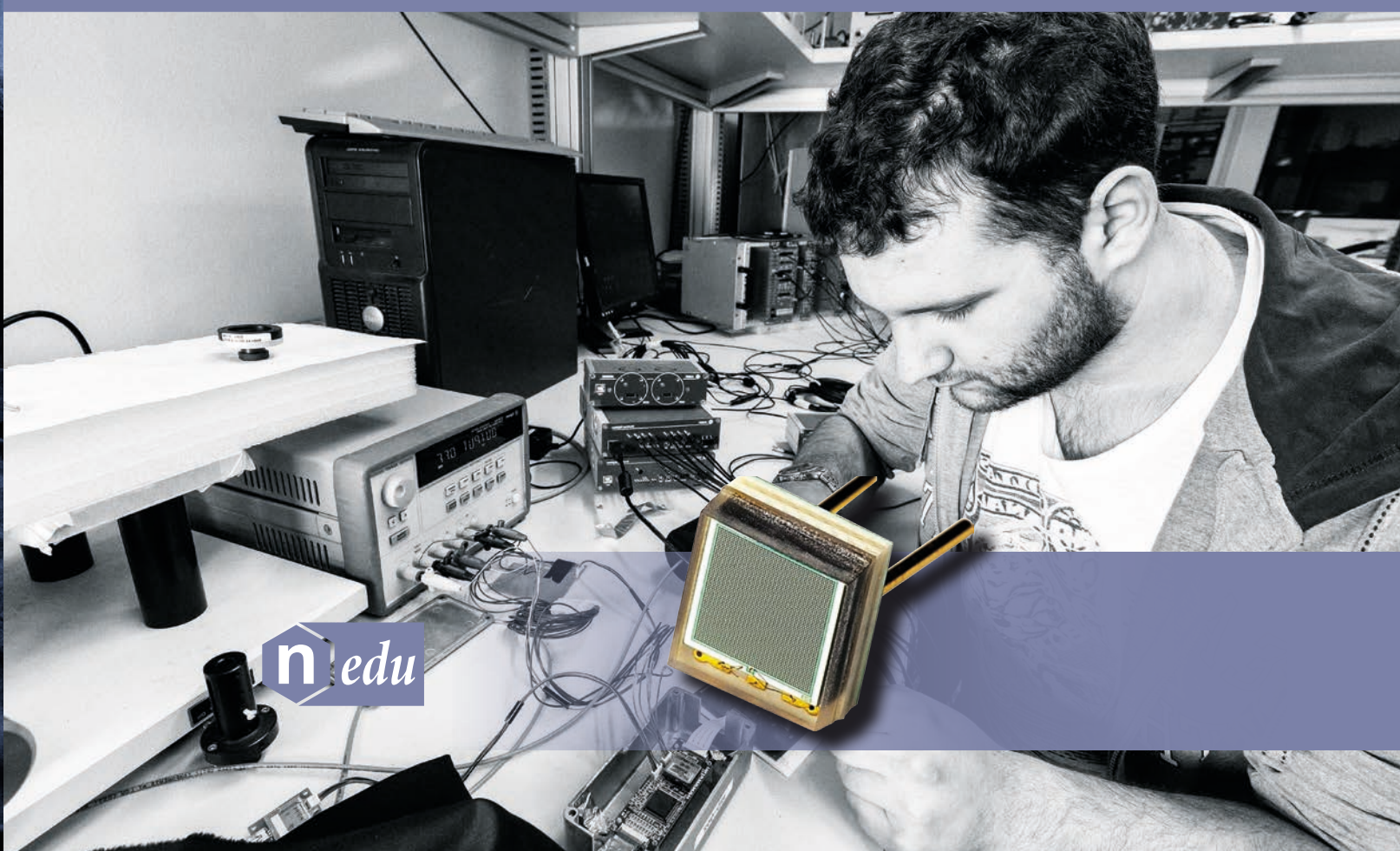


## A. Particle Detector Characterization





# A.1 Silicon Photomultipliers (SiPM): a state-of the art sensor to explore the quantum world



Exploring the quantum nature of phenomena is one of the most exiting experiences a physics student can live.

What is being proposed here has to do with light quanta, radioactive decays ( $\beta$  and  $\gamma$  rays) and cosmic rays. The experiments address the essence of the phenomenon as well as exemplary illustrations of their use in medical imaging and industry, complemented by basic and advanced statistical exercises.

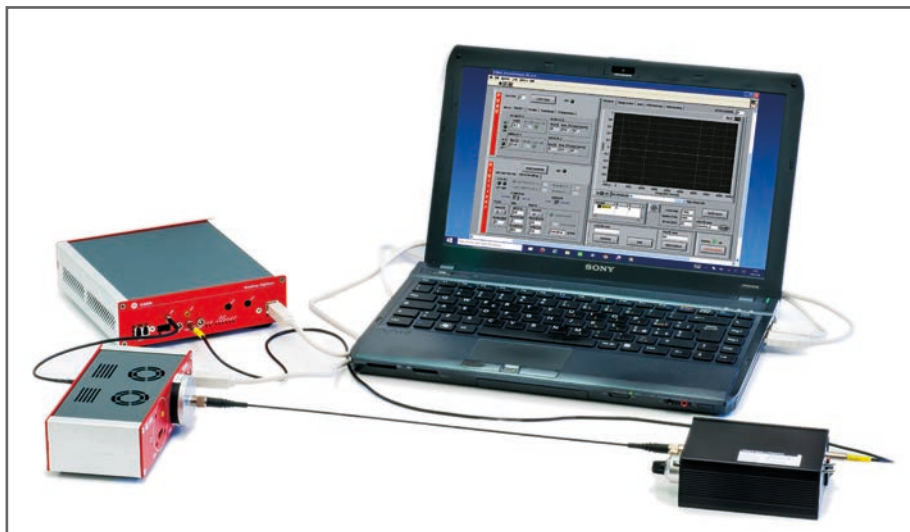
The set-up are all based on Silicon Photomultipliers (SiPM) state of-the-art sensor of light with single photon sensitivity and unprecedented photon number capability. In the field of light sensing and related appliances and instrumentation, SiPM are expected to have the same impact the transistor

had: well beyond the replacement of thermoionic valves, it triggered a revolution opening up new and unforeseen perspectives. As a consequence, it is quite natural to get started with activities aimed to introduce the student to the knowledge of the features of this class of sensors.

EDUCATIONAL PHOTON KIT	Model.	Description
	SP5600	Power Supply and Amplification Unit
	DT5720A	Desktop Digitizer 250 MS/s
	SP5601	LED Driver
	SP5650C	Sensor Holder for SP5600 with HAMAMATSU SiPM

# A.1.1 SiPM Characterization

SG6011



## Related Experiment

A.1.2

C.2.1

D.1

## Ordering Options

### Equipment

Code	Description
WK5600XEAAAA	SP5600E - Educational Photon Kit

or the all inclusive Premium Version

WK5600XANAAA	SP5600AN - Educational Kit - Premium Version
--------------	----------------------------------------------

## Purpose of the experiment

*Characterization of a SiPM detector using an ultra-fast pulsed LED.  
Estimation of the main features of the detector at fixed bias voltage.*

## Fundamentals

Silicon Photomultipliers (SiPM) consist of a high-density (up to  $\sim 10^4/\text{mm}^2$ ) matrix of diodes connected in parallel on a common Si substrate. Each diode is an Avalanche Photo Diode (APD) operated in a limited Geiger-Müller regime connected in series with a quenching resistor, in order to achieve gain at level of  $\sim 10^6$ . As a consequence, these detectors are sensitive to single photons (even at room temperature) feature a dynamic range well above 100 photons/burst and have a high Photon Detection Efficiency (PDE) up to 50%. SiPM measure the light intensity simply by the number of fired cells. However, this information is affected and biased by stochastic effects characteristic of the sensor and occurring within the time window: spurious avalanches due to thermally generated carriers (a.k.a. Dark Counts), delayed avalanches associated to the release of carriers trapped in metastable states (a.k.a. Afterpulses) and an excess of fired cells due to photons produced in the primary avalanche, travelling in Silicon and triggering neighboring cells (a phenomenon called Optical Cross Talk).

The typical SiPM response to a light pulse is characterized by multiple traces, each one corresponds to different numbers of fired cells, proportional to the number of impinging photons. Because of the high gain compared to the noise level, the traces are well separated, providing a photon number resolved detection of the light field.



Currently the Silicon Photomultipliers are the new technology used in many important physics experiments. The Cherenkov Telescope Array (CTA) is one of these experiments. The CTA project is an initiative to build the next generation ground-based very high energy gamma-ray instrument. It will serve as an open observatory to a wide astrophysics community and will provide a deep insight into the non-thermal high-energy universe. The aims of the CTA can be roughly grouped into three main themes, serving as key science drivers:

- Understanding the origin of cosmic rays and their role in the Universe
- Understanding the nature and variety of particle acceleration around black holes
- Searching for the ultimate nature of matter and physics beyond the Standard Model

<https://www.cta-observatory.org/>



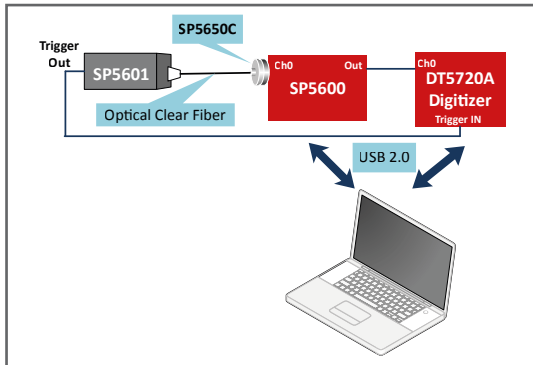
## Equipment

SP5600E - Educational Photon Kit

Model	SP5600	DT5720A	SP5601	SP5650C
Description	Power Supply and Amplification Unit	Desktop Digitizer 250 MS/s	LED Driver	Sensor Holder for SP5600 with SiPM
				
	p. 93	p. 93	p. 94	p. 94

## Requirements

No other tools are needed.



Experimental setup block diagram.

## Carrying out the experiment

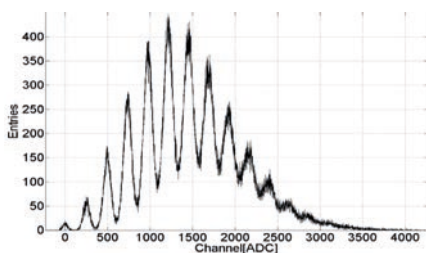
The light pulse from the SP5601 ultra-fast LED-Driver is driven through an optical clear fiber into the SP5650C SiPM holder housing the sensor under test and connected to the SP5600. The output signal (from the SP5600) is connected to the input channel of the DT5720A Desktop Digitizer equipped with the charge integration firmware, and triggered by the SP5601 LED-driver. The SP5600 and the DT5720A are connected to the PC through the USB. Use the default software values or optimize the bias voltage and discriminator threshold. The horizontal axis of the acquired spectrum is the ADC channels, therefore ADC channel conversion ( $ADC_{c.r.}$ ) factor can be calculated to perform the experiment and determine the main features of the SiPM.

## Results

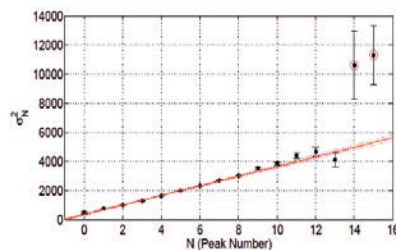
The gain of the SiPM is evaluated from the output charge of the sensor. After the estimation of the ADC channel conversion factor ( $ADC_{c.r.}$ ) and the distance between adjacent peaks ( $\Delta PP(ADC\_ch)$ ), the SiPM gain can be calculated according to the following equation:

$$Gain = \frac{\Delta PP(ADC\_ch) * ADC_{c.r.}}{e}$$

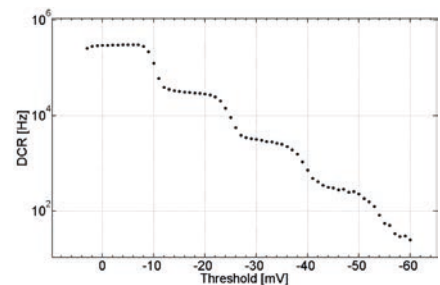
The resolution power of the system can be evaluated plotting the  $\sigma$  of each peaks versus the number of peaks. The counts frequency, in absence of light, at 0.5 p.e. threshold represents the DCR. The ratio between the dark count at 1.5 p.e. threshold ( $DCR_{1.5}$ ) and the value at 0.5 p.e. threshold ( $DCR_{0.5}$ ) give the crosstalk estimation of the detector.



Spectrum of Hamamatsu S10362-11-100C.



Peak  $\sigma$  versus peak number for Hamamatsu S10362-11-100C.

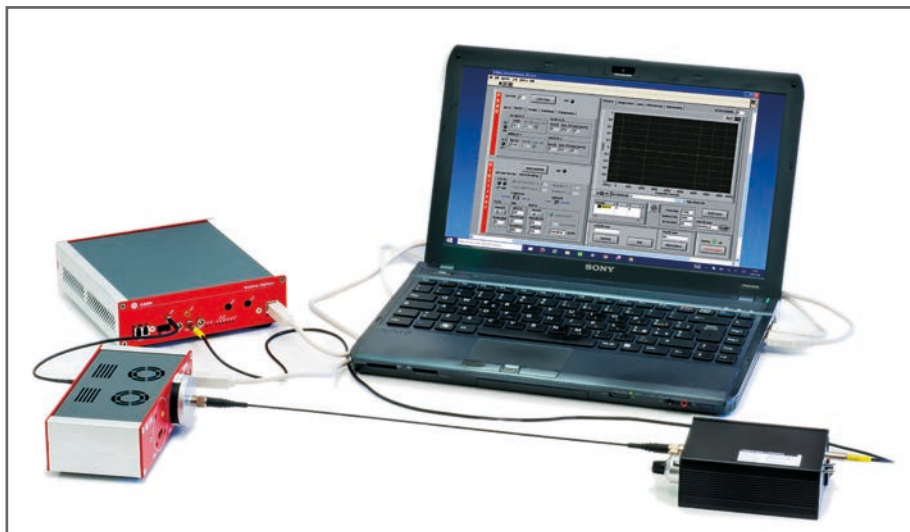


Sensor Dark Count frequency versus discrimination threshold.



## A.1.2 Dependence of the SiPM Properties on the Bias Voltage

SG6012



### Related Experiment

A.1.1

C.2.1

D.1

### Ordering Options

#### Equipment

Code	Description
WK5600XEAAAA	SP5600E - Educational Photon Kit

or the all inclusive Premium Version

WK5600XANAAA	SP5600AN - Educational Kit - Premium Version
--------------	----------------------------------------------

### Purpose of the experiment

*Study the dependence of the main SiPM figures of merit on the bias voltage. Measurement of the breakdown voltage and identification of the optimal working point. The experiment requires the use of the LED source included in the kit.*

### Fundamentals

The main features of the SiPM are expected to depend on the bias voltage or, more specifically, on the overvoltage, the voltage in excess of the breakdown value:

- The gain is expected to depend linearly on the overvoltage
- The triggering efficiency, i.e. the probability for a charge carrier to generate an avalanche by impact ionization, increases with the overvoltage till a saturation value is achieved. As a consequence, the Photon Detection Efficiency (PDE) increases together with the stochastic events (Dark Count Rate, Cross Talk and After Pulses) affecting the sensor response.

Actually, spurious events are expected to grow super-linearly and the determination of the optimal working point requires the definition of a proper figure of merit. Referring to the photon number resolving capability of the SiPM, the bias can be set to optimize the resolution power, i.e. the maximum number of resolved photons.



The Photomultipliers Tubes are a commercial product since 1934, at RCA; during the golden age of the discovery of the quantum world (Photoelectric effect, Einstein, 1905). Since then, the PMT continuously evolved, serving the industrial and scientific community with a wealth of different design & specification. In 1947, the transistor birth fixed the start of a new detectors generation that has brought to the Silicon Photomultipliers (SiPM) development. The SiPM are very appealing for different reason:

- high detection efficiency (single photo-electron discrimination)
- compactness and robustness
- low operating voltage and power consumption
- low cost
- withstanding to magnetic field

These features make this technology in fashionable in different application fields i.e. medical applications, homeland security, spectrometry, high energy physics ...

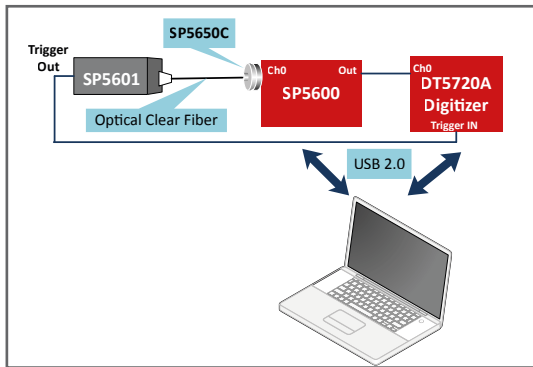
### Equipment

SP5600E - Educational Photon Kit

Model	SP5600	DT5720A	SP5601	SP5650C
Description	Power Supply and Amplification Unit	Desktop Digitizer 250 MS/s	LED Driver	Sensor Holder for SP5600 with SiPM
				
	p. 93	p. 93	p. 94	p. 94

### Requirements

No other tools or instruments are needed.



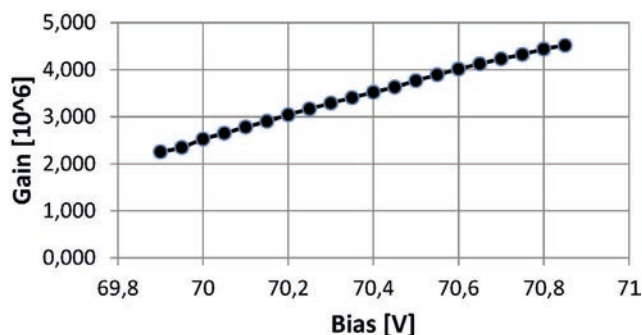
Experimental setup block diagram.

## Carrying out the experiment

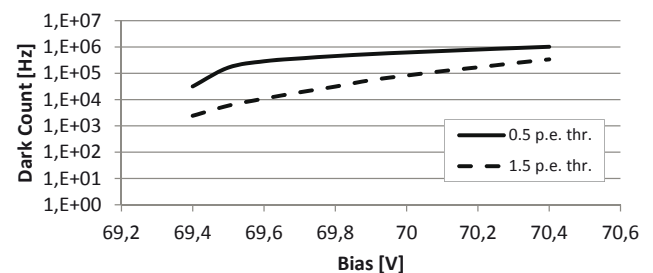
Mount one of the sensors (SP5650C) on the SP5600 and connect the analog output to the input of the DT5720A digitizer. Optically couple the LED and the sensor via the optical fiber, after having used the index matching grease on the tips. Set the internal trigger mode on the SP5601 and connect its trigger output on the DT5720A trigger IN. Connect via USB the modules to the PC and power ON the devices. Through the LabView graphical user interface (GUI), properly synchronize the signal integration and, for every voltage value, record the photon spectrum and measure directly the Dark Count and the Optical Cross talk. The measurement of the After Pulse is also possible but it requires most advanced analysis techniques.

## Results

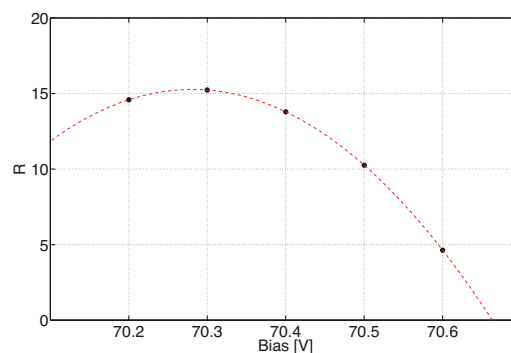
*As exemplary illustration, the trend of the gain vs. the bias voltage is shown, allowing as well the measurement of the breakdown voltage corresponding to the value at zero gain. The optimal working point by a measurement of the resolution power on the multi-photon peak spectrum is also shown.*



SiPM gain versus bias voltage.

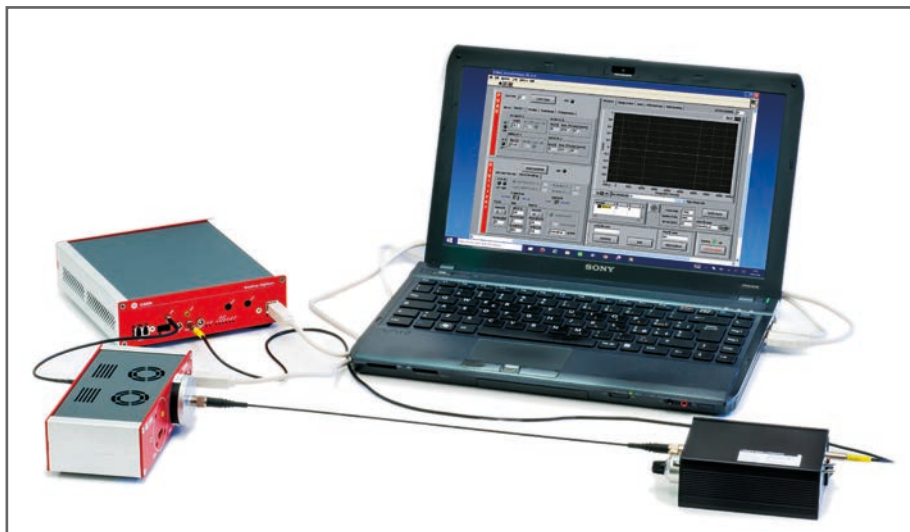


Dark count versus bias voltage.

Scan of the resolution power  $R$  as a function of the bias voltage.

# A.1.3 Temperature Effects on SiPM Properties

SG6013



## Ordering Options

Equipment	
Code	Description
WK5600XEAAAA	SP5600E - Educational Photon Kit

or the all inclusive Premium Version

WK5600XANAA	SP5600AN - Educational Kit - Premium Version
-------------	----------------------------------------------

## Purpose of the experiment


*Gain, noise and photon detection efficiency (at fixed bias voltage) are affected by temperature. The student is driven through the measurement of the dependence of these critical figures.*

## Fundamentals

The gain in a SiPM biased at fixed voltage changes with temperature since the breakdown voltage  $V_{br}$  does it. Gain stabilization is a must and can be pursued tracking the  $V_{br}$  changes and adjusting the bias voltage accordingly. The rate of variation depends on the sensor, through the material properties. Noise depends on the thermal generation of charge carriers, so a significant dependence is expected as well.

## Equipment

SP5600E - Educational Photon Kit

Model	SP5600	DT5720A	SP5601	SP5650C
Description	Power Supply and Amplification Unit	Desktop Digitizer 250 MS/s	LED Driver	Sensor Holder for SP5600 with SiPM
				
	p. 93	p. 93	p. 94	p. 94

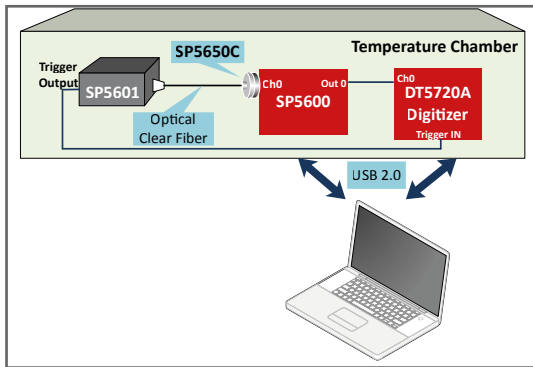


The NA62 is an experiment at CERN with the aim to measure the very rare kaon decay  $K^+ \rightarrow \pi^+ \nu \bar{\nu}$ . Carried on at CERN SPS the experiment aims to collect about 80  $K^+ \rightarrow \pi^+ \nu \bar{\nu}$  events at the SM prediction with a signal to background ratio of 10:1 in two years of data taking. In particular, the experiment makes also use of the Silicon Photomultipliers technology due to the properties similar to conventional photomultipliers but withstanding to high magnetic fields. CERN awarded CAEN with a contract for the design and production of the High Voltage power supply system for photomultiplier tubes for the NA62 Large Angle photon Veto (LAV), Muon Veto detectors (MUV), Differential Cherenkov counter (CEDAR) and the Calorimeter REAdout Module (CREAM) for the NA62 high resolution Liquid Krypton Calorimeter (LK<sub>r</sub>).

<http://na62.web.cern.ch/NA62/>


## Requirements

A temperature controlled box/room is essential.



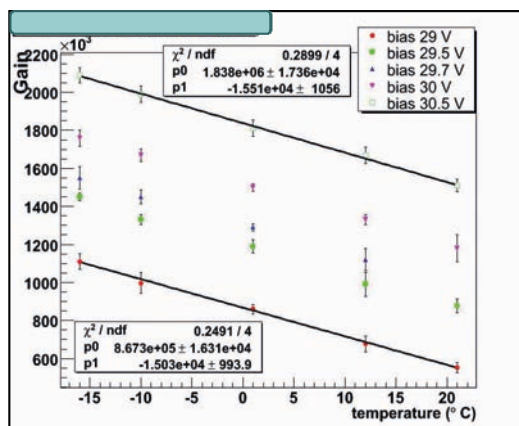
Experimental setup block diagram.

## Carrying out the experiment

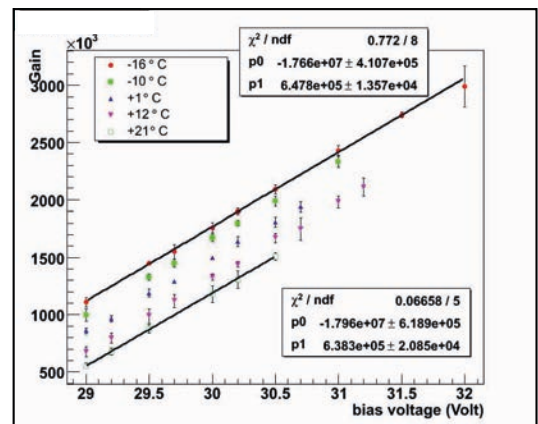
In a temperature controlled box, mount one of the sensors (SP5650C) on the SP5600 and connect the analog output to the input of the DT5720A digitizer. Optically couple the LED and the sensor via the optical fiber, after having used the index matching grease on the tips. Set the internal trigger mode on the P5601 and connect its trigger output on the DT5720A trigger IN. Connect via USB the modules to the PC and power ON the devices. Through the LabView graphical user interface (GUI), properly synchronize the signal integration and, for every temperature & voltage value, record the photon spectrum and measure directly the Dark Count and the Optical Cross talk.

## Results

Figures show the dependence of the gain upon temperature at various voltages and the voltage dependence at various temperatures. By the two set of results, the temperature coefficient of the sensor, i.e. the variation of the breakdown voltage with temperature, can be measured

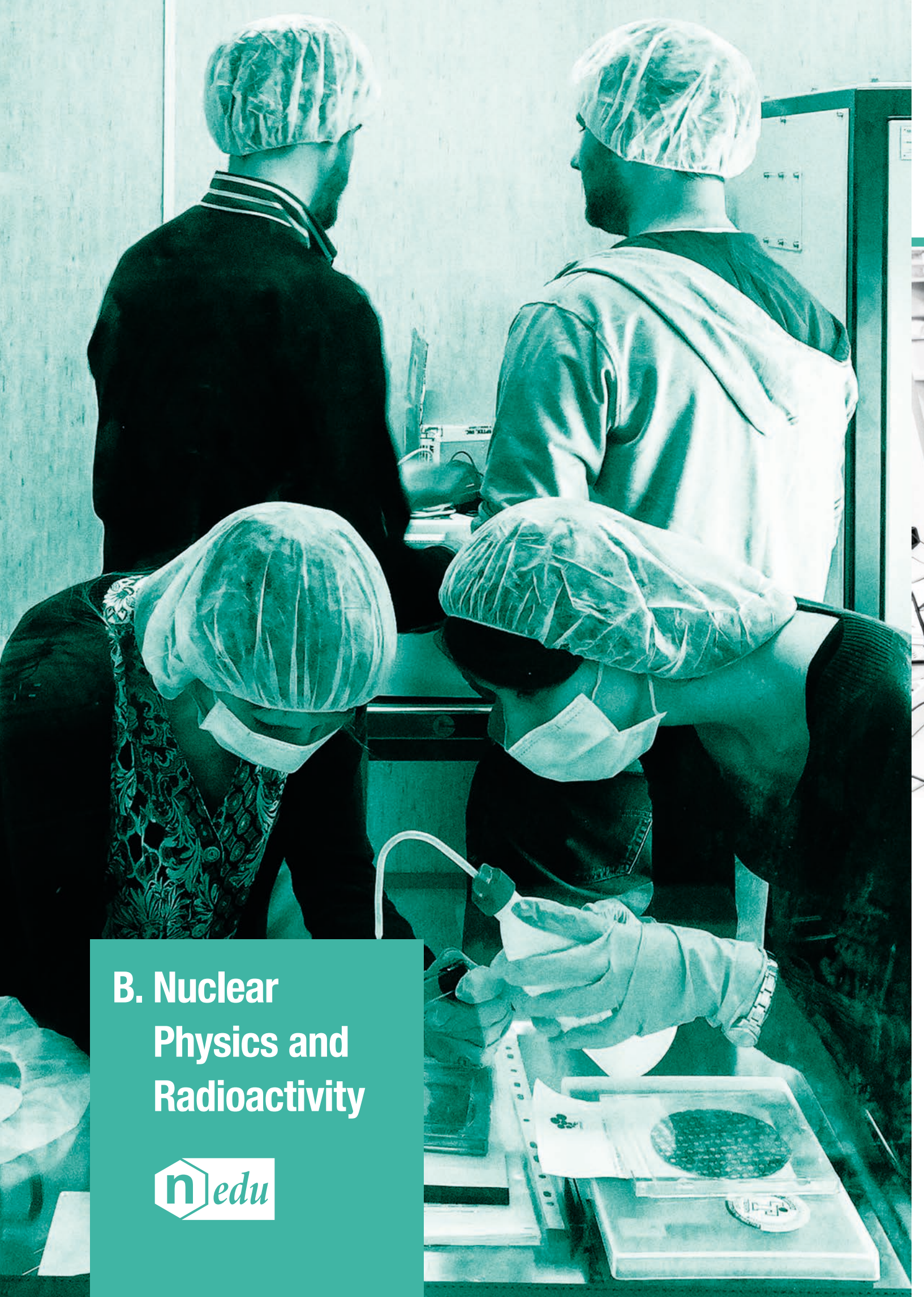


SiPM gain as a function of temperature, at different bias voltage values.



SiPM gain as a function of the bias voltage, at different temperature values.



A woman with long blonde hair, wearing a patterned top, is focused on adjusting a component of a complex scientific instrument. The instrument features various wires, a cylindrical metal part, and a small digital display. The scene is dimly lit, with a strong light source from the right, creating a dramatic effect. The overall color palette is dominated by teal and blue tones.

## B. Nuclear Physics and Radioactivity





## B.1 $\gamma$ Spectroscopy



In 1895 the radioactivity was discovered by H. Becquerel and in 1903 the Nobel Prize in Physics was assigned to Curie spouses for their studies on these phenomena. Radioactivity is around us and getting to know it experimentally is essential for physics students.

When an unstable nucleus decays in a cascade leading to a stable nuclide, it emits  $\alpha$  or  $\beta$  or  $\gamma$  quanta or a combination of them. Gamma rays are high energy photons and the spectroscopy of the emitted  $\gamma$  rays is instrumental for understanding the mechanism of the interaction with matter, the fundamentals about detection and the underlying nuclear physics. Moreover, it is relevant in basic and applied fields of science and technology, from nuclear to medical physics, from archaeometry to homeland security.

The  $\gamma$  spectroscopy experiments can be performed by using two different set-ups. The first one is the “Educational Gamma KIT”, characterized by a modular

structure that allows to execute all the applications.

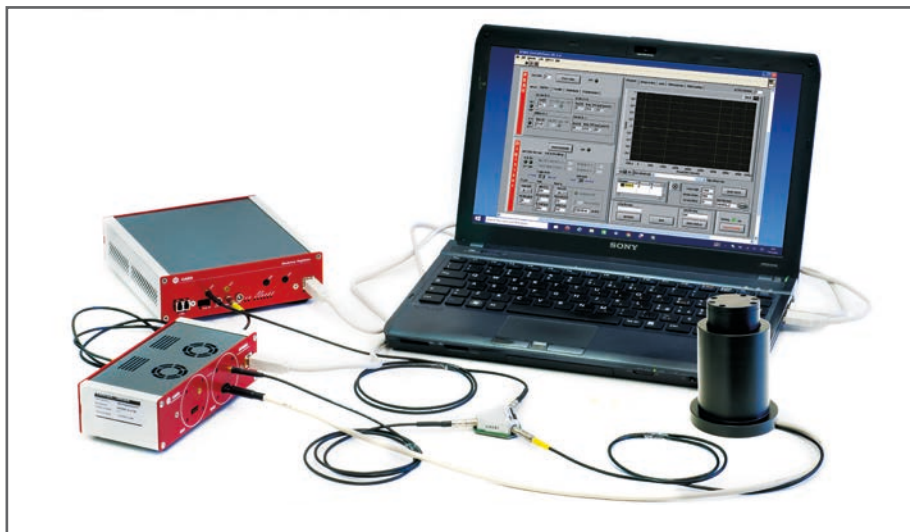
The alternative equipment is the “Emulation kit” based on the CAEN Digital Detector-Emulator (DT4800) together with Digital Multi-Channel Analyzer (DT5770). The latter allows to perform a series of lab experiments without using a radioactive source and a detector but simulating the signals produced by the interaction of particles with the detecting unit. The two set-ups are highly complementary.

EDUCATIONAL GAMMA KIT	Model.	Description
	SP5600	Power Supply and Amplification Unit
	DT5720A	Desktop Digitizer 250 MS/s
	SP5606	Mini-Spectrometer
	SP5607	Absorption tool
	A315	Splitter

EMULATION KIT	Model.	Description
	DT4800	Digital Detector Emulator
EMULATION KIT	DT5770	Digital Multi-Channel Analyzer

# B.1.1 Detecting $\gamma$ -Radiation

SG6111



## Ordering Options

Equipment	
Code	Description
WK5600XCAAAA	SP5600C - Educational Gamma Kit

or the all inclusive Premium Version

WK5600XANAAA	SP5600AN - Educational Kit - Premium Version
--------------	----------------------------------------------

## Purpose of the experiment

*Gamma radioactivity detection by using a system composed of a scintillating crystal coupled to a photon detector.*

## Fundamentals

Gamma rays interact with matter by three processes: Compton Scattering, Photoelectric Effect and Pair Production (whenever the energy exceeds the 1.022 MeV threshold corresponding to the  $e^+e^-$  rest mass). The cross section of each process depends on the energy of the gamma ray.

The Compton Effect is the inelastic scattering between the incoming photon and an atomic electron. In the Photoelectric Effect, the incident gamma ray transfers all of its energy to a bound electron which acquires a kinetic energy equal to the incoming gamma energy decreased by the binding energy.

These processes convert, totally or partially, the gamma ray energy into kinetic energy of electrons (or positrons, in case of pair production). The interaction of the charged particles with the atomic and molecular systems of the medium results in excited states whose decay, possibly mediated, leads to light in the visible or UV region, eventually detected by the light sensor. A wide range of scintillator products is available today, differing for the light yield, the material properties, the time characteristics of the scintillation light and, last but not least, cost. The choice of the scintillator is essentially dependent on the specific targeted application.



Marie Skłodowska Curie was a Polish and naturalized-

French physicist and chemist who conducted pioneering research on radioactivity. She was the first woman to win a Nobel Prize, the first person and only woman to win twice in multiple sciences. Together with her husband, she was awarded half of the Nobel Prize for Physics in 1903, for their study into the spontaneous radiation discovered by Becquerel, who was awarded the other half of the Prize. In 1911 she received a second Nobel Prize, this time in Chemistry, in recognition of her work in radioactivity. Radium discovery opened the door to deep changes in the way scientists think about matter and energy. She also led the way to a new era for medical knowledge and the treatment of diseases.

<https://www.aip.org/history/exhibits/curie/brief/index.html>



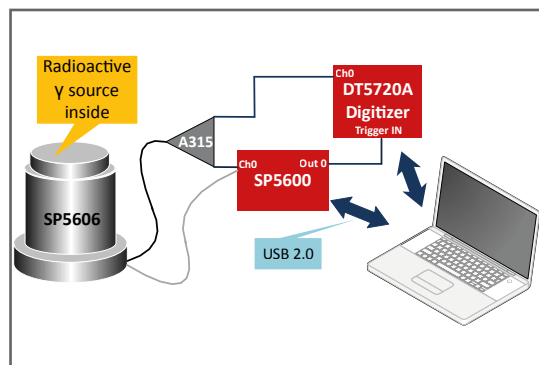
## Equipment

SP5600C - Educational Gamma Kit

Model	SP5600	SP5606	A315	DT5720A	SP5607
Description	Power Supply and Amplification Unit	Mini-Spectrometer	Splitter	Desktop Digitizer 250 MS/s	Absorption tool
	p. 93	p. 95	p. 95	p. 93	p. 96

## Requirements

Gamma Radioactive Source 



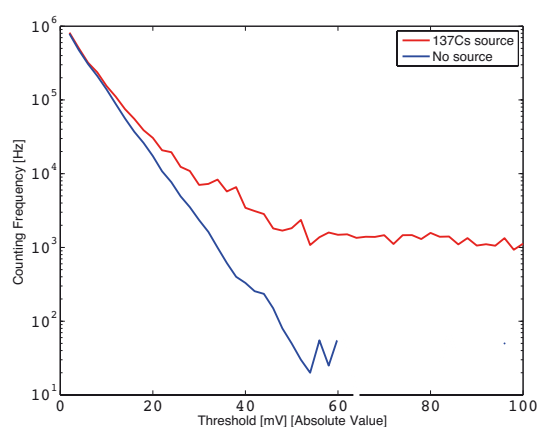
Experimental setup block diagram.

## Carrying out the experiment

The selected scintillator crystal shall be coupled to the SiPM in the SP5607, through a thin layer of index matching grease to maximize the light collection. In order to avoid saturation, the output of the SiPM is divided using the A315 splitter: one branch is connected to the DT5720A and will be digitized. The other branch will be amplified by the SP5600 module, generating the trigger for the integration signal by the on-board leading edge discriminator or simply counting the pulses induced by the detected gamma ray

## Results

The student may get acquainted with the presence of radioactivity with a simple preliminary measurement, namely comparing the counting frequency as a function of the discriminator threshold with/without the source. Presuming the source, essentially in contact to the crystal, to be point like with respect to the crystal surface, and assuming its activity is known, the student may estimate for every threshold value the detection efficiency and the signal over noise ratio, building up an efficiency-purity plot. Exemplary results obtained with a  $^{137}\text{Cs}$  source are shown. Moving away the source from the crystal, the law governing the variation of the flux can also be investigated.



Sensor output frequency as a function of the threshold in mV, with and without  $^{137}\text{Cs}$  source.



# B.1.2 Poisson and Gaussian Distribution

SG6112



## Ordering Options

### Equipment A

Code	Description
WK5600XCAAAA	SP5600C - Educational Gamma Kit

or the all inclusive Premium Version

WK5600XANAAA	SP5600AN - Educational Kit - Premium Version
--------------	----------------------------------------------

### Equipment B

Code	Description
WK5600XEMUAA	SP5600EMU - Emulation Kit

## Purpose of the experiment

Study the statistical distribution of the counting rates of a gamma radioactive source. Comparison of the data to the Poisson distribution, turning into a Gaussian as the mean number of counts grows. The study can be performed both experimentally, with the SiPM kit or simulating it with the emulation kit.

## Fundamentals

The number of radioactive particles detected over a time  $\Delta t$  is expected to follow a Poisson distribution with mean value  $\mu$ . It means that for a given radioactive source, the probability that  $n$  decays will occur over a given time period  $\Delta t$  is given by:

$$P_{\mu}(n) = \frac{\mu^n}{n!} e^{-\mu}$$

Where  $\mu$  is proportional to the sample size and to the time  $\Delta t$  and inversely proportional to the half-life  $T_{1/2}$  of the unstable nucleus. As long as  $\mu$  grows, the probability  $P_{\mu}(n)$  is well approximated by a Gaussian distribution:

$$P(n) = \frac{1}{\sqrt{2\pi}\sigma} e^{-\frac{(n-\mu)^2}{2\sigma^2}}$$

Where  $\sigma = \sqrt{\mu}$  is the standard deviation.

The experiment can be performed by using to different set-ups:




In the English-language literature the t-distribution takes its name from William Sealy Gosset's 1908 paper in Biometrika under the pseudonym "Student". Gosset worked at the Guinness Brewery in Dublin, Ireland, and was interested in the problems of small samples – for example the chemical properties of barley where sample sizes might be as few as 3. One version of the origin of the pseudonym is that Gosset's employer preferred staff to use pen names when publishing scientific papers instead of their real name, so he used the name "Student" to hide his identity. Another version is that Guinness did not want their competitors to know that they were using the t-test to determine the quality of raw material. Gosset's paper refers to the distribution as the "frequency distribution of standard deviations of samples drawn from a normal population". It became well-known through the work of Ronald Fisher, who called the distribution "Student's distribution" and represented the test value with the letter t.

[https://en.wikipedia.org/wiki/Student's\\_t-distribution](https://en.wikipedia.org/wiki/Student's_t-distribution)



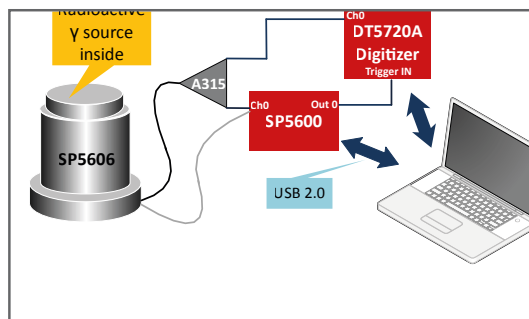
## EQUIPMENT A

### SP5600C - Educational Gamma Kit

Model	SP5600	SP5606	A315	DT5720A	SP5607
Description	Power Supply and Amplification Unit	Mini-Spectrometer	Splitter	Desktop Digitizer 250 MS/s	Absorption tool
					
	p. 93	p. 95	p. 95	p. 93	p. 96

## Requirements

Gamma Radioactive Source 



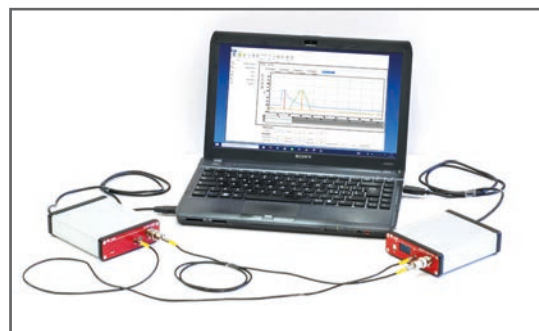
Block diagram of the experimental setup that makes use of the "Educational Gamma Kit".

## Carrying out the experiment

The selected scintillator crystal shall be coupled to the SiPM in the SP5607, through a thin layer of index matching grease to maximize the light collection. In order to avoid saturation, the output of the SiPM is divided using the A315 splitter: one branch is connected to the DT5720A and will be digitized. The other branch will be amplified by the SP5600 module, generating the trigger for the integration signal by the on-board leading edge discriminator or simply counting the pulses induced by the detected gamma ray. The discriminator threshold shall be defined looking at the spectrum and evaluating the dark count rate. Once this is properly set, the counting experiment shall be performed.

## EQUIPMENT B

### SP5600EMU - Emulation Kit



Model	DT4800	DT5770
Description	Digital Detector Emulator	Desktop Multi-Channel Analyzer
		

p. 97

p. 97

## Requirements

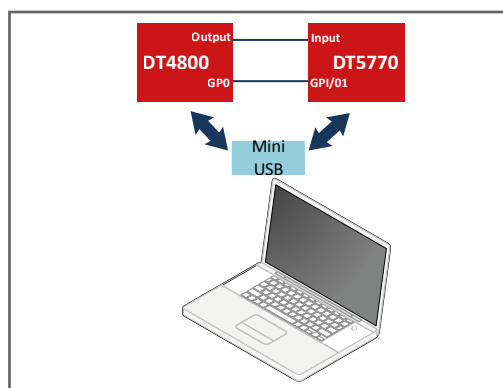
Gamma Radioactive Source is not needed.

## Carrying out the experiment

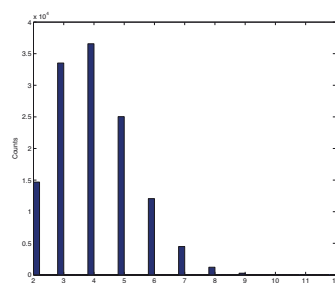
To perform the experiment connect the DT4800 output to the input channel of the MCA DT5770 and use the DT4800 GP0 as digitizer "trigger IN". The DT4800 Control Software Interface allows to generate exponential decay signals with programmable rise time and fall time and it is possible to emulate signals from a real energy spectrum linked to a radioactive source with variable activity.

## Results

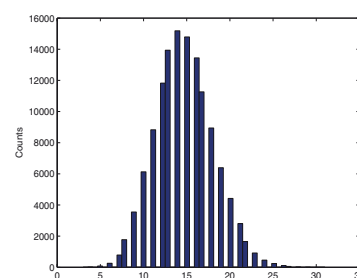
*Changing the counting window and/or the activity of the source or the threshold, the number of counts changes, with a probability density function moving from a Poissonian to a Gaussian shape. The student may play with the data, fitting them and comparing the expectations to the measurement.*



Block diagram of the experimental setup that makes use of the "Emulation Kit".



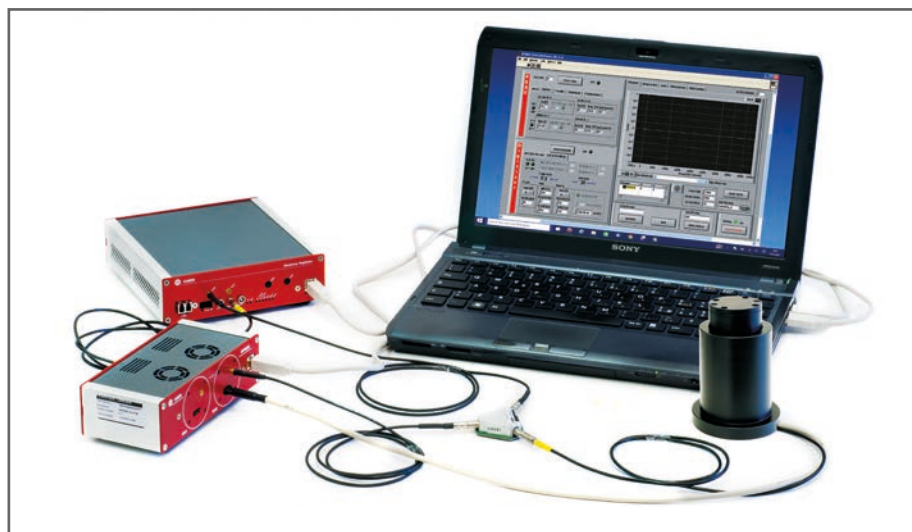
Poissonian distribution.



Gaussian distribution.

## B.1.3 Energy Resolution

SG6113



### Related Experiment

B.3.1

D.3

### Ordering Options

#### Equipment A

Code	Description
WK5600XCAAAA	SP5600C - Educational Gamma Kit

or the all inclusive Premium Version

WK5600XANAAA	SP5600AN - Educational Kit - Premium Version
--------------	----------------------------------------------

#### Equipment B

Code	Description
WK5600XEMUAA	SP5600EMU - Emulation Kit

### Purpose of the experiment

*The analysis of the spectrum of the deposited energy by a  $\gamma$  ray in a detector discloses the essence of the interaction of high energy photons with matter and allows to learn by doing the detector related effects.*

### Fundamentals

For  $\gamma$ -energy less than 2MeV, the interaction with matter is dominated by Compton scattering and Photo-absorption. The analysis of the Compton continuum of the deposited energy and of the photo-peak conveys information on the characteristics of the decaying isotope as well as the effects due to the system noise, the detected photon statistics, the stochastic terms in the detector and the intrinsic resolution of the scintillator. The experiment presumes to use  $^{137}\text{Cs}$  with its decays detected by a CsI crystal coupled to a Silicon Photomultiplier. The  $^{137}\text{Cs}$  source is particularly interesting due to its low energy X ray line at 30 keV and the high energy gamma emission at 662 keV. The former is relevant to optimize the lower detection limit of the system; the latter is a standard to evaluate the energy resolution. The use of the 2 lines and the analysis of the Compton spectrum characteristics allow to perform a rough measurement of the linearity with a single isotope.

The experiment can be performed by using to different set-ups:



ATLAS is one of two general-purpose detectors at the Large Hadron Collider (LHC). It investigates a wide range of physics, from the search for the Higgs boson to extra dimensions and particles that could make up dark matter. Although it has the same scientific goals as the CMS experiment, it uses different technical solutions and a different magnet-system design. Beams of particles from the LHC collide at the centre of the ATLAS detector making collision debris in the form of new particles, which fly out from the collision point in all directions. Six different detecting subsystems arranged in layers around the collision point record the paths, momentum, and energy of the particles, allowing them to be individually identified. A huge magnet system bends the paths of charged particles so that their momenta can be measured. Also this experiment makes use of the CAEN instrumentations.

<http://home.cern/about/experiments/atlas>



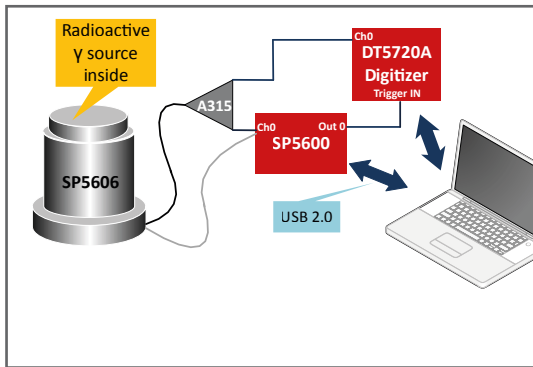
### EQUIPMENT A

#### SP5600C - Educational Gamma Kit

Model	SP5600	SP5606	A315	DT5720A	SP5607
Description	Power Supply and Amplification Unit	Mini-Spectrometer	Splitter	Desktop Digitizer 250 MS/s	Absorption tool
	p. 93	p. 95	p. 95	p. 93	p. 96

### Requirements

Gamma Radioactive Source

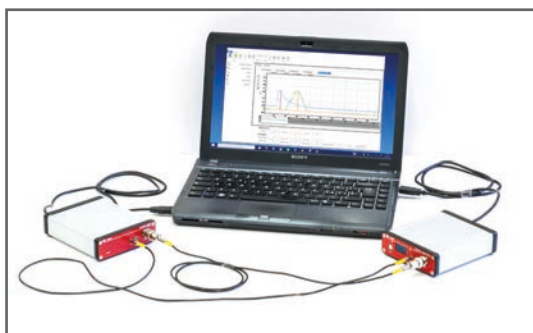


Block diagram of the experimental setup that makes use of the "Educational Gamma Kit".

## Carrying out the experiment

The CsI scintillator crystal shall be coupled to the SiPM in the SP5607, through a thin layer of index matching grease to maximize the light collection. In order to avoid saturation, the output of the SiPM is divided using the A315 splitter: one branch is connected to the DT5720A and will be digitized. The other branch will be amplified by the SP5600 module, generating the trigger for the integration signal by the on-board leading edge discriminator. The discriminator threshold shall be defined looking at the spectrum and evaluating the dark count rate. Once this is properly set and the radioactive source is properly positioned, the spectrum can be recorded.

## EQUIPMENT B

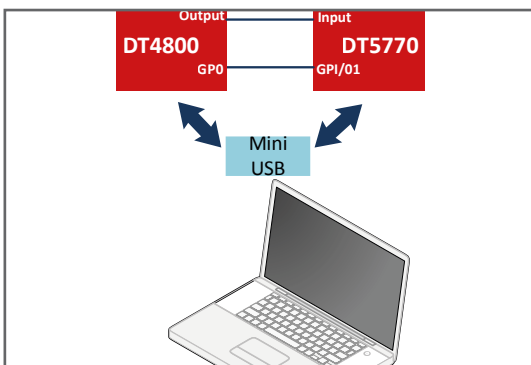


### SP5600EMU - Emulation Kit

Model	DT4800	DT5770
Description	Digital Detector Emulator	Desktop Multi-Channel Analyzer
		
	p. 97	p. 97

## Requirements

Gamma Radioactive Source is not needed.



Block diagram of the experimental setup that makes use of the "Emulation Kit".

## Carrying out the experiment

To perform the experiment connect the DT4800 output to input of the MCA DT5770 and use the DT4800 GP0 as digitizer "trigger IN". The DT4800 Control Software Interface allows to emulate signals from a real energy spectrum linked to a radioactive source with variable activity.

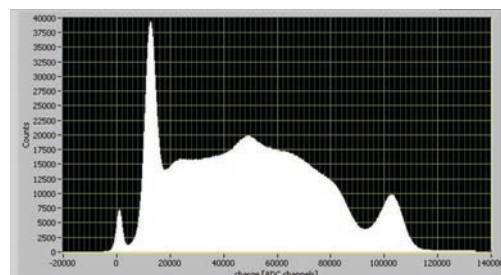
## Results

The figure shows a typical gamma spectrum, recorded with a very low energy threshold. The left over from the system noise is clearly visible, as well as the low energy line at 30 keV and the photopeak. For this specific spectrum, the energy resolution on the 662 keV peak corresponds to

$$\text{Energy Resolution} = \frac{\text{FWHM}_{\text{peak}}}{\mu_{\text{peak}}} * 100 \sim 10\%$$

$\text{FWHM}_{\text{peak}}$  = full width at half maximum of the peak

$\mu_{\text{peak}}$  = channel number of the peak centroid.

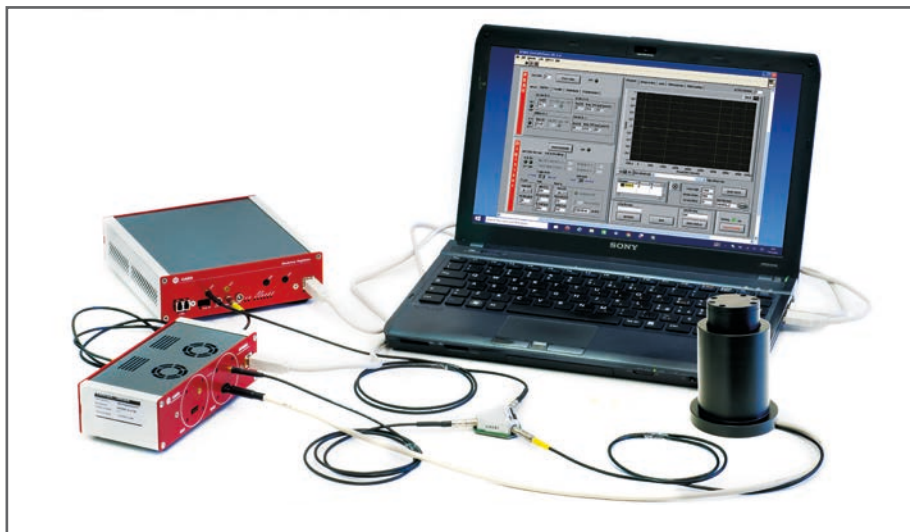


$^{137}\text{Cs}$  spectrum.



# B.1.4 System Calibration: Linearity and Resolution

SG6114



## Related Experiment

B.3.1

D.3

## Ordering Options

### Equipment A

Code	Description
WK5600XCAAAA	SP5600C - Educational Gamma Kit

or the all inclusive Premium Version

WK5600XANAAA	SP5600AN - Educational Kit - Premium Version
--------------	----------------------------------------------

### Equipment B

Code	Description
WK5600XEMUAA	SP5600EMU - Emulation Kit

## Purpose of the experiment

*Recording and comparing the  $\gamma$  energy spectra of several radioactive sources is the main goal of the experiment. The photo-peaks are used to calibrate the response of the system and to measure the energy resolution.*

## Fundamentals

Linearity and energy resolution are the main figures of merit of a spectrometric system. In the proposed experiment, based on a scintillating crystal coupled to a Silicon Photomultipliers, deviations in the linearity may be due to the sensor or the front-end electronics saturation. The student is guided through the analysis of the response curve using a series of isotopes up to the MeV energy by a  $^{60}\text{Co}$  source and to disentangle the different effects. At the same time, the energy resolution of the system is measured by the width of the photo-peaks and the results compared to what is expected by the fluctuations in the number of detected scintillation photons, the system noise, the sensor stochastic effects, the intrinsic resolution of the scintillator.

This is following an initial activity on the optimization of the operating parameters by an analysis of the photo-peak position and the resolution for a single isotope.

The experiment can be performed by using to different set-ups:



The kit instrumentation provides the CAEN digitizer DT5720A. This device is part of a complete family of digitizers in this form factor that consists of several models differing in sampling frequency, resolution, number of channel, memory size and other parameter. In parallel with the hardware development, CAEN have made a big effort in developing algorithms for the Digital Pulse Processing (DPP); you can install a DPP algorithm on the FPGA of the digitizer (firmware upgrade), run it on-line and implement new acquisition methods that go beyond the simple waveform recording. A digitizer with DPP becomes a new instrument that represents a fully digital replacement of most traditional modules such as Multi and Single Channel Analyzers, QDCs, TDCs, Discriminators and many others. CAEN digitizers are widely diffused in major physics experiments Worldwide.

[www.caen.it](http://www.caen.it)


## EQUIPMENT A

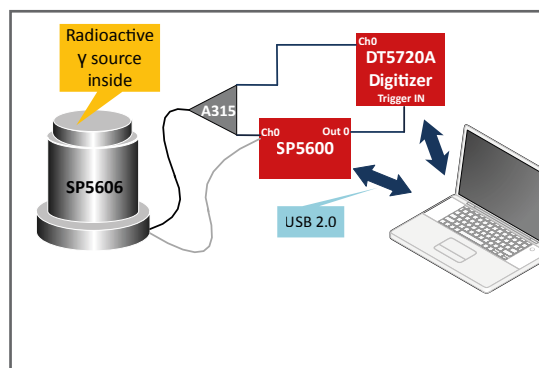
### SP5600C - Educational Gamma Kit

Model	SP5600	SP5606	A315	DT5720A	SP5607
Description	Power Supply and Amplification Unit	Mini-Spectrometer	Splitter	Desktop Digitizer 250 MS/s	Absorption tool
	p. 93	p. 95	p. 95	p. 93	p. 96

## Requirements

Gamma Radioactive Source





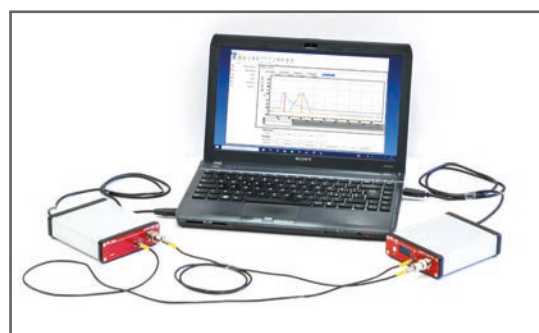
Block diagram of the experimental setup that makes use of the "Educational Gamma Kit".

## Carrying out the experiment

The scintillator crystal shall be coupled to the SiPM in the SP5607, through a thin layer of index matching grease to maximize the light collection. In order to avoid saturation, the output of the SiPM is divided using the A315 splitter: one branch is connected to the DT5720A and will be digitized. The other branch will be amplified by the SP5600 module, generating the trigger for the integration signal by the on-board leading edge discriminator. The discriminator threshold shall be defined looking at the spectrum and evaluating the dark count rate. Once this is set and the radioactive source is properly positioned, the spectrum can be recorded.

## EQUIPMENT B

### SP5600EMU - Emulation Kit



Model	DT4800	DT5770
Description	Digital Detector Emulator	Desktop Multi-Channel Analyzer
		
	p. 97	p. 97

## Requirements

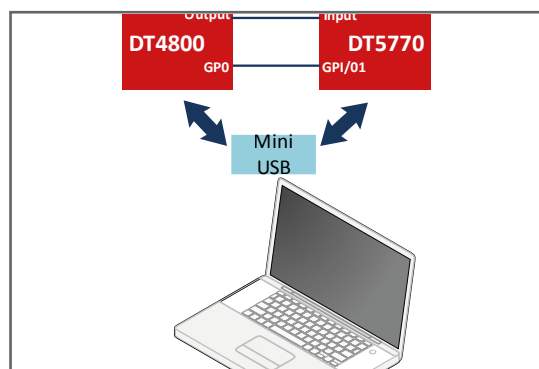
Gamma Radioactive Source is not needed.

## Carrying out the experiment

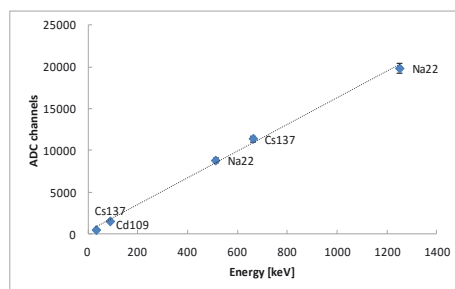
Carrying out the experiment: To perform the experiment connect the DT4800 output to the input channel of the MCA DT5770 and use the DT4800 GP0 as digitizer "trigger IN". The DT4800 Control Software Interface allows to emulate signals from a real energy spectrum linked to different radioactive sources with variable activity.

## Results

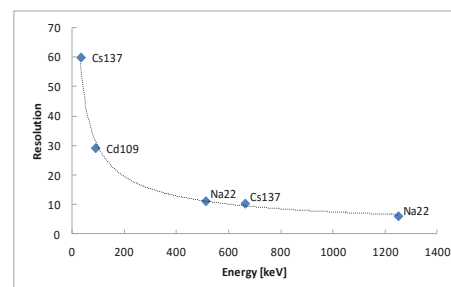
*By fitting the photo-peaks with a Gaussian curve, the system linearity as a function of energy is verified. The peak widths is determining the energy resolution. At more advanced level, the interpretation of the results accounting for the system properties may be performed.*



Block diagram of the experimental setup that makes use of the "Emulation Kit".



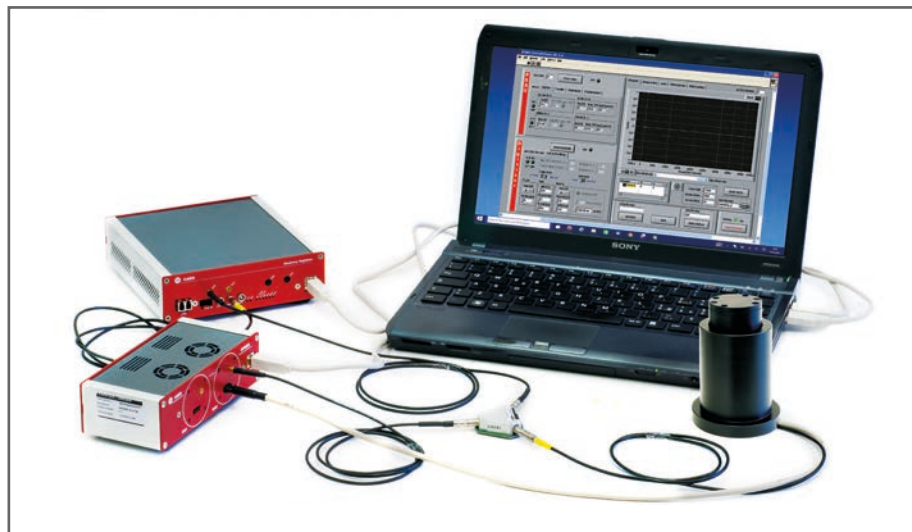
Energy Calibration



Energy dependence of the system resolution

# B.1.5 A Comparison of Different Scintillating Crystals: Light Yield, Decay Time and Resolution

## SG6115



### Ordering Options

Equipment	
Code	Description
WK5600XCAAAA	SP5600C - Educational Gamma Kit
or the all inclusive Premium Version	
WK5600XANAAA	SP5600AN - Educational Kit - Premium Version

### Purpose of the experiment

*Compare the basic characteristics of different scintillating crystals, namely the light yield and the decay time of the scintillation light. Verify the effect on the energy resolution.*

### Fundamentals

Scintillating materials have different characteristics related to the light yield and the characteristics time of the emission. The CAEN spectrometer is provided with three different crystals: BGO (Bismuth Germanate), LYSO(Ce) (Cerium-doped Lutetium Yttrium Orthosilicate), CsI(Tl) (Thallium-doped Cesium Iodide). All of them have the same volume ( $6 \times 6 \times 15 \text{ mm}^3$ ), are polished on all sides and coated with a white epoxy on 5 faces. One  $6 \times 6 \text{ mm}^2$  face is open in order to be coupled with the Silicon Photomultiplier. The main characteristics of the crystals are summarized in the following table:

	BGO	LYSO(Ce)	CsI(Tl)
Density ( $\text{g/cm}^3$ )	7.13	7.4	4.51
Decay Time (ns)	300	40	1000
Light Yield (ph./MeV)	8200	27000	52000
Peak emission (nm)	480	420	560
Radiation length (cm)	1.13	1.14	1.85
Reflective index	2.15	1.82	1.78

The light yield is having an impact on the energy resolution. This is also affected by the decay time, constraining the integration time and implying a different effect of the sensor stochastic effects (dark counts and afterpulses).



The scintillation is by physics definition the process by which ionization produced by charged particles excites a material causing light to be emitted during the de-excitation. When you excite a material and it subsequently gives off light, that is luminescence: fluorescence is photoluminescence or scintillation (i.e. excitation produced by ionizing radiation) that has a fast decay time (ns to  $\mu\text{s}$ ) and phosphorescence is the same, only with a much slower decay time (ms to seconds). Among the scintillator characteristics:

- light yield: high efficiency for converting ionization energy to light output [photons/MeV]
- decay time: how long it takes the excited states to de-excite and give off light (can be different for alphas and betas because depends on ionization density)
- density and Z: determine response to  $\gamma$ ,  $e^-$  and other electromagnetic processes.

Scintillator crystals are widely used in detectors for gamma-rays, X-rays, cosmic rays and particles whose energy is of the order of 1 keV and also greater than this value. A scintillator crystal is a crystal which is transparent in the scintillation wavelength range, which responds to incident radiation by emitting a light pulse. Such detectors are used especially in industry for thickness or weight measurements and in the fields of nuclear medicine, physics, chemistry and oil exploration

<http://www.physics.queensu.ca/~phys352/lect19.pdf>



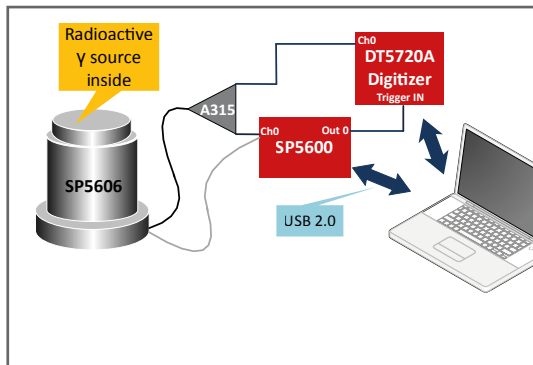
## Equipment

SP5600C - Educational Gamma Kit

Model	SP5600	SP5606	A315	DT5720A	SP5607
Description	Power Supply and Amplification Unit	Mini-Spectrometer	Splitter	Desktop Digitizer 250 MS/s	Absorption tool
					
	p. 93	p. 95	p. 95	p. 93	p. 96

## Requirements

Gamma Radioactive Source 



Experimental setup block diagram.

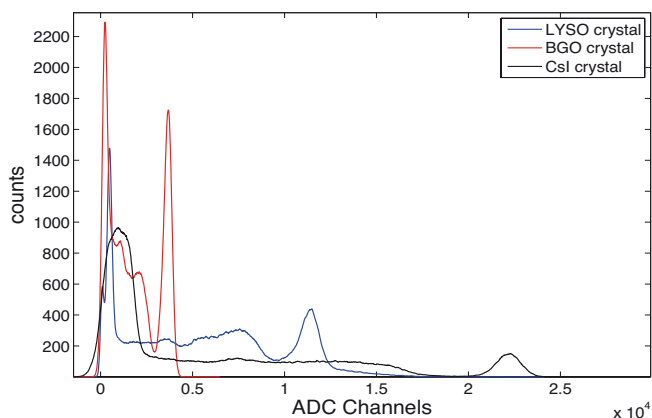
## Carrying out the experiment

The scintillator crystal shall be coupled to the SiPM in the SP5607, through a thin layer of index matching grease to maximize the light collection. In order to avoid saturation, the output of the SiPM is divided using the A315 splitter: one branch is connected to the DT5720A and will be digitized. The other branch will be amplified by the SP5600 module, generating the trigger for the integration signal by the on-board leading edge discriminator. The discriminator threshold shall be defined looking at the spectrum and evaluating the dark count rate. Once this is set and the radioactive source is properly positioned, the spectrum can be recorded. The procedure shall be repeated for every crystal.

## Results

*The crystal characteristics are investigated recording a source spectrum (for example  $^{137}\text{Cs}$ ) with the three different crystals, optimizing the integration time as a function of the scintillation decay time.*

*According to table, the Light Yield of the three crystal is very different. LYSO(Ce) has a light yield three times greater than the BGO, and CsI(Tl) light yield is twice than LYSO(Ce). The analysis of the signal waveform or the trend of the charge vs integration time leads to the measurement of the time characteristics of the scintillator.*



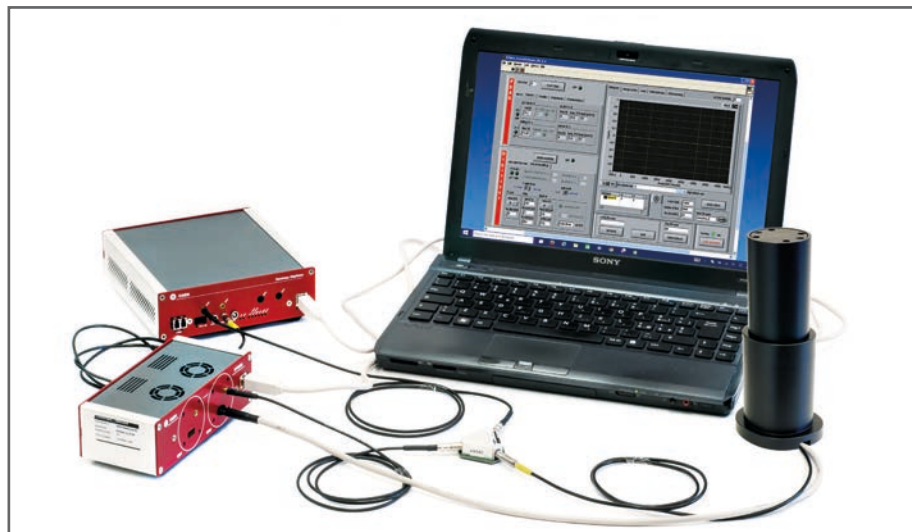
$^{137}\text{Cs}$  energy spectra. Blue spectrum corresponds to the acquisition through LYSO crystal, the red and black ones respectively with BGO and CsI crystals.

	Light Yield Ratio (from datasheet)	Peak Position Ratio
LYSO/CsI	0.52	~0.51
LYSO/BGO	3.29	~3.11
BGO/CsI	0.16	~0.16

Experimental results of Light Yield Ratio

# B.1.6 $\gamma$ -Radiation Absorption

SG6116



## Ordering Options

Equipment	
Code	Description
WK5600XCAAAA	SP5600C - Educational Gamma Kit

or the all inclusive Premium Version

WK5600XANAAA	SP5600AN - Educational Kit - Premium Version
--------------	----------------------------------------------

## Purpose of the experiment

The main goal of the experiment is the measurement of the  $\gamma$  radiation attenuation coefficient for different materials and different energies.

## Fundamentals

The attenuation of a  $\gamma$  radiation flux passing through matter is described by the exponential law

$$I(x) = I_0 * e^{-\mu x}$$

where  $I_0$  is the incident photon flux and  $I(x)$  measures the flux of  $\gamma$  rays emerging from a layer  $x$  of material without having interacted. The coefficient  $\mu$  depends on the material properties (atomic number, density) and on the energy of the impinging photon.

The student is guided towards the development of complementary measurement techniques based on counting and on the analysis of the spectrum, performing the experiment for different materials (including PMMA, a water equivalent solid state organic material used in medical dosimetry).

## Equipment

SP5600C - Educational Gamma Kit

Model	SP5600	SP5606	A315	DT5720A	SP5607
Description	Power Supply and Amplification Unit	Mini-Spectrometer	Splitter	Desktop Digitizer 250 MS/s	Absorption tool
					
	p. 93	p. 95	p. 95	p. 93	p. 96

## Requirements

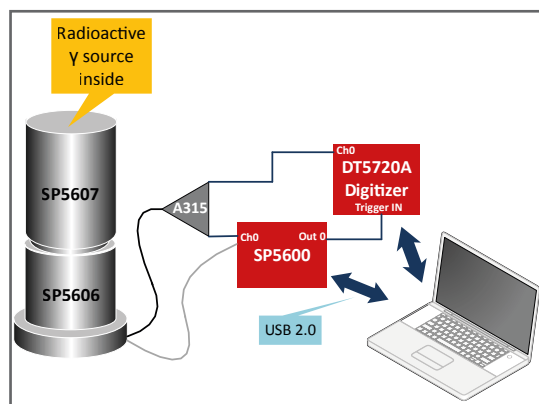
Gamma Radioactive Source 

## The Higgs Boson

On 4 July 2012, the ATLAS and CMS experiments at CERN's Large Hadron Collider announced they had each observed a new particle in the mass region around 126 GeV. This particle is consistent with the Higgs boson predicted by the Standard Model. The Higgs boson, as proposed within the Standard Model, is the simplest manifestation of the Brout-Englert-Higgs mechanism. Other types of Higgs bosons are predicted by other theories that go beyond the Standard Model. On 8 October 2013 the Nobel prize in physics was awarded jointly to François Englert and Peter Higgs "for the theoretical discovery of a mechanism that contributes to our understanding of the origin of mass of subatomic particles, and which recently was confirmed through the discovery of the predicted fundamental particle, by the ATLAS and CMS experiments at CERN's Large Hadron Collider."

<http://home.cern/topics/higgs-boson>





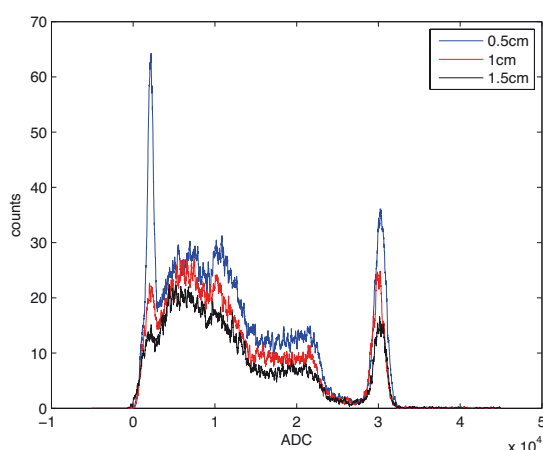
Experimental setup block diagram.

## Carrying out the experiment

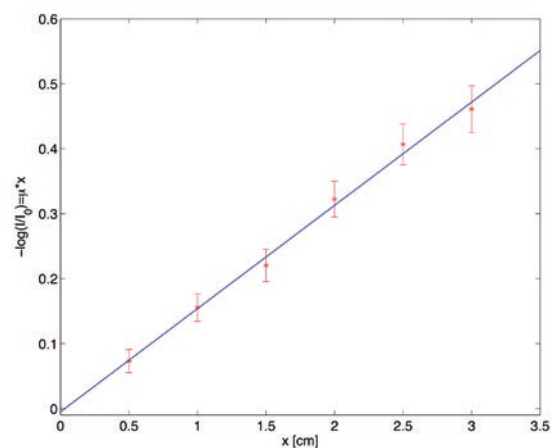
The scintillator crystal shall be coupled to the SiPM in the SP5607, through a thin layer of index matching grease to maximize the light collection. In order to avoid saturation, the output of the SiPM is divided using the A315 splitter: one branch is connected to the DT5720A and will be digitized. The other branch will be amplified by the SP5600 module, generating the trigger for the integration signal by the on-board leading edge discriminator. The discriminator threshold shall be defined looking at the spectrum and evaluating the dark count rate. Once this is set the SP5609 absorption tool shall be mounted. The experiment can be performed for every absorber thickness in counting mode and analysing the spectrum, measuring the events in the photo-peak for a constant predefined time interval.

## Results

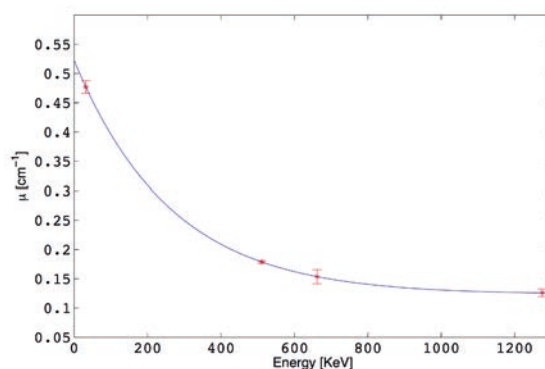
*Exemplary results are shown below, reporting the variation of the events in the photopeak for different absorber thickness, a plot verifying the exponential absorption law and the dependence of the absorption coefficient on the energy.*



Gamma spectra acquired with different absorber thicknesses.



Linear dependence of logarithmic intensity of gamma rays as a function of penetration thickness.

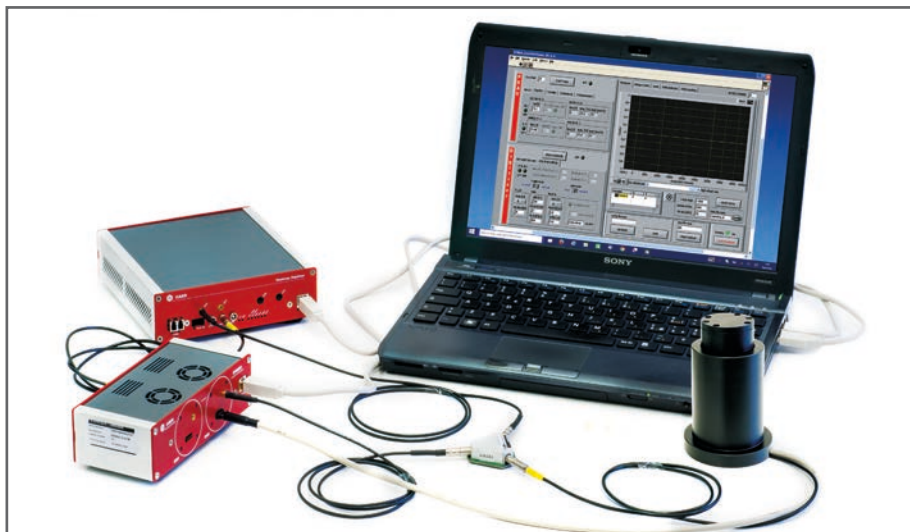


Gamma attenuation coefficient as a function of energy.



# B.1.7 Photonuclear cross-section / Compton Scattering cross-section

## SG6117



### Ordering Options

#### Equipment A

Code	Description
WK5600XCAAAA	SP5600C - Educational Gamma Kit

or the all inclusive Premium Version

WK5600XANAAA	SP5600AN - Educational Kit - Premium Version
--------------	----------------------------------------------

#### Equipment B

Code	Description
WK5600XEMUAA	SP5600EMU - Emulation Kit

### Purpose of the experiment

*Determination of the ratio of the effective cross-sections due to Compton and Photoelectric effects as a function of photons energy.*

### Fundamentals

In the energy range up to 2MeV, gamma rays interact with matter by two processes:

- Photoelectric Effect, dominant at energy less than 100 KeV. In this process the photon energy is completely transferred to atomic electron bounded  

$$\gamma + \text{atom} \rightarrow \text{ion} + e^-$$
- Compton Scattering, linked to the elastic collision between electrons and photons and relevant at 1MeV energy level  

$$\gamma + e^- \rightarrow \gamma' + e^{-'}$$

The predominant mode of interaction depends on the energy of the incident photons and the atomic number of the material with which they are interacting. From the acquired  $\gamma$ -spectrum, it is possible to estimate the fraction of events due to Compton scattering and those caused by the photoelectric. The ratio of the event fractions is used to determine the ratio of the two effective cross-sections that depends on the detector size.

The experiment can be performed by using to different set-ups:



Scintillating crystals can be organic or inorganic. Their different features make them adapted to particular applications. Organic single crystal scintillators (Anthracene, Stilbene) are aromatic hydrocarbon compounds which contain benzene ring structures composed of carbon and hydrogen atoms. These crystals are characterized by low light yield and high time response, features that make them adapted to be used as fast-neutron scintillators and for beta spectroscopy applications. Inorganic materials are composed of the alkali, alkaline earth and rare earth halide crystals generally have an activator dopant uniformly dispersed throughout the crystal lattice. They are characterized by good linearity and long response time and are useful for gamma spectroscopy applications. The most common scintillator crystal in use today are NaI(Tl), CsI(Tl), CsI(Na), LYSO, BGO and BaF<sub>2</sub>.  
<http://www.physics.queensu.ca/~phys352/lect19.pdf>



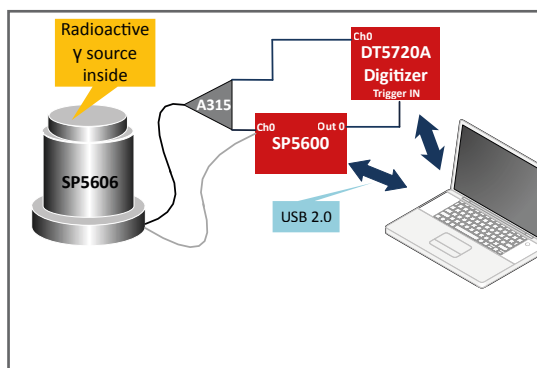
### EQUIPMENT A

SP5600C - Educational Gamma Kit

Model	SP5600	SP5606	A315	DT5720A	SP5607
Description	Power Supply and Amplification Unit	Mini-Spectrometer	Splitter	Desktop Digitizer 250 MS/s	Absorption tool
	p. 93	p. 95	p. 95	p. 93	p. 96

### Requirements

Gamma Radioactive Source

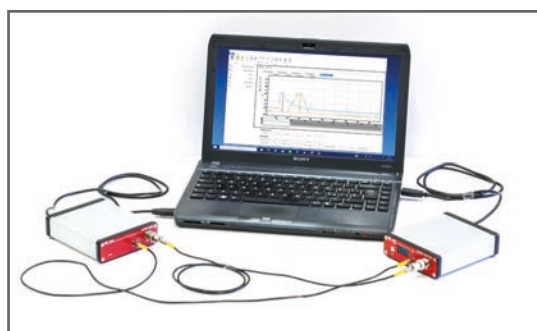


Block diagram of the experimental setup that makes use of the "Educational Gamma Kit".

## Carrying out the experiment

Spread the optical grease on the open face of the scintillating crystal, insert this crystal side in the SP5607 spectrometer. Connect the power cable to the SP5600 module and connect the other cable of the spectrometer to the splitter A315. Connect the two split outputs to SP5600 channel 0 and DT5720A channel 0. Use the SP5600 digital output as DT5720A "trigger IN". Use the default software values or optimize the parameters to choose the discriminator cut-off threshold in mV. Switch off the power supply, open the spectrometer and insert the radioactive gamma source to acquire the first spectrum. After that, switch off the power supply, open the spectrometer, change the radioactive gamma source and repeat the measurement.

## EQUIPMENT B

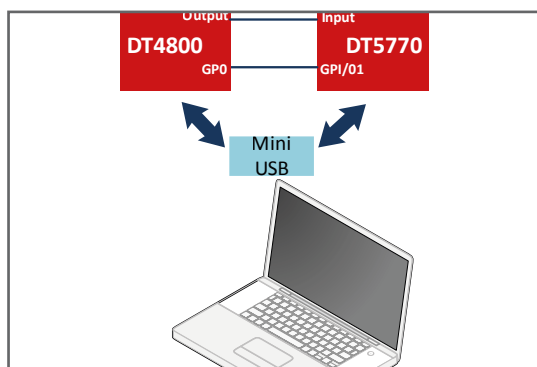


### SP5600EMU - Emulation Kit

Model	DT4800	DT5770
Description	Digital Detector Emulator	Desktop Multi-Channel Analyzer
		
	p. 97	p. 97

## Requirements

Gamma Radioactive Source is not needed.



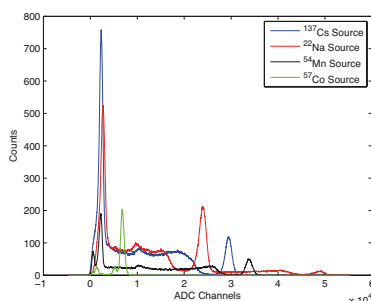
Block diagram of the experimental setup that makes use of the "Emulation Kit".

## Carrying out the experiment

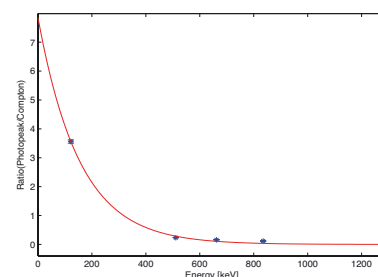
To perform the experiment connect the DT4800 output to the input channel of the MCA DT5770 and use the DT4800 GP0 as digitizer "trigger IN". The DT4800 Control Software Interface allows to emulate signals from real energy spectra of several gamma radioactive source.

## Results

*By using several radioactive sources or spectra simulated by DT4800, the energy dependence of the ratio between the cross-sections of two phenomena can be examined, by verifying that the Photoelectric Effect cross section decreases with increasing energy compared to the Compton Scattering cross section for the used detector size.*

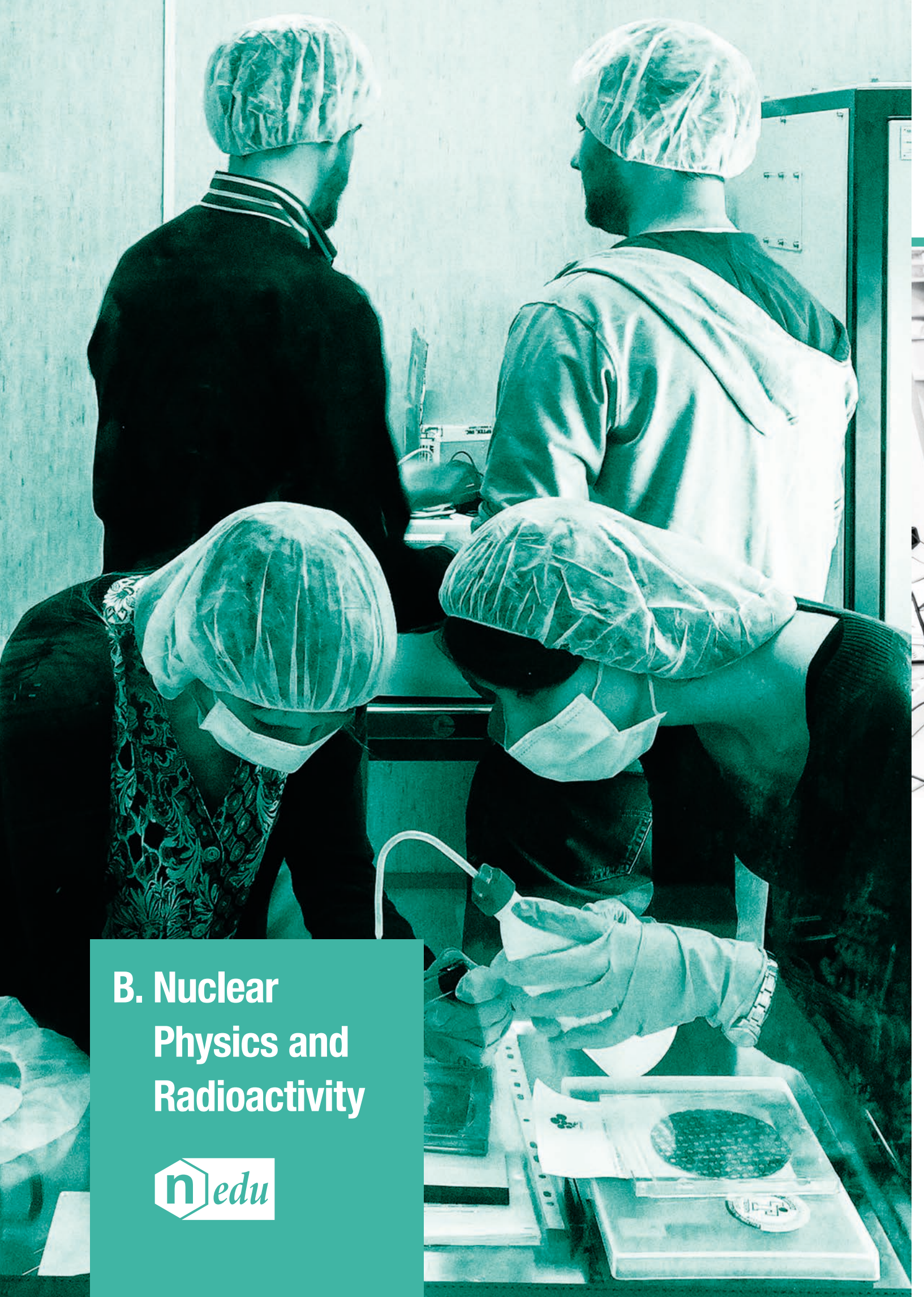


Spectra of radioactive sources used to estimate the ratio of Photonuclear and scattering Compton cross sections.



Behaviour of the ratio between Photo-Peak and Compton contributions as a function of energy.



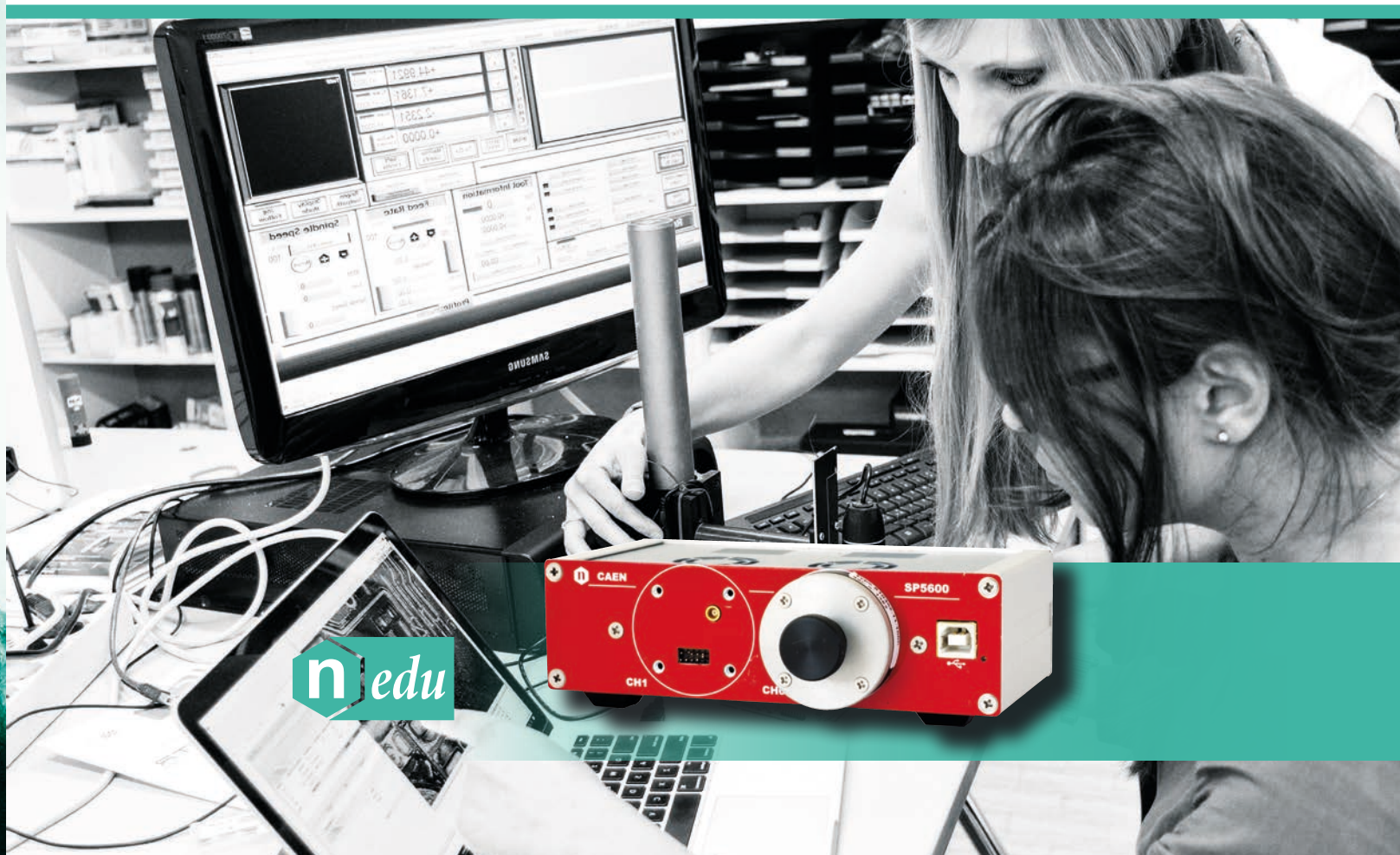


## B. Nuclear Physics and Radioactivity





## B.2 $\beta$ Spectroscopy



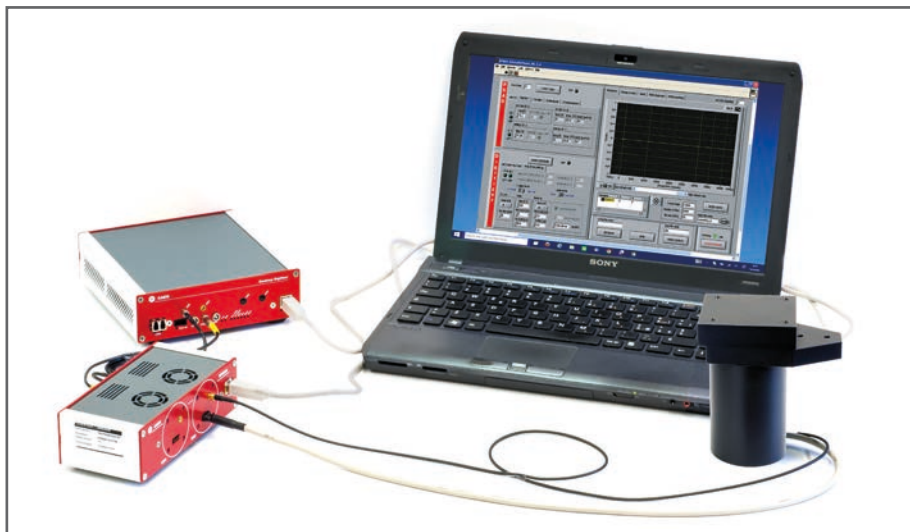
After radioactivity discovery, E. Rutherford separated radioactive emissions into two types: alpha ( $\alpha$ ) and beta ( $\beta^-$ ) radiations, based on matter penetration and ability to cause ionization. The  $\beta^-$  particles have higher penetration and lower specific ionization than alpha particles. Beta particles are electrons ( $\beta^-$ ) or positrons ( $\beta^+$ ), resulting by nucleon decays in unstable nuclei. Since beta decay is a three body process, the  $\beta$  energy spectrum is continuum.

The  $\beta$  spectroscopy experiments are performed using the “Educational Beta KIT”, comprising by the modules listed in the following table.

EDUCATIONAL BETA KIT	Model.	Description
	SP5600	Power Supply and Amplification Unit
	DT5720A	Desktop Digitizer 250 MS/s
	SP5608	Scintillating tile coupled to SiPM

## B.2.1 Response of a Plastic Scintillating Tile

SG6121



### Ordering Options

Equipment	
Code	Description
WK5600XDAAA	SP5600D - Educational Beta Kit
or the all inclusive Premium Version	
WK5600XANAA	SP5600AN - Educational Kit - Premium Version

### Purpose of the experiment

*To get acquainted with a set-up based on a plastic scintillator tile coupled to a Silicon Photo-multiplier.*

### Fundamentals

Particle detectors based on scintillating material coupled to a photosensor are in common use in nuclear and particle physics, medical, industrial and environmental applications. The choice of the scintillator is dependent on the end-user specifications but for a large set of applications plastic scintillators represent a cost effective viable solution. The CAEN kit comprises a plastic scintillator tile of  $5 \times 5 \times 1 \text{ cm}^3$  volume, directly coupled to a  $6 \times 6 \text{ mm}^2$  SiPM. The sensitive area is a trade off between the requests for some of applications (e.g. cosmic ray detection or inspection of thin layers or filters) and the homogeneity of the response of the system.

Before addressing a variety of lab applications, the student is guided through the basics of the system.



One hundred years ago, amidst glowing glass tubes and the hum of electricity, the British physicist J.J. Thomson was venturing into the interior of the atom. At the Cavendish Laboratory at Cambridge University, Thomson was experimenting with currents of electricity inside empty glass tubes. He was investigating a long-standing puzzle known as "cathode rays." His experiments prompted him to make a bold proposal: these mysterious rays are streams of particles much smaller than atoms, they are in fact minuscule pieces of atoms. He called these particles "corpuscles," and suggested that they might make up all of the matter in atoms. It was startling to imagine a particle residing inside the atom--most people thought that the atom was indivisible, the most fundamental unit of matter.

<https://www.aip.org/history/exhibits/electron/>



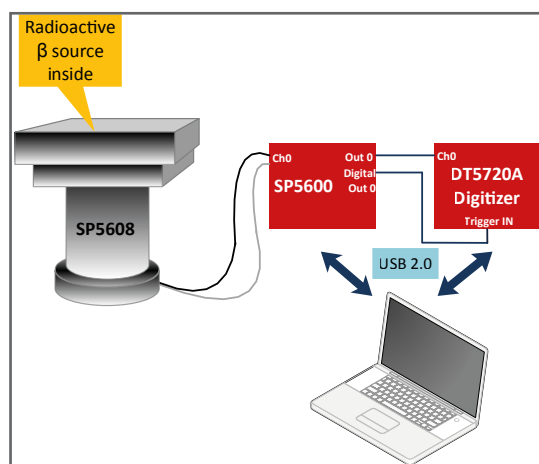
### Equipment

SP5600D - Educational Beta Kit

Model	SP5600	SP5608	DT5720A
Description	Power Supply and Amplification Unit	Scintillating tile	Desktop Digitizer 250 MS/s
			
	p. 93	p. 96	p. 93

### Requirements

Beta Radioactive Source 



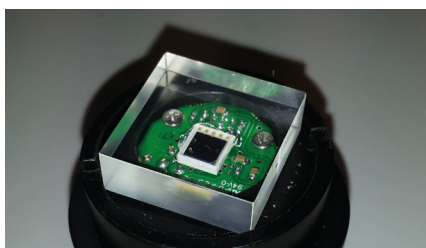
Experimental setup block diagram.

### Carrying out the experiment

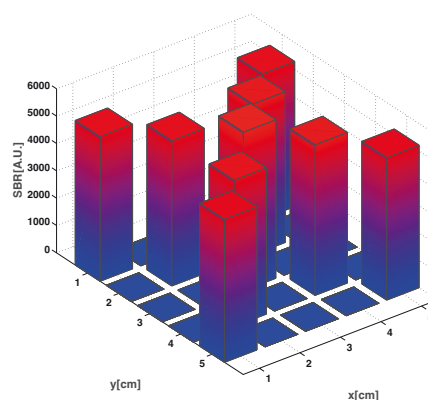
Connect the power and the MCX cables of the SP5608 tile to one channel of the SP5600. Connect the two channel outputs to DT5720A: the analog output to the channel 0 and the digital output to “trigger IN” of the digitizer. Use the GUI to optimize the system parameters (bias, gain, discriminator threshold). Once this is done, switch off the power supply, open the SP5608 top cover and position the beta source on the scintillating tile in the center. Close the support top, switch ON the power supply and measure the counting rate. Repeat the measurement moving the source in several positions over the tile and acquiring the signal/background ratio.

### Results

*In response to the incoming beta particles, the system is designed to deliver a high signal. However, the student shall consider the optimal setting of the discriminator threshold, taking into account the dark count rate, the variation in the beta source counts, the signal to noise ratio and the quality of the recorded beta spectrum. Moreover, for the optimal setting it is significant to monitor the homogeneity of the response as the source is moved across the tile.*



Scintillating tile coupled to a sensor.

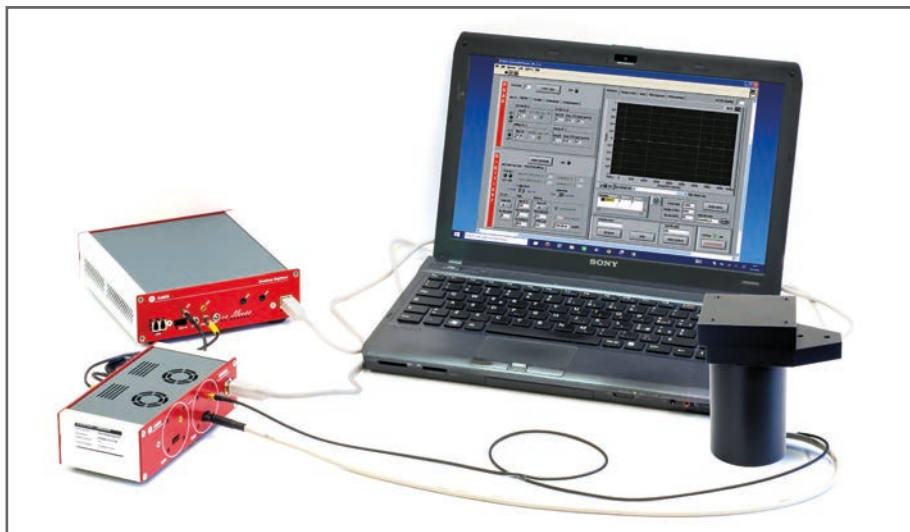


Homogeneity of tile response to a beta source.



## B.2.2 $\beta$ Spectroscopy

SG6122



### Ordering Options

Equipment	
Code	Description
WK5600XDAAAA	SP5600D - Educational Beta Kit

or the all inclusive Premium Version

WK5600XANAAA	SP5600AN - Educational Kit - Premium Version
--------------	----------------------------------------------

### Purpose of the experiment

After gamma spectrometry, the student is introduced to the measurement and interpretation of  $\beta$  spectra, using a plastic scintillator tile.

### Fundamentals

There are three different beta decays:

$\beta^-$  decay (electron emission):  $n \rightarrow p + e^- + \bar{\nu}_e$

$\beta^+$  decay (positron emission):  $p \rightarrow n + e^+ + \nu_e$

Electron capture (EC):  $p + e^- \rightarrow n + \nu_e$

Where p identifies the proton, n the neutron and  $\nu$  the weakly interacting neutrino. Because of the three body kinematics and the energy associated to the neutrino, the  $\beta$  spectrum is continuum up to a maximum energy depending on the isotope under study (and the neutrino mass).

### Equipment

SP5600D - Educational Beta Kit

Model	SP5600	SP5608	DT5720A
Description	Power Supply and Amplification Unit	Scintillating tile	Desktop Digitizer 250 MS/s
			
	p. 93	p. 96	p. 93

### Requirements

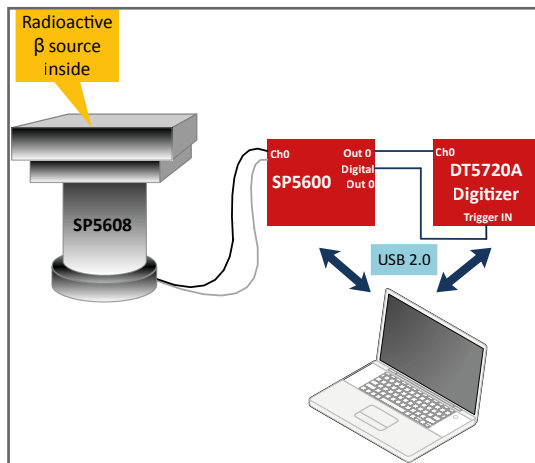
Beta Radioactive Source 



In the first decade of the 20th century, physicists believed that the  $\beta$  particles emitted in radioactive decay were monoenergetic and that such monoenergetic electrons would be absorbed exponentially in passing through matter. Conversely, they also believed that if electrons followed an exponential absorption law then they were monoenergetic. William Wilson showed conclusively that this view was wrong. After Wilson's work, physicists changed the experimental technique they used to investigate the phenomena. Instead of using absorption to measure the decay energy, they now used magnetic spectroscopy with various detectors as their standard method. Although Wilson's work changed the entire practice of the field and showed that the accepted view on electron absorption was wrong, references to it soon disappeared. Perhaps more surprisingly, after 1912 Wilson himself no longer published work on  $\beta$  particles and disappeared from the physics literature completely. The reasons for this also will be discussed.

<http://phys.colorado.edu/sites/default/files/williamwilsonandbetarays.pdf>





Experimental setup block diagram.

### Carrying out the experiment

Connect the power and the MCX cables of the SP5608 tile to one channel of the SP5600. Connect the two channel outputs to DT5720A: the analog output to the channel 0 and the digital output to "trigger IN" of the digitizer. Use the default software values or optimize the parameters to evaluate the contribution not coming from the beta source and choose the discrimination threshold in mV. After that, switch off the power supply, open the SP5608 top and place the beta source on the scintillating tile. close the support top, switch ON the power supply and acquire the beta spectrum.

### Results

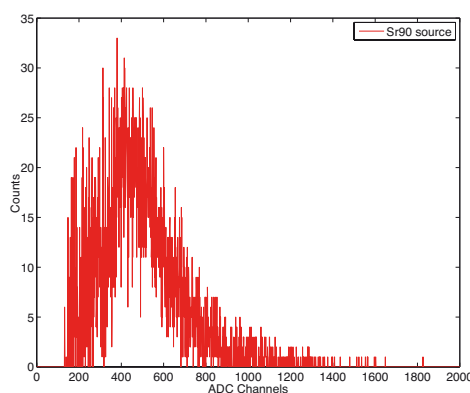
*Measurement and interpretation of  $\beta$  spectra introduce the student into the field of special relativity and weak interactions of radioactive decays. Observation of the beta spectrum is very important to understand the theory of beta decay. Historically, experimental beta-ray spectra introduced enormous problems in the interpretation of beta decay due to the ostensible violation of the energy conservation. The introduction of neutrinos explaining the continuous beta-ray spectra solved not the problem conservation of energy, momentum and lepton number.*

*As first approach to beta spectroscopy, it is interesting to determine the maximum energy available in the decay process and to verify that the most probable energy value  $E_{avg}$  can be expressed as:*

$$E_{avg} \cong 1/3 * E_{max}$$

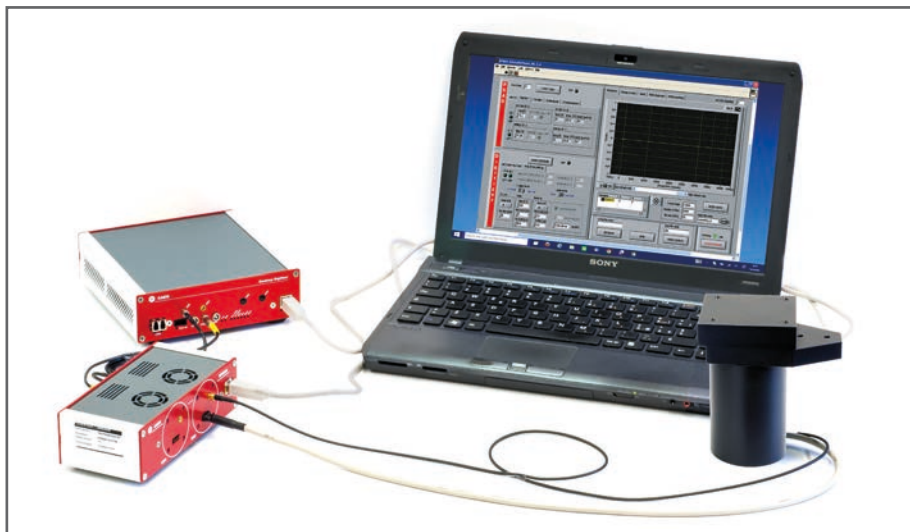
*By using several  $\beta$ -sources, different energy values  $E_{avg}$  can be estimated, each one corresponds to the total energy released in the specified  $\beta$  decay.*

*An example of  $^{90}\text{Sr}$  spectrum is shown in the figure. For a most complete analysis on beta spectrum, other application notes are recommended.*

Experimental beta spectrum of  $^{90}\text{Sr}$  radioactive source.

## B.2.3 $\beta$ Radiation: Transmission through Matter

SG6123



### Ordering Options

Equipment	
Code	Description
WK5600XDAAA	SP5600D - Educational Beta Kit

or the all inclusive Premium Version

WK5600XANAA	SP5600AN - Educational Kit - Premium Version
-------------	----------------------------------------------

### Purpose of the experiment

*Attenuation measurement of the intensity of  $\beta$  radioactive source as a function of the absorber thickness by using two absorber materials: aluminium and paper sheets.*

### Fundamentals

$\beta$ -particle is a charged particle that interacts with matter in several ways depending on its initial energy: ionization process, Bremsstrahlung process, Cherenkov and Transition radiation. When  $\beta$ -radiation crosses a matter thickness, it releases completely or part of its energy due to collisions with absorber atoms; this phenomenon depends on the initial  $\beta$ -energy and on the crossed material density. Beta particles are less massive than alpha particles and only carry a charge of  $1e$ ; consequently, beta particles can appreciably penetrate many potential shielding materials although their penetrating capacity is considerably lower compared with  $\gamma$ -rays. These different radiation behaviours are essential for those attempting to shield locations from gamma radiation, either for sensitive experiments or for the safety of humans.

The transmission of beta particles is frequently calculated in the same fashion as that of gamma rays, where the mass attenuation coefficient is defined by the slope of the exponential function. Due to the fact that the  $\beta$ -particles with lower energies are less penetrating hence they are completely absorbed at smaller values of thickness, the initial decrease of the absorption curve is too rapid to be fit by exponential function. This approximation is verified only in a particular region of the transmission curve: a minimal absorber thickness so that the beta counting are very well separated from the "background level".



### $\beta$ -Tracers

Radioisotopes are commonly used as tracers in chemical and biological research. By synthesizing molecules containing a radioactive atom, the path and fate of that type of molecule in a particular reaction or metabolic process can be followed by tracking the radioactive signal of the isotope. One radioisotope used for this process is carbon-14 which can be inserted into organic or biological molecules and followed by its beta radiation signal.

[http://www.ehow.com/info\\_8278087\\_uses-beta-rays.html](http://www.ehow.com/info_8278087_uses-beta-rays.html)



### Equipment

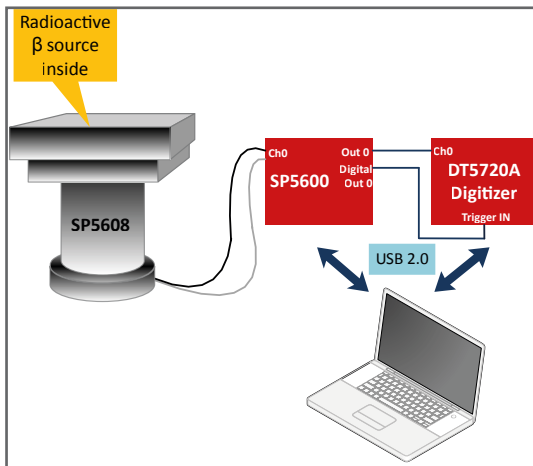
SP5600D - Educational Beta Kit

Model	SP5600	SP5608	DT5720A
Description	Power Supply and Amplification Unit	Scintillating tile	Desktop Digitizer 250 MS/s
			
	p. 93	p. 96	p. 93



## Requirements

Beta Radioactive Source 



Experimental setup block diagram.

## Carrying out the experiment

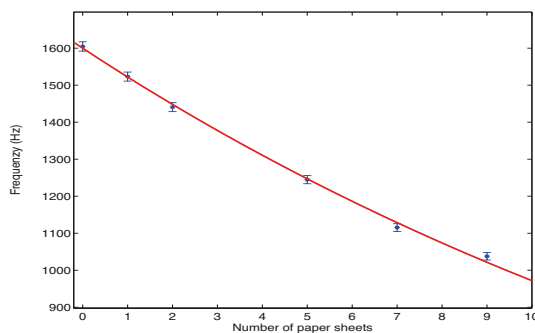
Insert the beta source support in the SP5608 and connect power and MCX cables to one channel of the SP5600. Connect the two channel outputs to DT5720A: the analog output to the channel 0 and the digital output to "trigger IN" of the digitizer. Use the default software values or optimize the parameters to evaluate the contribution not coming from the beta source and choose the discrimination threshold in mV. After that, switch off the power supply, open the SP5608 top and place the beta source on the plastic support and close the support top. Switch ON the power supply and measure the counting rate. Repeat the measurement by adding layers of the same absorber and later change the absorber type.

## Results

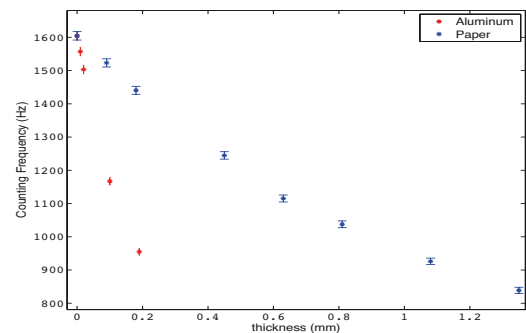
By using different absorber thicknesses, the near-exponential decreasing of  $\beta$ -radiation intensity  $I$  as a function of the absorber thickness  $x$ , is verified. This behaviour does not have a fundamental basis like gamma rays attenuation, but it is very well described by

$$I = I_0 * e^{-nx}$$

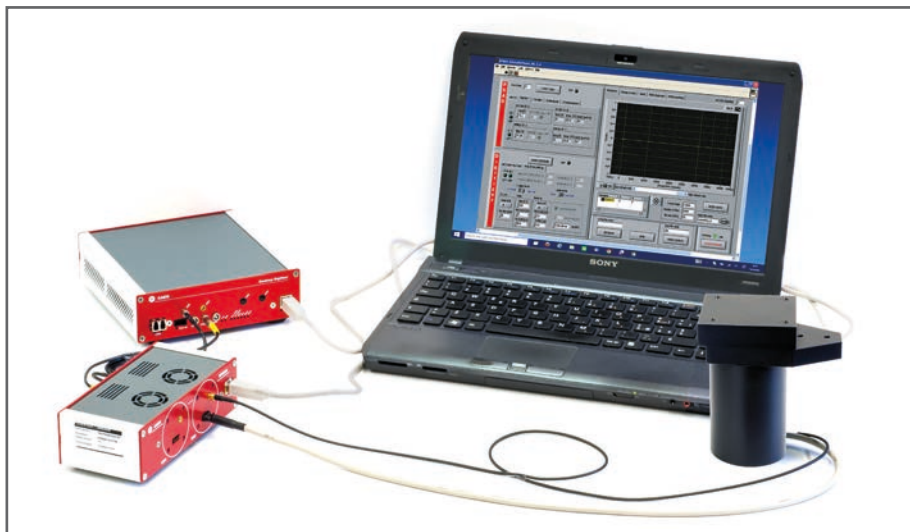
where  $n$  is the absorption coefficient. This coefficient correlates the endpoint energy of beta source for a particular absorbing material. From absorption curves of beta particles, the absorption coefficients and ranges of  $\beta$  particles in aluminium and in paper sheets can be determined.



Exponential behaviour of the transmitted counting rate of Sr90 source with respect to number of paper sheets.



Behaviour of the transmitted counting rate of Sr90 source as a function of different absorbing materials.

**B.2.4****SG6124** **$\beta$  Radiation as a Method to Measure Paper Sheet Grammage and Thin Layer Thickness****Ordering Options**

Equipment	
Code	Description
WK5600XDAAAA	SP5600D - Educational Beta Kit

or the all inclusive Premium Version

WK5600XANAAA	SP5600AN - Educational Kit - Premium Version
--------------	----------------------------------------------

**Purpose of the experiment**

*Estimate of the instrument sensitivity in the measurement of thin layer thickness by beta particle attenuation.*

**Fundamentals**

Beta attenuation represents a golden standard in the quality control of paper industry and in the measurement of thin layer thickness. The latter has several applications, including the concentration of fine particulate matter deposited on a filter. The use of high activity sources with relatively soft spectrum and highly efficient detectors guarantees that this technique, used since the 50's, is yet today a standard.

**Equipment**

SP5600D - Educational Beta Kit

Model	SP5600	SP5608	DT5720A
Description	Power Supply and Amplification Unit	Scintillating tile	Desktop Digitizer 250 MS/s
			
	p. 93	p. 96	p. 93

**Requirements**Beta Radioactive Source **Gravitational Wave Detected 100 Years After Einstein's Prediction.**

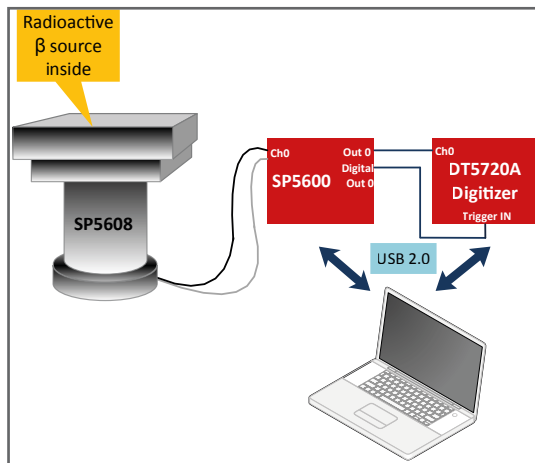
For the first time, scientists have observed ripples in the fabric of spacetime called gravitational waves, arriving at the earth from a cataclysmic event in the distant universe. This confirms a major prediction of Albert Einstein's 1915 general theory of relativity and opens an unprecedented new window onto the cosmos.

Gravitational waves carry information about their dramatic origins and about the nature of gravity that cannot otherwise be obtained. Physicists have concluded that the detected gravitational waves were produced during the final fraction of a second of the merger of two black holes to produce a single, more massive spinning black hole. This collision of two black holes had been predicted but never observed.

The gravitational waves were detected on September 14, 2015 at 5:51 a.m. Eastern Daylight Time (09:51 UTC) by both of the twin Laser Interferometer Gravitational-wave Observatory (LIGO) detectors, located in Livingston, Louisiana, and Hanford, Washington, USA. The LIGO Observatories are funded by the National Science Foundation (NSF), and were conceived, built, and are operated by Caltech and MIT. The discovery, accepted for publication in the journal Physical Review Letters, was made by the LIGO Scientific Collaboration (which includes the GEO Collaboration and the Australian Consortium for Interferometric Gravitational Astronomy) and the Virgo Collaboration using data from the two LIGO detectors.

<https://www.ligo.caltech.edu/news/ligo20160211>





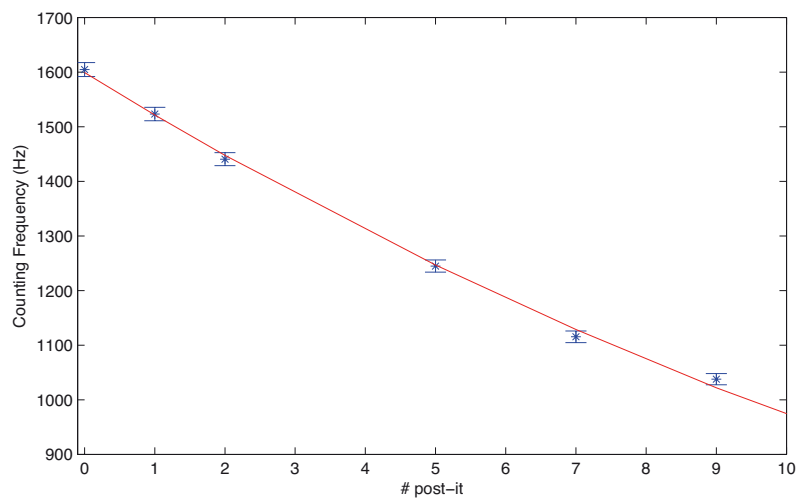
Experimental setup block diagram.

### Carrying out the experiment

Insert the beta source support in the SP5608 and connect power and MCX cables to one channel of the SP5600. Connect the two channel outputs to DT5720A: the analog output to the channel 0 and the digital output to “trigger IN” of the digitizer. Use the default software values or optimize the parameters to evaluate the contribution not coming from the beta source and choose the discrimination threshold in mV. After that, switch off the power supply, open the SP5608 top and place the beta source on the plastic support and close the support top. Switch ON the power supply and measure the counting rate. Repeat the measurement by adding paper sheets.

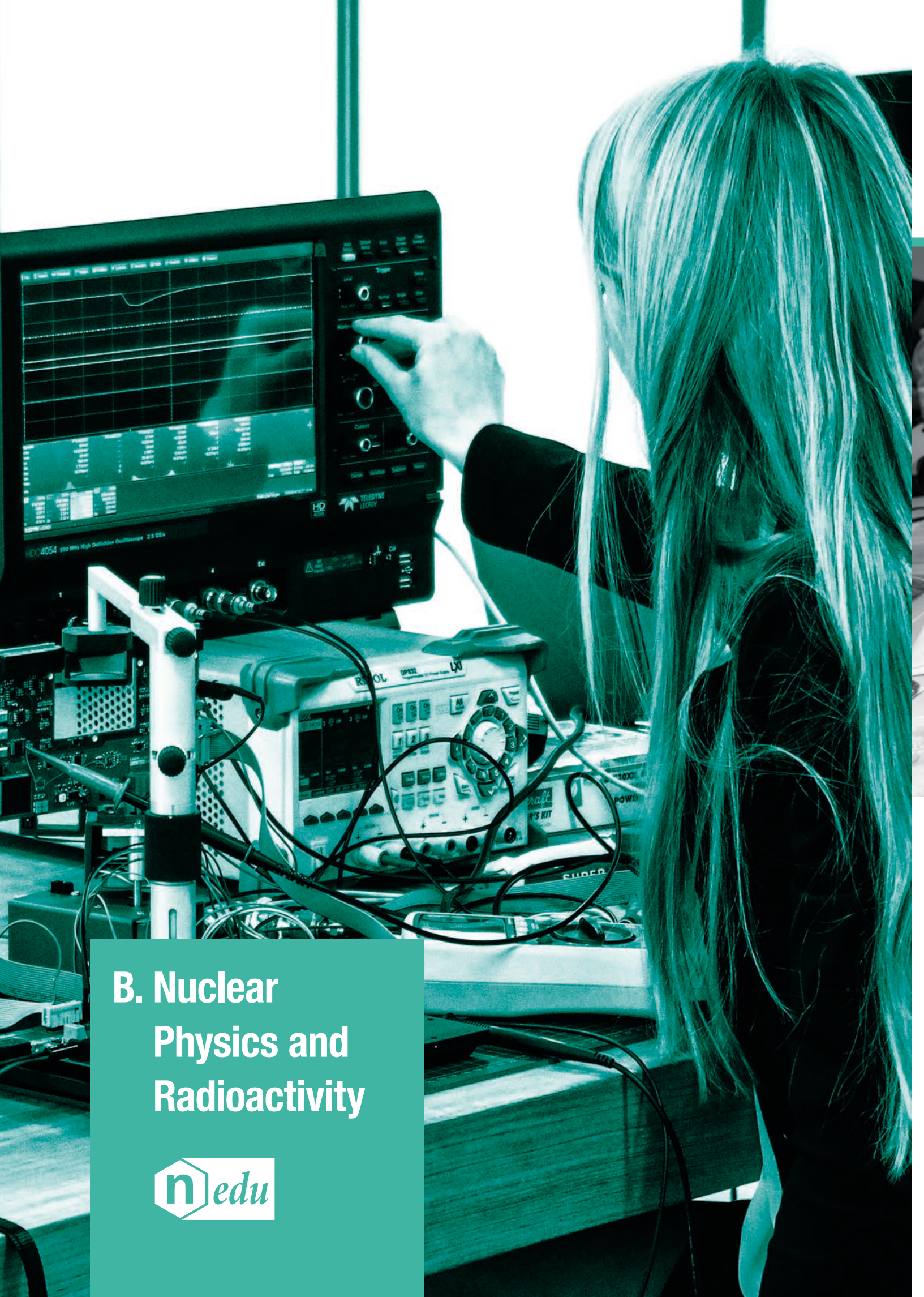
### Results

*The industrial results are provided by using high activity  $\beta$  source (1 GBq). This experiment allows to estimate the instrument sensibility and the time needed to obtain a certain percentage of sensibility through the attenuation curve of a  $\beta$  source with “student compliant” activity. The results are very surprising:  $3\sigma$  of confidence level to distinguish one or two post-it in 250 ms and 25 seconds to reach sensibility 10%.*



Counting frequency of the beta rays as a function of the number of crossed paper sheets.





## B. Nuclear Physics and Radioactivity





## B.3 Nuclear Imaging - PET



universidade  
de aveiro

Nuclear Instruments

Positron Emission Tomography (PET) scanner is the state-of-the-art medical imaging system, capable of providing detailed functional information of physiological processes inside the human body. PET represents a beautiful example of integration of skills and competences from medicine, nuclear chemistry, physics and information technology.

The SP5700-EasyPET, sketched in the table, opens the possibility of teaching by doing the basics behind PET imaging, which is certainly an asset to high-level educational laboratories. Some details about EasyPET components and concept are reported in the Products section.

The experiments proposed in this section are

performed by using the CAEN portable didactic PET system, developed by University of Aveiro (PT). Moreover, to perform some experiments it is also necessary to use the Multi Channel Analyzer DT5770, that together with EasyPET device is included in the SP5701-EasyPET Kit.

EasyPET	Components
	Two detectors: scintillating crystal + SiPM
	Printed Circuit Board (PCB)
	Two stepper motors
	Microcontroller unit

## B.3.1 Basic Measurements: $\gamma$ Spectroscopy and System Linearity

SG6131



### Related Experiment

B.1.3

B.1.4

D.3

### Ordering Options

#### Equipment

Code	Description
WK5701XAAAAA	SP5701 – EasyPET Kit

### Purpose of the experiment


*Gamma spectroscopy studies by using a gamma radioactive sources and by analysing the signals produced by the interaction of the gamma with one of the scintillating crystals of the system.*

### Fundamentals

The EasyPET detector system is composed of two Silicon Photomultipliers (SiPM) coupled to scintillating crystals. The EasyPET operation principle is simple: the two small detector cells, each composed of a small scintillator crystal coupled to a silicon photomultiplier (SiPM), develop a signal when they detect a photon emitted by the source. In order to perform the gamma spectroscopy measurements using one of the two detector systems, it is important underline that the detector is characterized by a noise component, caused by spurious events occurring randomly and independently from the illumination field. This noise, called Dark Count Rate (DCR), depends mainly on the sensor technology and on the operating temperature, with a rate from 100kHz up to several MHz per mm<sup>2</sup> at 25 °C. The DCR decreases with the lowering of the temperature (about a factor 2 of DCR reduction every 8 °C). In addition, the operating voltage has an impact on the DCR since it's connected to the electric field and as a consequence to the active volume of the sensor and to the triggering probability of the charge carrier. This noise component affects the resolution of a generic gamma spectrum composed of system noise peak, Compton distribution and Photo-peak.

### Equipment

SP5701 - EasyPET Kit

Model	SP5700	DT5770
Description	EasyPET	Desktop Multi-Channel Analyzer
		

p. 98

p. 97



#### The First X-ray, 1895.

The discovery of a new and mysterious form of radiation in the late 19th century led to a revolution in medical imaging.

At the end of the 19th century, while studying the effects of passing an electrical current through gases at low pressure, German physicist Wilhelm Röntgen accidentally discovered X-rays—highly energetic electromagnetic radiation capable of penetrating most solid objects. His discovery transformed medicine almost overnight. Within a year, the first radiology department opened in a Glasgow hospital, and the department head produced the first pictures of a kidney stone and a penny lodged in a child's throat. Shortly after, an American physiologist used X-rays to trace food making its way through the digestive system. The public also embraced the new technology—even carnival barkers touted the wondrous rays that allowed viewing of one's own skeleton. At the close of 1895, Röntgen published his observations and mailed his colleagues a photograph of the bones of his wife's hand, showing her wedding ring on her fourth finger.

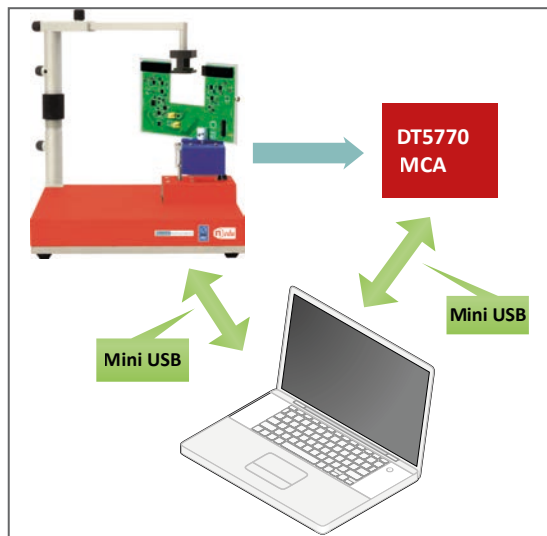
<http://www.the-scientist.com/?articles.view/articleNo/30693/title/The-First-X-ray--1895/>





## Requirements

$^{22}\text{Na}$  Radioactive source (recommended: 1/2 inch disc, 10  $\mu\text{Ci}$ ) 



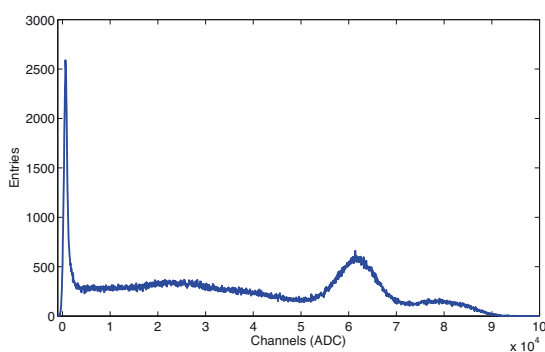
Experimental setup block diagram.

## Carrying out the experiment

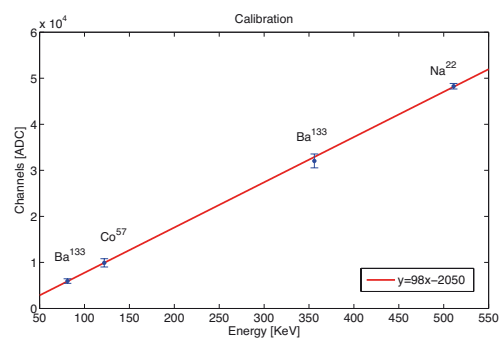
Mount the arm of the source holder on the column fixed to the system base, fix the U-shaped board to the top stepper motor and connect the flat cable to the U-shaped board and to the control unit. Connect to PC and power ON the system. Choose one detection system and connect its analog output to channel input of the DT5770, then use the comparator output to trigger the MCA and choose the threshold in mV of the signal output. Place the radioactive source as close as possible to the detector chosen and acquire the energy spectrum thanks to a Multi Channel Analyzer. Repeat the measurements with several gamma radioactive source in order to study the linearity system.

## Results

*The  $\gamma$  spectrum shows the Compton continuum, related to the continuum of energies released by the Compton scattered electrons, and the Photo-Peak, the full-energy peak corresponding to the photoelectric absorption of the incident gamma. The peak around zero represents the system noise. The conversion between the channels number and the energy can be performed by a calibration. The system linearity is checked by using several radioactive sources. If the response of the system is linear, the output signals are directly proportional to the incident gamma energies.*



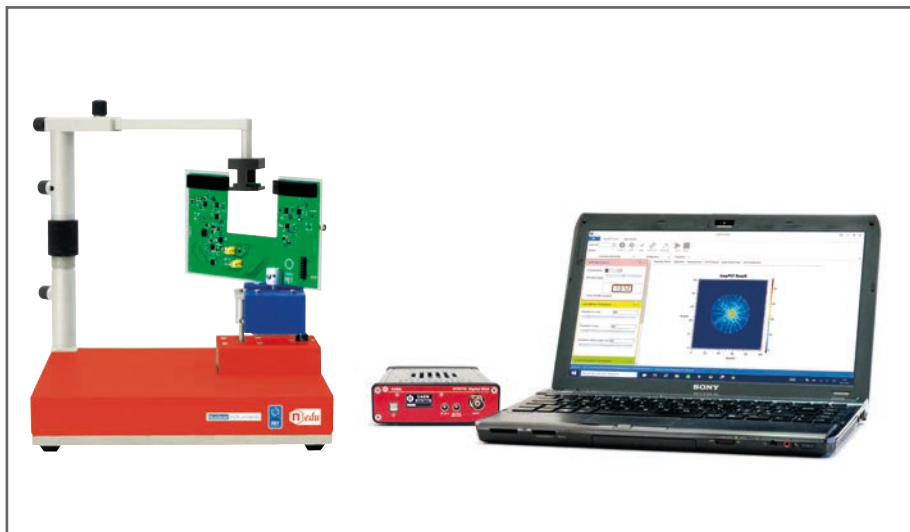
Energy spectrum of  $^{22}\text{Na}$  source.



Energy Calibration.

## B.3.2 Positron Annihilation Detection

SG6132



### Ordering Options

Equipment	
Code	Description
WK5701XAAAAA	SP5701 – EasyPET Kit

### Purpose of the experiment

*Positron annihilation detection by using a couple of detectors composed of a LYSO scintillating crystal coupled to a Silicon Photomultiplier (SiPM).*

### Fundamentals

The underlying principle to PET systems is the detection of high energy radiation emitted from a chemical marker, a molecule labelled with a radioisotope, administered to a patient. The marker is properly chosen in order to associate to molecules involved in biochemical or metabolic processes under investigation. This allows studying the function of a particular organ or evaluating the presence of disease, revealed by the excessive concentration of the marker in specific locations of the body. The radioisotope emits positrons which, after annihilating with atomic electrons, result in the isotropic emission of two photons back to back with an energy of 511 keV. The two photons are detected by a ring of detectors, which allows a pair of them to detect two back to back photons in any direction.

EasyPET comprehends only two detector modules that move together and execute two types of independent movements, around two rotation axes, so as to cover a field of view similar to that of a complete ring of detectors. A fast electronic readout system allows detecting coincident events resulting from the same decay process.





Positron emission tomography (PET) is a test that uses a special type of camera and a tracer (radioactive chemical) to look at organs in the body. The tracer usually is a special form of a substance (such as glucose) that collects in cells that are using a lot of energy, such as cancer cells. During the test, the tracer liquid is put into a vein (intravenous, or IV) in your arm. The tracer moves through your body, where much of it collects in the specific organ or tissue. The tracer gives off tiny positively charged particles (positrons). The camera records the positrons and turns the recording into pictures on a computer. PET scan pictures do not show as much detail as computed tomography (CT) scans or magnetic resonance imaging (MRI) because the pictures show only the location of the tracer. The PET picture may be matched with those from a CT scan to get more detailed information about where the tracer is located. A PET scan is often used to evaluate cancer, check blood flow, or see how organs are working.

<http://www.webmd.com/cancer/lymphoma/positron-emission-tomography>



### Equipment

SP5701 - EasyPET Kit

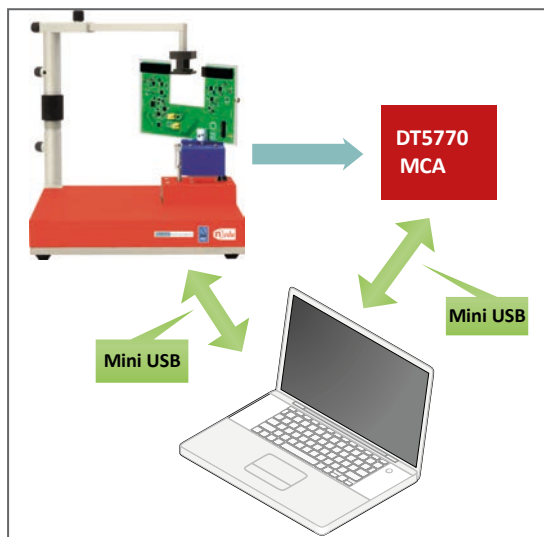
Model	SP5700	DT5770
Description	EasyPET	Desktop Multi-Channel Analyzer
		

p. 98

p. 97

## Requirements

$^{22}\text{Na}$  Radioactive source (recommended: 1/2 inch disc, 10  $\mu\text{Ci}$ ) 



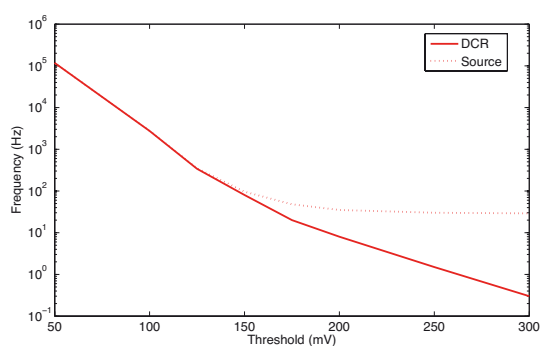
Experimental setup block diagram.

## Carrying out the experiment

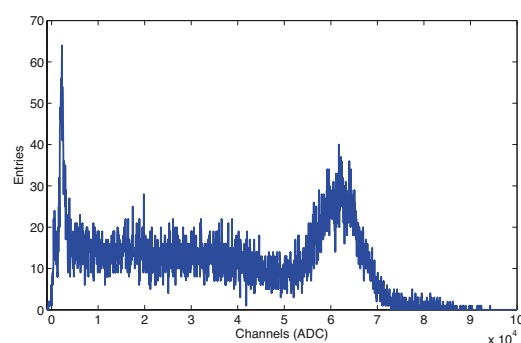
Mount the arm of the source holder on the column fixed on the system base, fix the U-shaped board to the top stepper motor and connect the flat cable to the U-shaped board and to control unit. Connect to PC and power ON the system. Connect the analog output of one detector to channel input of the DT5770 and use as MCA "trigger IN" the coincidence output characterized by the occurring of the comparator output of each detector within a time window. Place the source holder between the two detectors and measure the DCR frequency as a function of the threshold. Place the  $^{22}\text{Na}$  radioactive source in the holder and repeat the measurement. Chose a threshold and acquire the coincidence spectrum thanks to a Multi Channel Analyzer.

## Results

*The coincidence detection allows to reduce significantly the system noise due to the SiPM DCR. In the optimization of the acquisition conditions, the coincidence detection introduces the parameter of the time window width in addition to the bias voltage and the threshold. In order to find the best parameter values is necessary to analyse the response of the system in coincidence mode to the radioactive source with respect to the random events, at fixed operating voltage. The simple geometry of the system with only two opposite and aligned detectors and the implementation of the coincidence detection ensures that, in the energy distribution, the Compton scattering occurring in one or even in both scintillating crystals comes from the same annihilation event.*



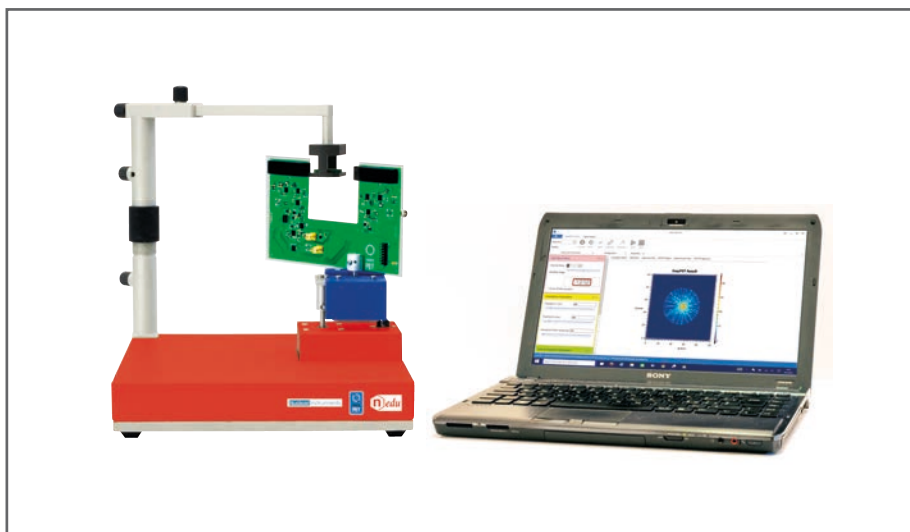
Coincidence frequency, with and without  $^{22}\text{Na}$  source, as a function of the threshold.



Coincidence spectrum of  $^{22}\text{Na}$  radioactive source.

## B.3.3 Two-dimensional Reconstruction of a Radioactive Source

SG6133



### Ordering Options

Equipment	
Code	Description
WSP5700XAAAA	SP5700 – EasyPET
or	
WK5701XAAAA	SP5701 – EasyPET Kit

### Purpose of the experiment

*Understanding the technique of the nuclear imaging and the setup optimization of the parameters by performing two-dimensional image reconstruction of  $^{22}\text{Na}$  radioactive source.*

### Fundamentals

The EasyPET operation principle is simple: two detector modules move together and execute two types of independent movements, around two rotation axes, so as to cover a field of view similar to that of a complete ring of detectors.

The rotation movements are executed by two stepper motors. The bottom motor has a fixed axis, whose position defines the center of the field of view. The bottom motor supports and performs a complete rotation of a second motor, in predefined steps of amplitude  $\alpha$ . The axis of the top motor is thus always positioned within a circumference of radius equal to the distance between the two axes. The top motor, in its turn, supports and moves a U-shaped printed circuit board, where a pair of aligned and collinear detector modules is mounted, performing a symmetric scan of range  $\theta$  around the center, for each position of the bottom motor. In this way, EasyPET can reconstruct an image of a radioactive source placed anywhere within a cylindrical field of view between the pair of detectors. The diameter of the field of view is defined by the amplitude of  $\theta$ , the range of the top motor scan.




Computed tomography (CT) is a diagnostic imaging test used to create detailed images of internal organs, bones, soft tissue and blood vessels. The cross-sectional images generated during a CT scan can be reformatted in multiple planes, and can even generate three-dimensional images which can be viewed on a computer monitor, printed on film or transferred to electronic media. CT scanning is often the best method for detecting many different cancers since the images allow your doctor to confirm the presence of a tumor and determine its size and location. CT is fast, painless, non-invasive and accurate. In emergency cases, it can reveal internal injuries and bleeding quickly enough to help save lives. The first commercially viable CT scanner was invented by Sir Godfrey Hounsfield in United Kingdom at EMI Central Research Laboratories using X-rays.

<http://www.radiologyinfo.org/en/submenu.cfm?pg=ctscan>



### Equipment

SP5700 - EasyPET

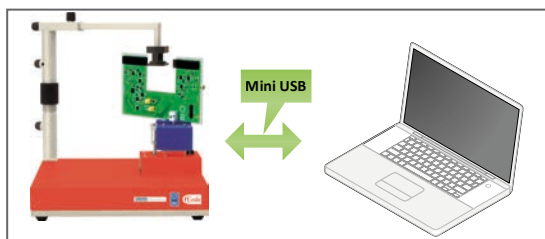
Model	SP5700
Description	EasyPET 

p. 98



## Requirements

$^{22}\text{Na}$  Radioactive source (recommended: 1/2 inch disc, 10  $\mu\text{Ci}$ ) 



Experimental setup block diagram.

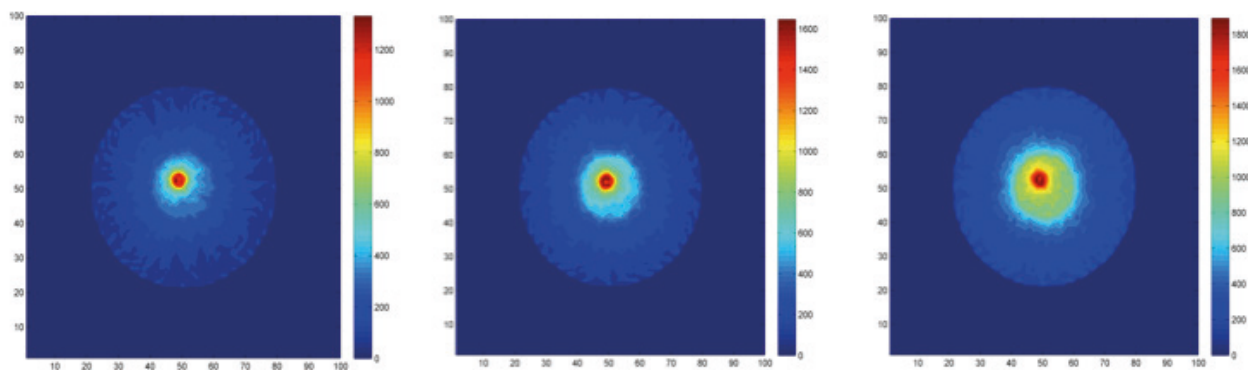
## Carrying out the experiment

Mount the arm of the source holder on the column fixed on the system base, fix the U-shaped board to the top stepper motor and connect the flat cable to the U-shaped board and to control unit. Connect to PC and power ON the system. The parameters involved in the setup optimization for the two-dimensional reconstruction of the source image are three: the detectors operating voltage, the coincidence time window and the threshold. Place the source holder between the two detector modules and tune the parameters to estimate the DCR contribution.

Place the  $^{22}\text{Na}$  radioactive source in the holder and repeat the measurement tuning the parameters in order to obtain a good image reconstruction of the radioactive source.

## Results

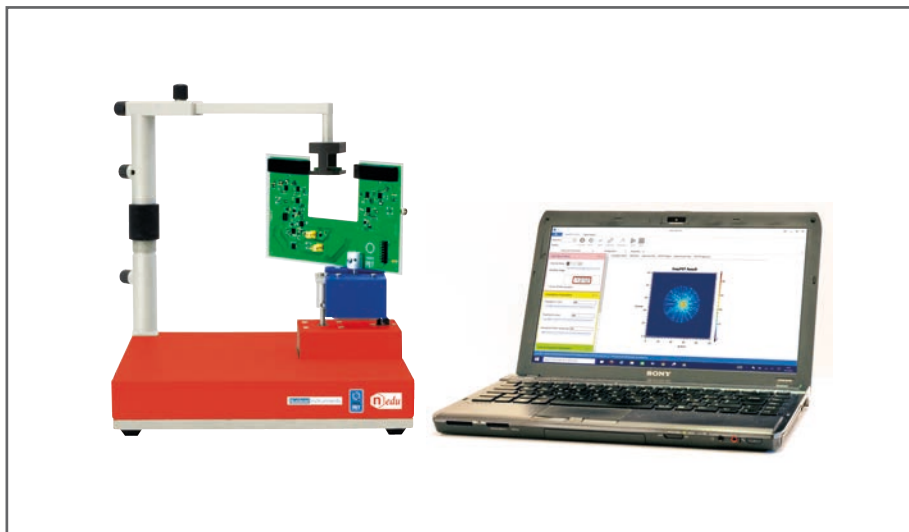
*Tuning the parameters, the students can directly observe and understand their effects on the imaging measurements. At fixed threshold, the image contrast changes due to the time window width. The use of the lowest possible coincidence time window of the system is mandatory to achieve a good image contrast. Fixing the bias voltage and the time window, it is interesting to observe how the threshold affects the image contrast. This parameter choice is dictated by a trade off between the signal to noise ratio and efficiency maximization. The threshold value and the coincidence time window should be set by choosing the best compromise.*



$^{22}\text{Na}$  source distribution image as a function of coincidence time window, at fixed threshold and bias voltage.

## B.3.4 Spatial Resolution

SG6134



### Ordering Options

Equipment	
Code	Description
WSP5700XAAAA	SP5700 – EasyPET
or	
WK5701XAAAAA	SP5701 – EasyPET Kit

### Purpose of the experiment

*Evaluation of the spatial resolution of a PET system composed of two detector modules.*

### Fundamentals


The main goal of the PET studies is to obtain a good quality and detailed image of an object by the PET scanner. The parameters involved and critical to good quality image formation are several: spatial resolution, sensitivity, noise, scattered radiations, and contrast.

The spatial resolution is a fundamental characteristics of a tomographic system and its determination is mandatory for a PET system. The spatial resolution of a PET scanner is a measure of the ability of the device to faithfully reproduce the image of an object. It is empirically defined as the minimum distance between two points in an image that can be detected by a scanner.

In the EasyPET the dominant factor determining the spatial resolution is represented by the width of the scintillating crystals. Another effect that degrades the spatial resolution of the system is the so-called sampling error. It is associated to the distribution of the lines of response in the field of view and is a direct consequence of the rotation and scanning granularity.

### Equipment

SP5700 - EasyPET

Model	SP5700
Description	EasyPET
	

p. 98



### Small-Animal PET

The importance of animal model-based research lead to the production of small dimension PET systems to perform preclinical imaging studies on small animals. These devices give a fundamental contribution to biological and medical research and to the pharmaceutical industry. In fact, small animal PET allows the development of new radiopharmaceuticals and provides the opportunity to investigate disease progression, therapeutic response and eventually consequences of the therapy. Since the physical dimensions of the organs of small animals are of the order of mm, small dimension PET systems require a much better spatial resolution (ideally under 1 mm FWHM) than human PET systems (of the order of 4-6 mm FWHM).

<http://www.acsu.buffalo.edu/~rutaoyao/2012-jnmt-animalPET.pdf>



## Requirements

$^{22}\text{Na}$  Radioactive source (recommended: 1/2 inch disc, 10  $\mu\text{Ci}$ ) 



Experimental setup block diagram.

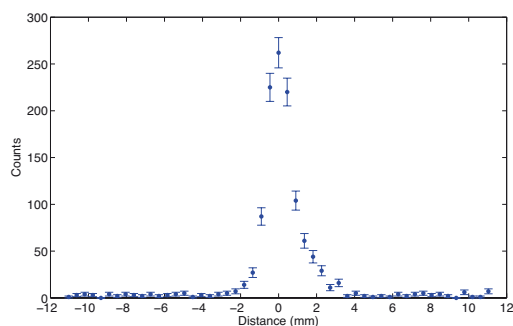
## Carrying out the experiment

Mount the arm of the source holder on the column fixed on the system base, fix the U-shaped board to the top stepper motor and connect the flat cable to the U-shaped board and to control unit. Connect to PC and power ON the system. Set and optimize the parameters as bias voltage, threshold and coincidence time windows. In order to perform the spatial resolution measurement, the radioactive source is placed between the two detectors, on the line of response passing through the center. Its position is kept fixed while the system acquires

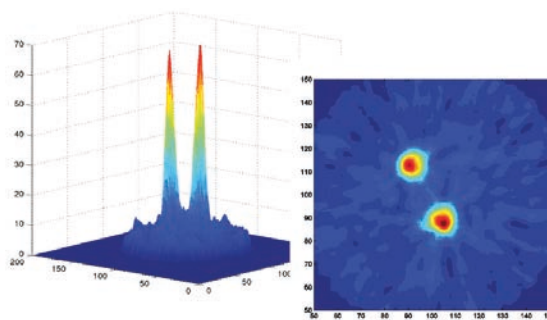
the number of coincidence counts for successive scanning positions of the detector pair. The acquisition time is chosen in relation to the source activity to have enough statistics. The system response function is obtained plotting the number of coincidence counts for each position as a function of the distance between the source and the line of response (the distance is calculated as the product of the source-scanning axis distance and the scanning angle tangent). The resulting curve can be interpreted as the radioactive source distribution convoluted with the system spatial resolution.

## Results

*The estimated spatial resolution is  $\sim (1.45 \pm 0.4)$  mm, which is comparable to the spatial resolution of the small animal PET systems.*



Counting frequency of the beta rays as a function of the number of crossed paper sheets.



$^{22}\text{Na}$  sources, 5  $\mu\text{Ci}$ , 2.7 mm  $\varnothing$  and 9 mm apart.





## C. Particle Physics





# C.1 Cosmic Rays



The cosmic radiation, discovered by Victor Hess<sup>1</sup> in 1912, includes all stable charged particles and it is composed by two component: “primary” and “secondary” cosmic rays. Essentially, the first ones are composed by heavy nucleus, protons (~90%) and helium (~10%), but also electrons, neutrinos, photons, some light nucleus and antimatter (positron and antiprotons). These particles are accelerated by astrophysical sources and by interacting with the terrestrial atmosphere, they mainly produce the “secondary” cosmic rays: pions, kaons and electromagnetic showers. Muons and neutrinos are products of the decay chain of charged mesons, while electrons and photons originate in decays of neutral mesons.

The experiments on cosmic rays proposed in this section are performed by using the “Educational Beta KIT”. The first application is qualitative and it is based on the verification of the cosmics. The second experiment allows the measure the cosmic flux on horizontal scintillating tile.

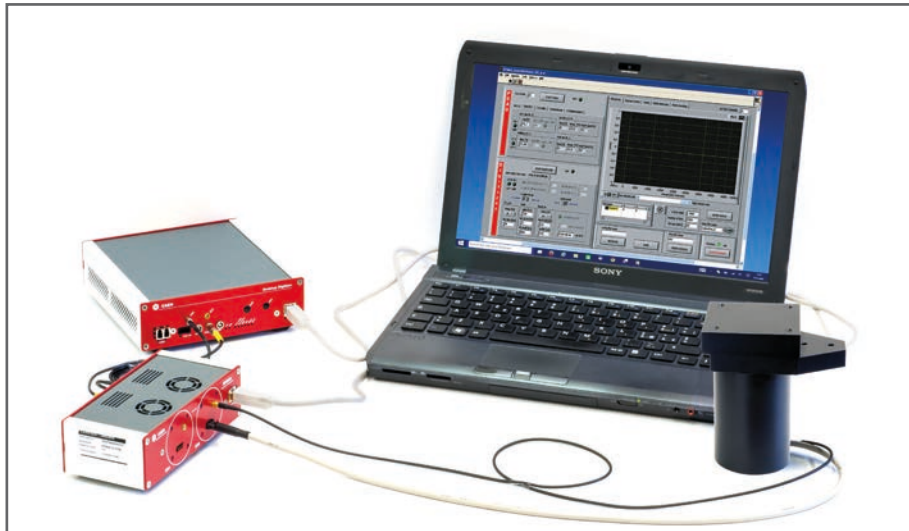
Coming soon a Cosmic telescope will be available in order to perform the third step and measure the flux azimuthal variation.

<sup>1</sup> Nobel Prize in Physics in 1936.

EDUCATIONAL PHOTON KIT	Model.	Description
	SP5600	Power Supply and Amplification Unit
	DT5720A	Desktop Digitizer 250 MS/s
	SP5608	Scintillating tile coupled to SiPM
	COMING SOON	Cosmic telescope

# C.1.1 Muons Detection

SG6211



## Ordering Options

Equipment	
Code	Description
WK5600XDAAA	SP5600D - Educational Beta Kit

or the all inclusive Premium Version

WK5600XANAA	SP5600AN - Educational Kit - Premium Version
-------------	----------------------------------------------

## Purpose of the experiment

*Cosmic rays detection by using a system composed of a plastic scintillating tile directly coupled to a Silicon Photomultiplier detector.*

## Fundamentals


The muons, produced by the decay of pions and kaons generated by the hadronic interaction of the primary cosmic rays with atmospheric nuclei, are the most cosmic rays at sea level.

Cosmic muons are charged particles, produced high in the atmosphere (typically 15 km) with highest penetration capability in matter. Their mass ( $\sim 200$  times the electron mass), the absence of strong interactions and their long lifetime ( $\tau \sim 2,2 \times 10^{-6}$  s), allow muons to cross the atmosphere and reach the Earth's surface.

The muon average energy at sea level is around 4 GeV.

## Equipment

SP5600D - Educational Beta Kit

Model	SP5600	SP5608	DT5720A
Description	Power Supply and Amplification Unit	Scintillating tile coupled to SiPM	Desktop Digitizer 250 MS/s
			
	p. 93	p. 96	p. 93

## Requirements

No other tools are needed.

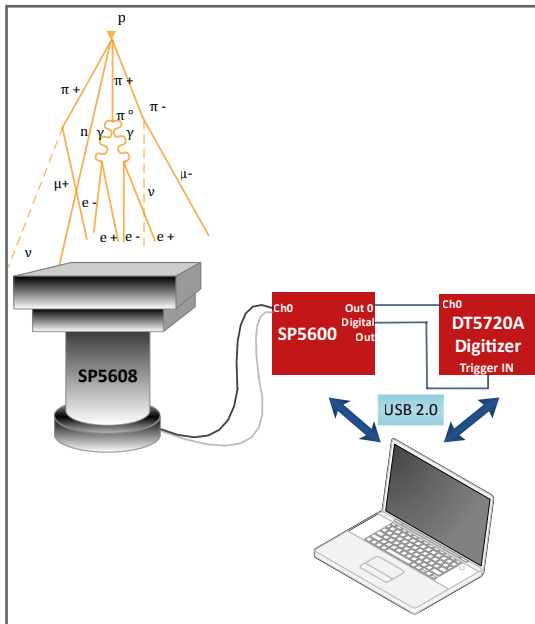


### 1932, physics "annus mirabilis": the positron

1932 was an extraordinary year for nuclear physics: J. Chadwick discovered the neutron, C. D. Anderson identified the positron and the first artificial disintegration was realised with a particle accelerator by J. Cockcroft and E. Walton. These 3 discoveries transformed nuclear physics by providing basis on which any new research could be led. The neutron allowed the discovery of artificial radioactivity by Joliot - Curie in 1934 and later the discovery of nuclear fission by O. Hahn, F. Strassman and L. Meitner. The positron brought new concepts about cosmic radiation and drew the way to the discovery of new particles. Artificial disintegration paved the way to the ever-bigger machines. It was the beginning of the era of breaking nuclei. 1932 deserves its title of "annus mirabilis" of physics. This article presents the quick evolution of ideas, concepts in nuclear physics in the thirties. (A.C.)

[https://inis.iaea.org/search/search.aspx?orig\\_q=RN:30014612](https://inis.iaea.org/search/search.aspx?orig_q=RN:30014612)





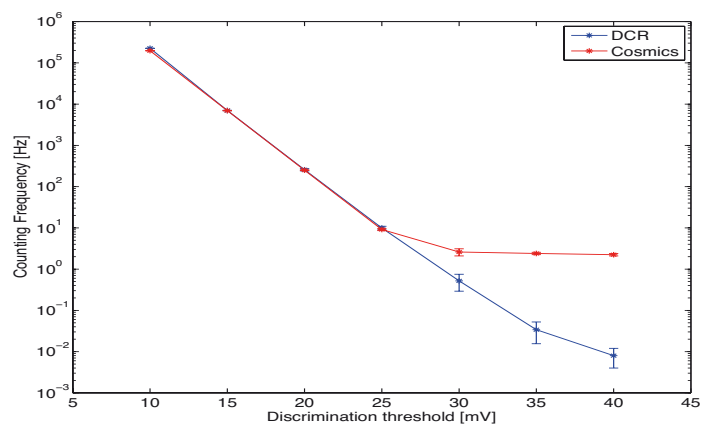
Experimental setup block diagram.

### Carrying out the experiment

Open the SP5608 and remove the plastic scintillating tile. Close the SP5608 and connect its power cable and its MCX cable to one channel of the SP5600. Connect the two outputs of the chosen channel to DT5720A: the analog output to the channel 0 and the digital output to "trigger IN" of the digitizer. Use the default software values or optimize the parameters to evaluate the noise contribution of the sensor, called Dark Count Rate (DCR). Measure the DCR as a function of the discrimination threshold in mV. Because of the DCR, the system has to be made sensitive to the cosmic ray flux relying on the acquisition time of the sensor signal. Switch off the power supply, open the SP5608 top, spread the optical grease on the SiPM and insert the scintillating tile. Close the support top, switch ON the power supply and restore the previous configuration parameters. Measure the counting rate scanning the values of the threshold.

### Results

*The cut-off threshold has a key role in the cosmic ray detection and it shall be set to reduce the random coincidence rate below the Hertz level and measure the cosmic rate.*

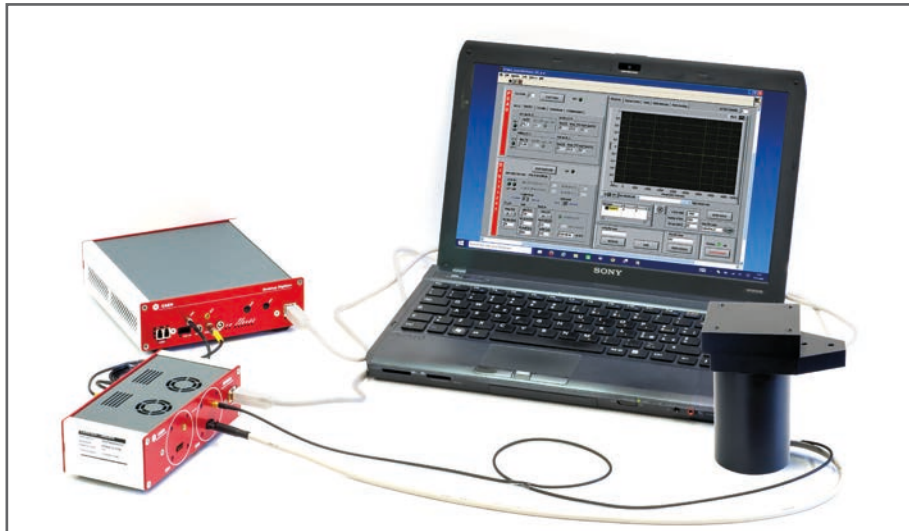


Signal frequency as a function of discriminator threshold. The red line represents the cosmic contribution, the black one the noise.



# C.1.2 Muons Vertical Flux on Horizontal Detector

SG6212



## Ordering Options

Equipment	
Code	Description
WK5600XDAAA	SP5600D - Educational Beta Kit
or the all inclusive Premium Version	
WK5600XANAA	SP5600AN - Educational Kit - Premium Version

## Purpose of the experiment

*Measurement of the muon vertical flux on a plastic scintillating tile.  
Estimation of the detection efficiency of the system by comparison between the expected rate and the measured one.*

## Fundamentals

Muons lose about 2 GeV to ionization before reaching the ground with average energy around 4 GeV. The production spectrum, energy loss in the atmosphere and decay of the muons are convoluted in their energy and angular distribution. The integral intensity of vertical muons is

$$I_v \approx 82 \text{ m}^{-2}\text{s}^{-1}\text{sr}^{-1}$$

and their flux for horizontal detectors is  $\approx 1 \text{ cm}^{-2}\text{min}^{-1}$  at energies higher than 1 GeV at sea level, as know in literature<sup>2</sup>.






Cosmic ray muon radiography is a technique capable of imaging variations of density inside a hundreds of meters of rock. With resolutions up to tens of meters in optimal detection conditions, muon radiography can give us images of the top region of a volcano edifice with a resolution that is significantly better than the one typically achieved with conventional gravity methods and in this way can give us information on anomalies in the density distribution, such as expected from dense lava conduits, low density magma supply paths or the compression with depth of the overlying soil.

[www.mu-ray.fisica.unina.it](http://www.mu-ray.fisica.unina.it)



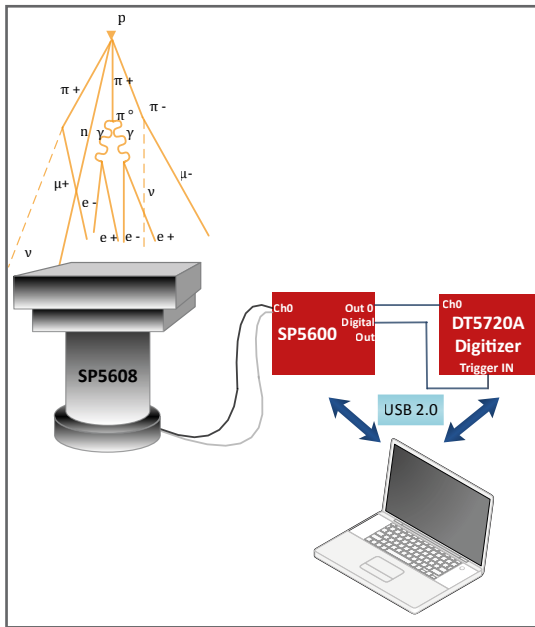
## Equipment

SP5600D - Educational Beta Kit

Model	SP5600	SP5608	DT5720A
Description	Power Supply and Amplification Unit	Scintillating tile coupled to SiPM	Desktop Digitizer 250 MS/s
			
	p. 93	p. 96	p. 93

## Requirements

No other tools are needed.



Experimental setup block diagram.

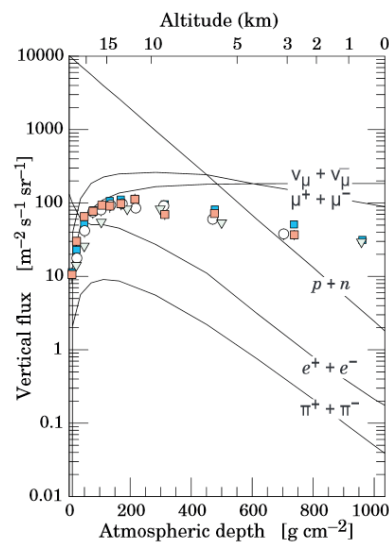
## Carrying out the experiment

Open the SP5608 and remove the plastic scintillating tile. Close the SP5608 and connect its power cable and its MCX cable to one channel of the SP5600. Connect the two outputs of the chosen channel to DT5720A: the analog output to the channel 0 and the digital output to "trigger IN" of the digitizer. Use the default software values or optimize the operating voltage of the sensor to reach an higher photon detection efficiency (PDE). The first measurement step is the evaluation of the noise (Dark Count Rate) as a function of the discriminator threshold. Because of the DCR, the system has to be made sensitive to the cosmic ray flux relying on the acquisition time of the sensor signal. The thresholds shall be set to reduce the random coincidence rate below the Hertz level. Switch off the power supply, open the SP5608 top, spread the optical grease on the SiPM and insert the scintillating tile. Close the support top, switch ON the power supply and reset the previous configuration parameters. Measure the muons counting rate and estimate the cosmic flux.

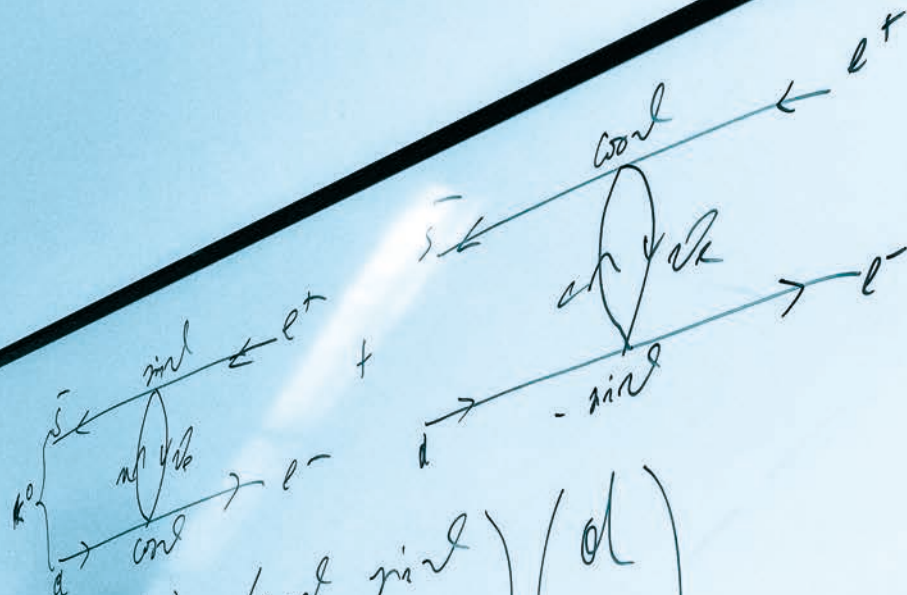
## Results

*The expected rate of muons across the scintillating tile is very low, requiring a fine tuning of the system in order to achieve a significant reduction of the random count rate and enhance the system sensitivity.*

*Considering the zenith dependence of flux ( $I(\theta) = I_V \cos\theta^2$ ) and the integration over the solid angle, the expected cosmic rate due to the geometry system can be estimated and the detection efficiency can be evaluated.*

Cosmic vertical flux as a function of altitude and atmospheric depth<sup>2</sup>.

<sup>2</sup> K.A. Olive et al. (Particle Data Group), Chin. Phys. C, 38, 090001 (2014).



$$\begin{pmatrix} d_u \\ s_u \end{pmatrix} = \begin{pmatrix} \cos\theta & \sin\theta \\ -\sin\theta & \cos\theta \end{pmatrix} \begin{pmatrix} d \\ s \end{pmatrix}$$

$$\text{MECHANISM} \Rightarrow \begin{pmatrix} u \\ d \end{pmatrix} \begin{pmatrix} c \\ s \end{pmatrix}$$

$$= c\bar{c} \quad M_{J/\psi} \approx 3.1 \text{ GeV} \quad \Gamma_{J/\psi} \approx 90 \text{ keV}$$



SLAC / BNL  
1974

## C. Particle Physics





## C.2 Photons



The Elementary Particles can be divided into fermions, which are matter or antimatter particles as quarks, antiquarks, electrons, antielectrons and so on, and bosons which generally are "force particles" that mediate interactions among fermions.

Photon is an elementary particle belonging to the boson family. It is massless, stable and it has no electric charge. As a boson, it has an integer spin and it obeys to Bose-Einstein Statistics.

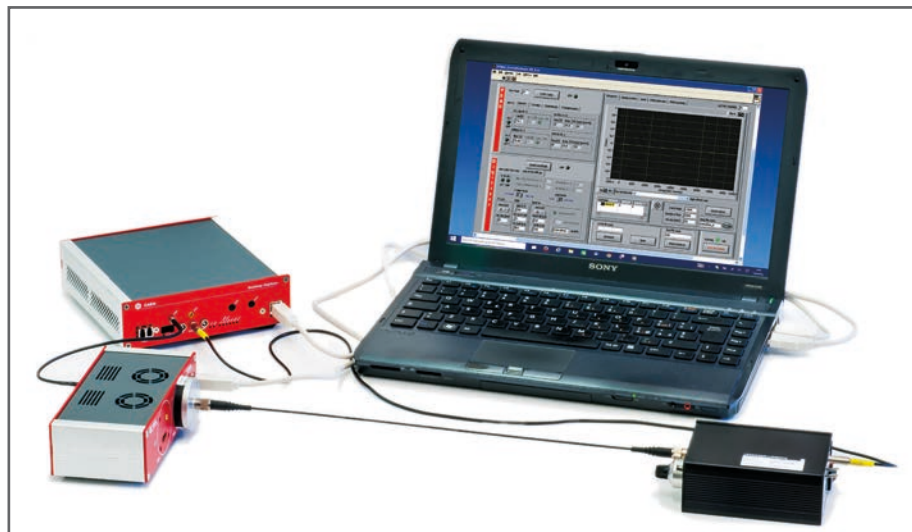
The photon is the gauge boson for electromagnetism.

The experiments related the photons are performed thanks to the CAEN "Educational Photon Kit".

EDUCATIONAL PHOTON KIT	Model.	Description
	SP5600	Power Supply and Amplification Unit
	DT5720A	Desktop Digitizer 250 MS/s
	SP5601	LED Driver
	SP5650C	Sensor Holder for SP5600 with HAMAMATSU SiPM

# C.2.1 Quantum Nature of Light

SG6221



## Related Experiment

A.1.1

D.1

## Ordering Options

### Equipment

Code	Description
WK5600XEAAAA	SP5600E - Educational Photon Kit

or the all inclusive Premium Version

WK5600XANAAA	SP5600AN - Educational Photon Kit - Premium Version
--------------	-----------------------------------------------------

## Purpose of the experiment

Exploring the quantum nature of light thanks to bunches of photons emitted in a few nanoseconds by an ultra-fast LED and sensed by a state-of-the-art detector, a Silicon Photomultiplier (SiPM).


## Fundamentals

In the XVII century the concept of wave-particle duality was developed, starting from the wave nature of light postulated by Huygens to the Einstein Photoelectric Effect, which postulates light quanta existence.

A basic principle of quantum mechanics is complementarity: each quantum-mechanical object has both wave-like and particle-like properties. With this approach the photon is at the same time wave and particle, but they can never be observed simultaneously in the same experiment, not even if the uncertainty principle is successfully bypassed.

## Equipment

SP5600E - Educational Photon Kit

Model	SP5600	DT5720A	SP5601	SP5650C
Description	Power Supply and Amplification Unit	Desktop Digitizer 250 MS/s	LED Driver	Sensor Holder for SP5600 with SiPM
				
	p. 93	p. 93	p. 94	p. 94

## Requirements

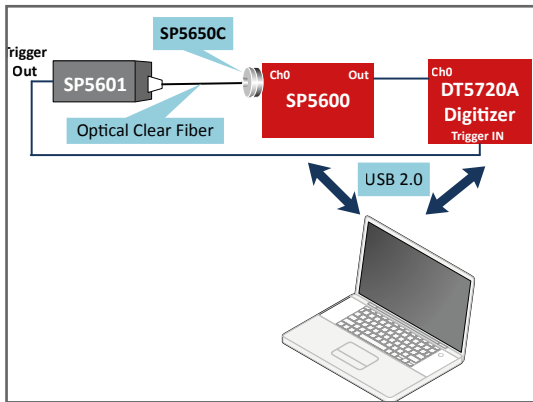
No other tools are needed.



Like the special theory of relativity, Einstein's quantum hypothesis arose from an experimental puzzle and an asymmetry or duality in physical theories. The duality consisted of the well-known distinction between material atoms and continuous ether, or, as Einstein wrote in the opening sentence of his light quantum paper, "between the theoretical conceptions that physicists have formed about gases and other ponderable bodies and the Maxwell theory of electromagnetic processes in so-called empty space." As noted earlier, Boltzmann and others conceived of gases as consisting of myriads of individual atoms, while Maxwell and Lorentz envisioned electromagnetic processes as consisting of continuous waves. Einstein sought a unification of these two viewpoints by removing the asymmetry in favor of a discontinuous, "atomic," or quantum, theory of light. Resolution of an experimental puzzle encouraged this approach. The Nobel Prize in Physics 1921 was awarded to Albert Einstein "for his services to Theoretical Physics, and especially for his discovery of the law of the photoelectric effect".

<https://www.aip.org/history/exhibits/einstein/essay-photoelectric.htm>





Experimental setup block diagram.

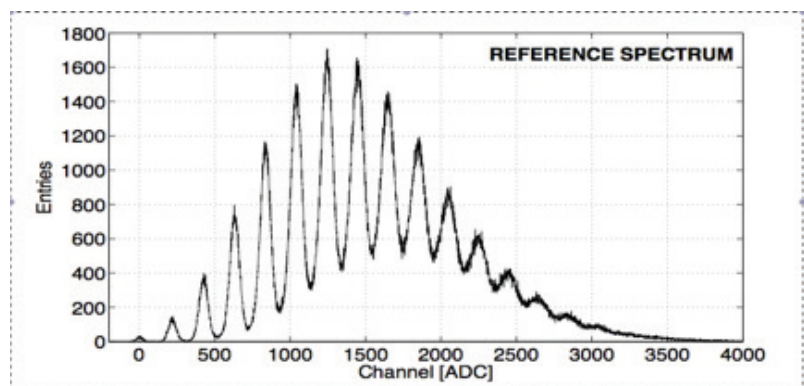
## Carrying out the experiment

Plug in the SP5650A into one channel of SP5600 and connect the analog output to DT5720A channel 0. Remove the protection cover of the SP5601 and SP5650A, spread the optical grease on both ends of the optical fiber and connect them. Use internal trigger mode on SP5601 and connect its trigger output on the DT5720A trigger IN. Connect via USB the modules to PC and power ON the devices. Use the default software values or optimize the parameters to acquire the light spectrum.

In the spectrum of the SiPM response to a light pulse, every entry corresponds to the digitized released charge, measured integrating the electrical current spike during a predefined time interval. The peaks correspond to different number of cells fired at the same time by incoming photons.

## Results

*This detector can count the number of impacting photons, shot by shot, allowing to observe how the light is composed by photons. Moreover the SiPM measures the light intensity simply by the number of fired cells.*

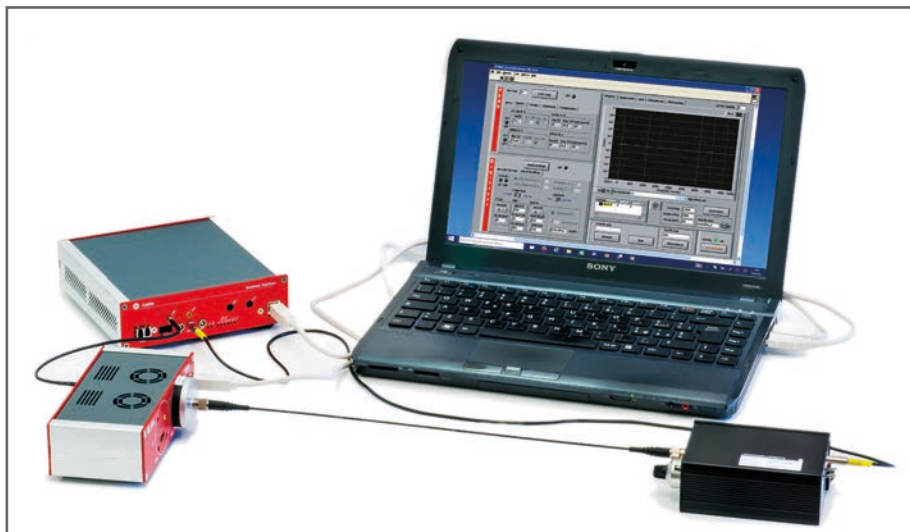


Spectrum of the photons emitted by a LED Driver and detected by a Silicon Photomultiplier.



## C.2.2 Hands-on Photon Counting Statistics

SG6222



### Related Experiment

A.1.1

B.1.2

C.2.1

D.1

### Ordering Options

#### Equipment

Code	Description
WK5600XEAAA	SP5600E - Educational Photon Kit

or the all inclusive Premium Version

WK5600XANAAA	SP5600AN - Educational Kit - Premium Version
--------------	----------------------------------------------

### Purpose of the experiment

*Statistical properties of the light pulses emitted by a LED driver.*

### Fundamentals

Spontaneous emission of light results from random decays of excited atoms and it is expected to be Poissonian. SiPM can count the number of impacting photons, shot by shot, opening up the possibility to apply basic skills in probability and statistics while playing with light quanta displaying the spectrum of the SiPM response to a high statistics of pulses. The spectrum is composed by a series of peaks, each ones correspond to different number of cells fired at the same time. Each peak is well separated and occurs with a probability linked at first order to the light intensity fluctuations. In SiPM the homogeneity of the response is quite high, however, since fired cells are randomly distributed in the detector sensitive area residual differences in the gain become evident broadening the peak.

A key point in the analysis technique was the estimation of the area underneath every peak, essential to reconstruct the probability density function of the emitted number of photons per pulse. An easy procedure is to consider each peak as a gaussian, so spectra recorded in response to photons impacting on the sensor can be seen as a superposition of Gaussians, each corresponding to a well defined number of fired cells. A binned Gaussian distribution of  $N_{pk}$  events may be written as:

$$y_i = y_{max} e^{\frac{-(x_i - x_0)^2}{2\sigma^2}}$$

where  $y_i$  is the number of events in the bin centred on  $x_i$  and  $y_{max}$  is the peak value, measured in  $x_0$ . Since  $y_{max} = N_{pk}/(\sigma\sqrt{2\pi})$ , knowing the content of the bin centred in  $x_0$  and estimating  $\sigma$  leads to  $N_{pk}$ . The standard deviation can also be calculated in a simple way by the Full Width at Half Maximum (FWHM), obtained searching for the position of the bins with a content equals to  $y_{max}/2$  and presuming that  $FWHM = 2.355\sigma$



### Schrödinger's Cat Paradox

Schrödinger's cat is a famous illustration of the principle in quantum theory of superposition, proposed by Erwin Schrödinger (Nobel Prize in Physics in 1933). Schrödinger's cat serves to demonstrate the apparent conflict between what quantum theory tells us is true about the nature and behaviour of matter on the microscopic level and what we observe to be true about the nature and behaviour of matter on the macroscopic level -- everything visible to the unaided human eye.





Here's Schrödinger's thought experiment: We place a living cat into a steel chamber, along with a device containing a vial of hydrocyanic acid. There is, in the chamber, a very small amount of hydrocyanic acid, a radioactive substance. If even a single atom of the substance decays during the test period, a relay mechanism will trip a hammer, which will, in turn, break the vial and kill the cat.

<http://whatis.techtarget.com/definition/Schrodingers-cat>



## Equipment

SP5600E - Educational Photon Kit

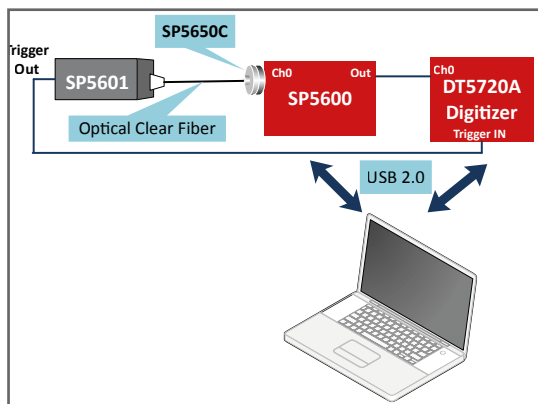
Model	SP5600	DT5720A	SP5601	SP5650C
Description	Power Supply and Amplification Unit	Desktop Digitizer 250 MS/s	LED Driver	Sensor Holder for SP5600 with SiPM
				
	p. 93	p. 93	p. 94	p. 94

## Requirements

No other tools are needed.

## Carrying out the experiment

Plug in the SP5650A into one channel of SP5600 and connect the analog output to DT5720A channel 0. Remove the protection cover of the SP5601 and SP5650A, spread the optical grease on both ends of the optical fiber and connect them. Use internal trigger mode on SP5601 and connect its trigger output on the DT5720A trigger IN. Connect via USB the modules to PC and power ON the devices. Use the default software values or optimize the parameters to perform the experiment.



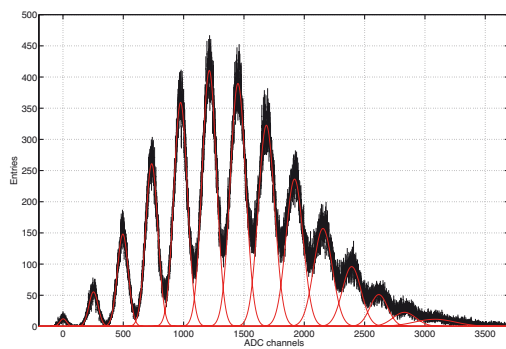
Experimental setup block diagram.

## Results

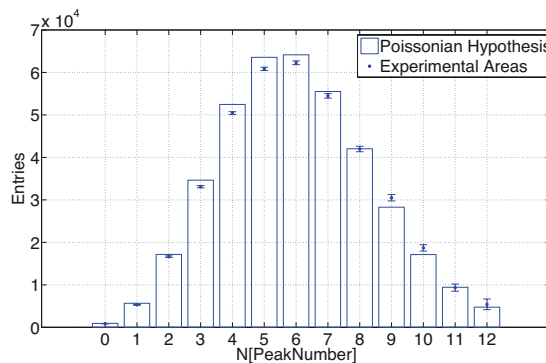
The probability density function of the emitted number of photons per pulse can be estimated by the evaluation of the area underneath every peak.

Two different hypothesis can be investigated to evaluate the statistical model and mean number of photoelectrons: Model Independent (the mean photon number is nothing but the mean) and Poissonian hypothesis (mean value obtained by presuming a pure Poissonian behaviour and by referring to the probability  $P(0)$  of having no fired cell when the expected average value).

A complete and more complex analysis that include also considerations about detector structure is reported in the following section in the D.1 note.



Photoelectron spectrum probing a LED source measured with a Hamamatsu SiPM. The Individual Gaussians are shown in red.



Data from the light spectrum compared to a simple Poissonian.



A photograph of a laboratory setting. In the foreground, a woman with long dark hair is seated at a table, focused on adjusting a piece of scientific equipment. The equipment consists of a vertical metal frame with various components, including what appears to be a detector or sensor assembly. In the background, a man with a beard and a striped shirt is standing and writing on a whiteboard. The whiteboard has the word "PERIOD" written on it. The entire scene is bathed in a warm, yellowish light.

## **D. Advanced Statistics based on Silicon Photomultiplier Detectors**





## D. Advanced Statistics based on Silicon Photomultiplier Detectors

D.1 An Educational Kit Based on a Modular Silicon Photomultiplier System p. 66

D.2 A simple and robust method to study after-pulses in Silicon Photomultipliers p. 79

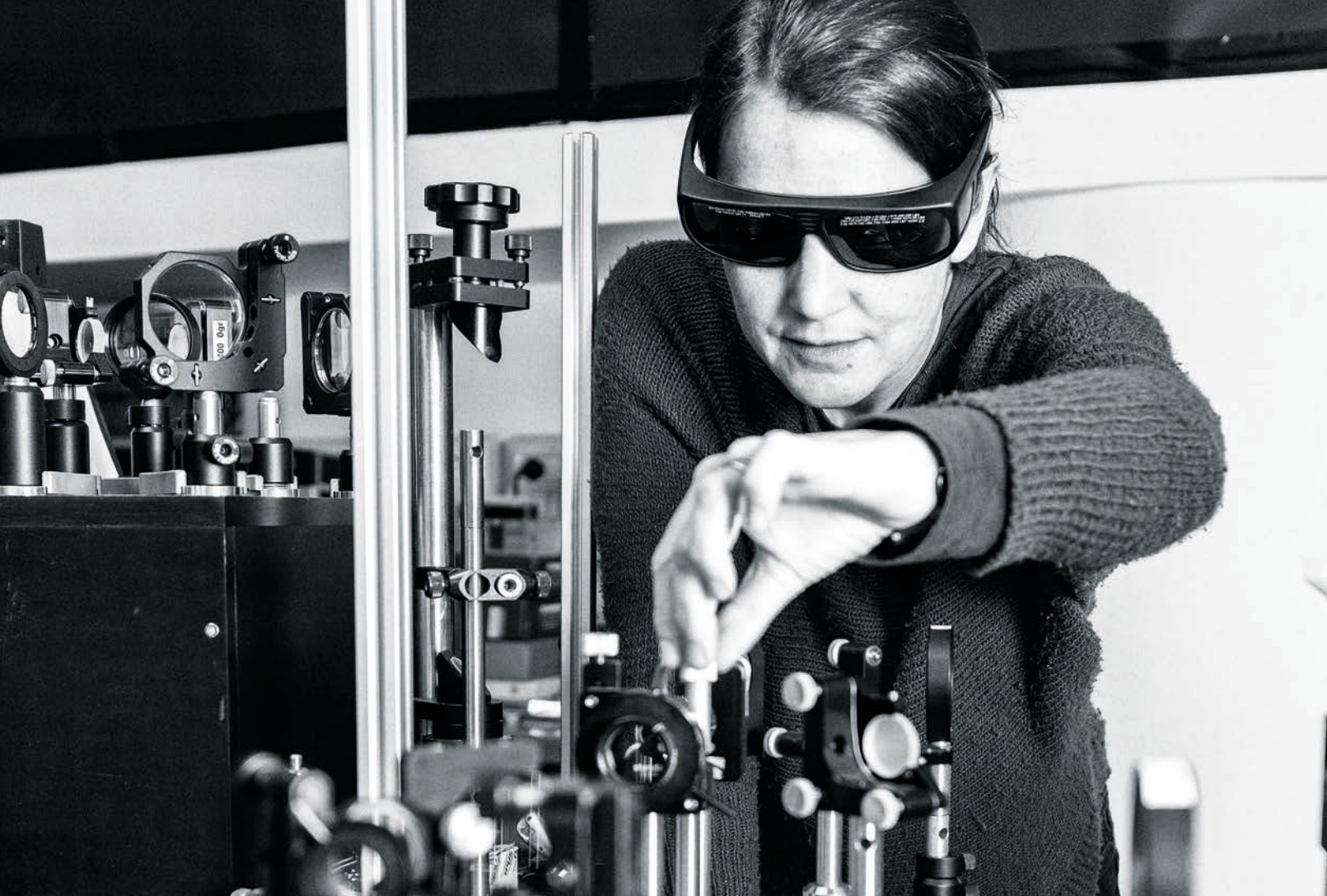
D.3 Background removal procedure based on the SNIP algorithm for  $\gamma$ -ray spectroscopy with the CAEN Educational Kit p. 84



A series of experiments covering several applications has been carried out and are presented in this section through detailed Educational Notes. The collaboration with the University of Insubria allows to offer experiments based on Silicon Photo-Multiplier detectors for advanced laboratories using the latest instrumentation generation developed by CAEN for the major experiments Worldwide.

For every topic, an accompanying suite is being developed, including an 'instructor' guide, indications on the analysis and a library of routines in MATLAB, a platform widely distributed in the academic community.

EDUCATIONAL KIT - "PREMIUM VERSION"	Model.	Description
	SP5600	Power Supply and Amplification Unit
	DT5720A	Desktop Digitizer 250 MS/s
	SP5601	LED Driver
	SP5650C	Sensor Holder for SP5600 with HAMAMATSU SiPM
	SP5606	Spectrometer
	SP5607	Absorption Tool
	A315	Splitter
	SP5608	Scintillating tile coupled to SiPM



## D.1 An Educational Kit Based on a Modular Silicon Photomultiplier System

ED3127

### Equipment

#### SP5600E - Educational Photon Kit

Model	SP5600	DT5720A	SP5601	SP5650A
Description	Power Supply and Amplification Unit	Desktop Digitizer 250 MS/s	LED Driver	Sensor Holder for SP5600 with SiPM
				
	p. 93	p. 93	p. 94	p. 94

Related Experiment
C.2.1
A.1.1

#### Ordering Options

Equipment	
Code	Description
WK5600XEAAAA	SP5600E - Educational Photon Kit

or the all inclusive Premium Version

WK5600XANAAA	SP5600AN - Educational Kit - Premium Version
--------------	----------------------------------------------



Data analysis code developed in MATLAB is available.



# An Educational Kit Based on a Modular Silicon Photomultiplier System

Valentina Arosio, Massimo Caccia, Valery Chmill, Amedeo Ebolese, Marco Locatelli, Alexander Martemiyarov, Maura Pieracci, Fabio Risigo, Romualdo Santoro and Carlo Tintori

**Abstract**—Silicon Photo-Multipliers (SiPM) are state of the art light detectors with unprecedented single photon sensitivity and photon number resolving capability, representing a breakthrough in several fundamental and applied Science domains. An educational experiment based on a SiPM set-up is proposed in this article, guiding the student towards a comprehensive knowledge of this sensor technology while experiencing the quantum nature of light and exploring the statistical properties of the light pulses emitted by a LED.

**Keywords**—Silicon Photo-Multipliers, Photon Statistics, Educational Apparatus

## I. INTRODUCTION

EXPLORING the quantum nature of phenomena is one of the most exciting experiences a physics student can live. What is being proposed here has to do with light bullets, bunches of photons emitted in a few nanoseconds by an ultra-fast LED and sensed by a state-of-the-art detector, a Silicon Photo-Multiplier (hereafter, SiPM). SiPM can count the number of impacting photons, shot by shot, opening up the possibility to apply basic skills in probability and statistics while playing with light quanta. After an introduction to the SiPM sensor technology (Section II), the basics of the statistical properties of the random process of light emission and the sensor related effects are introduced (Section III). The experimental and data analysis techniques are described in Section IV, while results and discussions are reported in Section V.

## II. COUNTING PHOTONS

SiPMs are cutting edge light detectors essentially consisting of a matrix of photodiodes with a common output and densities up to  $10^4/mm^2$ . Each diode is operated in a limited Geiger-Muller regime in order to achieve gains at the level of  $\approx 10^6$  and guarantee an extremely high homogeneity in the cell-to-cell response. Subject to the high electric field in the depletion zone, initial charge carriers generated by an absorbed photon or by thermal effects trigger an exponential charge multiplication by impact ionization, till when the current spike across the quenching resistance induces a drop in the operating voltage, stopping the process [1], [3], [4].

M. Caccia, V. Chmill, A. Ebolese, A. Martemiyarov, F. Risigo and R. Santoro are with the Dipartimento di Scienza e Alta Tecnologia, Università degli Studi dell'Insubria, 22100, Como, Italy (e-mail: massimo.caccia@uninsubria.it).

M. Locatelli, M. Pieracci and C. Tintori are with the CAEN S.p.A., 55049, Viareggio, Italy (e-mail: m.locatelli@caen.it).

SiPM can be seen as a collection of binary cells, providing altogether an information about the intensity of the incoming light by counting the number of fired cells.

Fig. 1 shows the typical response by a SiPM to a light pulse: traces correspond to different numbers of fired cells, proportional to the number of impinging photons. Because of the high gain compared to the noise level, traces are well separated, providing a photon number resolved detection of the light field.

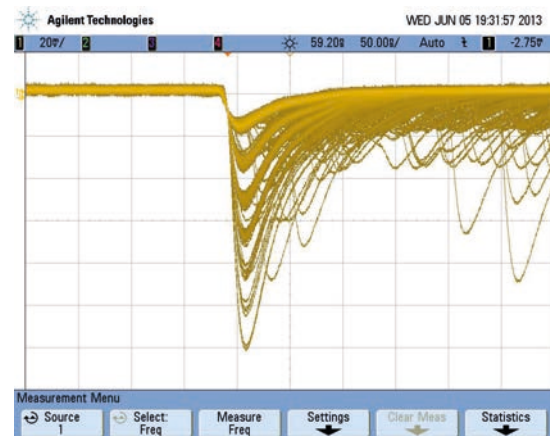


Fig. 1: Response of a SiPM Hamamatsu MPPC S10362-11-100C illuminated by a light pulse.

This is also shown in Fig. 2, displaying the spectrum of the SiPM response to a high statistics of pulses: every entry corresponds to the digitized released charge, measured integrating the electrical current spike during a pre-defined time interval. The peaks correspond to different number of cells fired at the same time. Each peak is well separated and occurs with a probability linked at first order to the light intensity fluctuations. An analysis of the histogram is revealing other significant characteristics:

- The peak at 0 corresponds to no detected photons and its width measures the noise of the system, i.e. the stochastic fluctuations in the output signal in absence of any stimulus. In the displayed histogram,  $\sigma_0 = 29 \pm 1$  ADC channels.
- The peak at 1 detected photon has a width  $\sigma_1 = 38.1 \pm 0.4$  ADC channels, by far exceeding  $\sigma_0$ . The extra



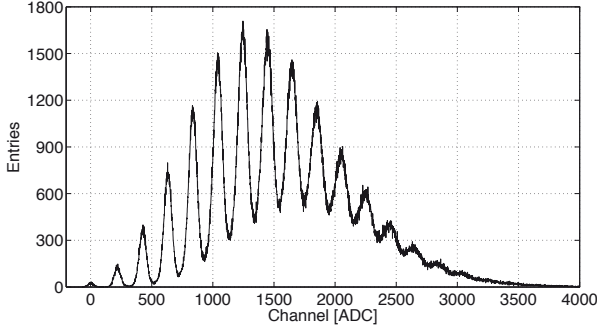


Fig. 2: Photoelectron spectrum probing a LED source measured with a Hamamatsu MPPC S10362-11-100C at a bias voltage of 70.3V and temperature of 25°C.

contribution may be related to the fact that not all of the cells were born equal. In SiPM the homogeneity of the response is quite high [5], [6], however, since fired cells are randomly distributed in the detector sensitive area residual differences in the gain become evident broadening the peak.

- As a consequence the peak width is increasing with the number  $N$  of fired cells with a growth expected to follow a  $\sqrt{N}$  law, eventually limiting the maximum number  $M$  of resolved peaks.

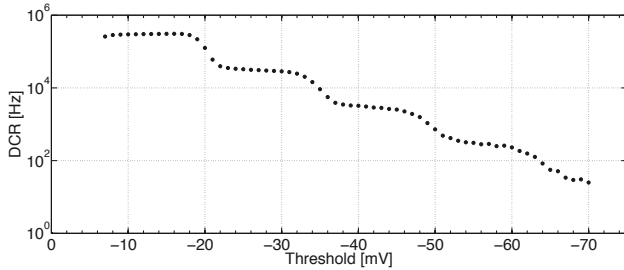


Fig. 3: Measurement of the DCR of the SiPM performed at 25°C.

The detector working conditions can be optimized to maximize  $M$ , properly tuning the bias voltage  $V_{bias}$  and balancing competing effects. On one hand, the peak-to-peak distance is linked to the single cell gain and it is expected to grow linearly with the over-voltage as:

$$Gain = \frac{C \Delta V}{q_e}, \quad (1)$$

where  $\Delta V = V_{bias} - V_{Breakdown}$ ,  $C$  is the diode capacitance of the single cell and  $q_e$  the electron charge [3]. Effects broadening the peaks may grow faster dumping the expected resolution. Among these effects it is worth mentioning Dark Counts, Optical Cross-Talk and After-Pulsing:

- Free charge carriers may also be thermally generated. Results are spurious avalanches (Dark Counts) occurring

randomly and independently from the illumination field. The Dark Count Rate (DCR) does depend from several factors: substrate, processing technology, sensor design and operating temperature [4]. The over-voltage has an impact since the junction thickness volume grows with it together with the triggering probability, namely the probability that a charge carrier develops an avalanche [4], [5]. The DCR can be measured in different ways. A *Stair Case Plot* is presented in Fig. 3 where the output from a sensor is compared to the threshold of a discriminator and the rate with which the threshold is exceeded is counted. A typical DCR is about  $0.5 \text{ MHz/mm}^2$ .

- Dark Counts may be considered as statistically independent. However, optical photons developed during an avalanche have been shown to trigger secondary avalanches [4] involving more than one cell into spurious pulses. This phenomenon is named Optical Cross-Talk (OCT). The OCT is affected by the sensor technology [4], [7], [8], [9] and strongly depends on the bias voltage increasing the triggering probability and the gain forming the optical photon burst. The OCT can be measured by the ratio of the Dark Counts frequencies for pulses exceeding the 0.5 and 1.5 levels of the single cell amplitude, namely:

$$OCT = \frac{\nu_{1.5pe}}{\nu_{0.5pe}}. \quad (2)$$

The OCT typically ranges between 10% and 20% [5], [9], [10].

- Charge carriers from an initial avalanche may be trapped by impurities and released at later stage resulting in delayed avalanches named After-Pulses. For the detectors in use here, an After-Pulse rate at about the 25% level has been reported for an overvoltage  $\Delta V = 1 \text{ V}$ , with a linear dependence on  $V_{bias}$  and a two-component exponential decay time of 15 ns and 80 ns [5].

Dark Counts, Optical Cross-Talk and After-Pulses occur stochastically and introduce fluctuations in the multiplication process that contribute to broaden the peaks in the spectrum. An exhaustive study of this effect, also known as Excess Noise Factor (ENF), exceeds the goals of this work and will not be addressed here (see for example [3], [6], [8] and [12]). However, the resolving power that will be introduced in the following may be considered a figure of merit accounting for the ENF and measuring the ability to resolve the number of detected photons.

### III. PHOTON COUNTING STATISTICS

Spontaneous emission of light results from random decays of excited atoms. Occurrences may be considered statistically independent, with a decay probability within a time interval

$\Delta t$  proportional to  $\Delta t$  itself. Being so, the statistics of the number of photons emitted within a finite time interval  $T$  is expected to be Poissonian, namely:

$$P_{n,\text{ph}} = \frac{\lambda^n e^{-\lambda}}{n!}, \quad (3)$$

where  $\lambda$  is the mean number of emitted photons.

The detection of the incoming photons has a stochastic nature as well, at the simplest possible order governed by the Photon Detection Probability (PDE)  $\eta$ , resulting in a Binomial probability to detect  $d$  photons out of  $n$ :

$$B_{d,n}(\eta) = \binom{n}{d} \eta^d (1-\eta)^{n-d}. \quad (4)$$

As a consequence, the distribution  $P_{d,\text{el}}$  of the number of detected photons is linked to the distribution  $P_{n,\text{ph}}$  of the number of generated photons by

$$P_{d,\text{el}} = \sum_{n=d}^{\infty} B_{d,n}(\eta) P_{n,\text{ph}}. \quad (5)$$

However, the photon statistics is preserved and  $P_{d,\text{el}}$  is actually a Poissonian distribution of mean value  $\mu = \lambda\eta$  [9], [10]. For the sake of completeness, the demonstration is reported in Appendix A.

Detector effects (especially OCT and After-Pulses) can actually modify the original photo-electron probability density function, leading to significant deviations from a pure Poisson distribution. Following [9] and [10], OCT can be accounted for by a parameter  $\epsilon_{XT}$ , corresponding to the probability of an avalanche to trigger a secondary cell. The probability density function of the number of fired cells, the random discrete variable  $m$ , can be written at first order as:

$$P \otimes B = \sum_{k=0}^{\text{floor}(m/2)} B_{k,m-k}(\epsilon_{XT}) P_{m-k}(\mu), \quad (6)$$

where  $\text{floor}$  rounds  $m/2$  to the nearest lower integer and  $B_{k,m-k}(\epsilon_{XT})$  is the binomial probability for  $m-k$  cells fired by a photon to generate  $k$  extra hit by OCT.  $P \otimes B$  is characterized by a mean value and variance expressed as:

$$\bar{m}_{P \otimes B} = \mu(1 + \epsilon_{XT}) \quad \sigma_{P \otimes B}^2 = \mu(1 + \epsilon_{XT}). \quad (7)$$

In order to perform a more refined analysis, the probability density function of the total number of detected pulses can be calculated taking into account higher order effects [13]. The result is achieved by assuming that every primary event may produce a single infinite chain of secondary pulses with the same probability  $\epsilon_{XT}$ . Neglecting the probability for an event to trigger more than one cell, the number of secondary hits, described by the random discrete variable  $k$ , follows a geometric distribution with parameter  $\epsilon_{XT}$ :

$$G_k(\epsilon_{XT}) = \epsilon_{XT}^k (1 - \epsilon_{XT}) \quad \text{for } k = 0, 1, 2, 3, \dots \quad (8)$$

The number of primary detected pulses is denoted by the random discrete variable  $d$  and belongs to a Poisson distribution with mean value  $\mu$ . As a consequence, the total number of detected pulses  $m$  represents a compound Poisson process given by:

$$m = \sum_{i=1}^d (1 + k_i). \quad (9)$$

Then, the probability density function of  $m$  is expressed as a compound Poisson distribution:

$$P \otimes G = \frac{e^{-\mu} \sum_{i=0}^m B_{i,m} \mu^i (1 - \epsilon_{XT})^i \epsilon_{XT}^{m-i}}{m!}, \quad (10)$$

where

$$B_{i,m} = \begin{cases} 1 & \text{if } i = 0 \text{ and } m = 0 \\ 0 & \text{if } i = 0 \text{ and } m > 0 \\ \frac{m!(m-1)!}{i!(i-1)!(m-i)!} & \text{otherwise} \end{cases}$$

The mean value and the variance of the distribution are respectively given by:

$$\bar{m}_{P \otimes G} = \frac{\mu}{1 - \epsilon_{XT}} \quad \sigma_{P \otimes G}^2 = \frac{\mu(1 + \epsilon_{XT})}{(1 - \epsilon_{XT})^2}. \quad (11)$$

These relations can be calculated referring to the definition of the probability generating function and exploiting its features [13]. The full demonstration is available in Appendix B.

#### IV. EXPERIMENTAL TECHNIQUES

In this section the experimental set-up and the analysis methods are presented. The optimization of the working point of a SiPM is addressed together with the recorded spectrum analysis technique.

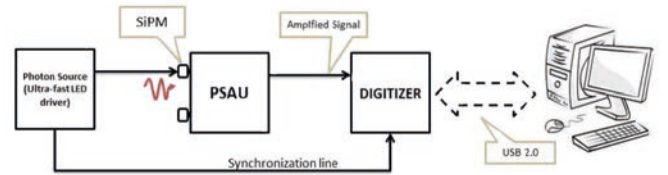


Fig. 4: Schematic layout of the experimental set-up.

##### A. Set-up and measurements

The experimental set-up is based on the CAEN Silicon Photomultiplier Kit. The modular plug and play system contains:

- The Two channel SP5600 CAEN Power Supply and three-stage Amplification Unit (PSAU) [14], with SiPM

embedding head unit. The PSAU integrates a leading edge discriminator per channel and coincidence logic.

- The two channels DT5720A CAEN Desktop Digitizer, sampling the signal at 250 MS/s over a 12 bit dynamic range. The available firmware enables the possibility to perform charge Integration (DPP-CI), pulse shape discrimination (DPP-PSD) and advanced triggering [15].
- The ultra-fast LED (SP5601 [16]) driver emitting pulses at 400 nm with FWHM of 14 nm. Pulses are characterized by an exponential time distribution of the emitted photons with a rising edge at sub-nanosecond level and a trailing edge with  $\tau \approx 5$  ns. The driver is also providing a synchronization signal in NIM standard.

In the current experiments the SiPM that was used is a Multi Pixel Photon Counter (MPCC) S10362-11-100C produced by HAMAMATSU Photonics<sup>1</sup> (see Table I).

TABLE I: Main characteristics of the SiPM sensor (Hamamatsu MPCC S10362-11-100C) at a temperature of 25°C

Number of Cells:	100
Area:	$1 \times 1 \text{ mm}^2$
Diode Dimension:	$100 \mu\text{m} \times 100 \mu\text{m}$
Breakdown Voltage:	69.2V
DCR:	600 kHz at 70.3V
OCT:	20% at 70.3V
Gain:	$3.3 \times 10^6$ at 70.3V
PDE ( $\lambda = 440\text{nm}$ ):	75% at 70.3V

The block diagram of the experimental set-up is presented in Fig.4 with light pulses conveyed to the SiPM sensor by an optical fiber.

The area of the digitized signal is retained as a figure proportional to the total charge generated by the SiPM in response to the impacting photons. The integration window (or *gate*) is adjusted to match the signal development and it is synchronized to the LED driver pulsing frequency.

The proposed experimental activities start with the optimal setting of the sensor bias voltage, defined maximizing the resolving power defined as:

$$R = \frac{\Delta_{pp}}{\sigma_{gain}}, \quad (12)$$

where  $\Delta_{pp}$  is the peak-to-peak distance in the spectrum and  $\sigma_{gain}$  accounts for the single cell gain fluctuations:

$$\sigma_{gain} = (\sigma_1^2 - \sigma_0^2)^{1/2}, \quad (13)$$

being  $\sigma_{0,1}$  the standard deviations of the 0- and 1-photoelectron peaks [17]. R is a figure of merit measuring the capability to resolve neighboring peaks in the spectrum. In

fact, following the Sparrow criterion [18] according to which two peaks are no longer resolved as long as the dip half way between them ceases to be visible in the superposed curves, the maximum number  $N_{max}$  of identified peaks is given by:

$$N_{max} < \frac{R^2}{4}, \quad (14)$$

where it has been assumed the width of the peaks to grow as the squared root of the number of cells (as confirmed by the data reported in Fig. 5).

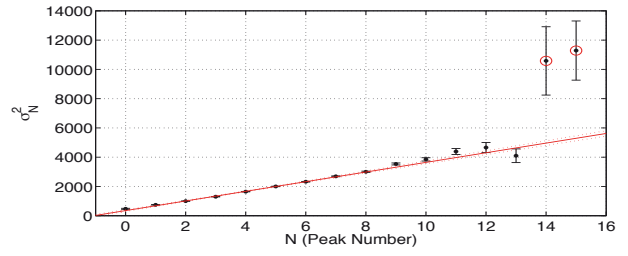


Fig. 5: Peaks width for the spectrum Fig.2 by a multi-Gaussian fit. The dash lines represent the 95% C.L. for the fit, shown with the solid line. The circles indicate the outliers.

The outliers, the data points that are statistically inconsistent with the rest of the data, are identified with the Thompson Tau method [19] and discarded.

A typical plot of the resolving power versus the bias voltage is presented in Fig. 6. The optimal biasing value corresponds to the maximum resolution in the plot and it is used as a working point. After the sensor calibration, spectra for different light intensities are recorded and analyzed as reported below.

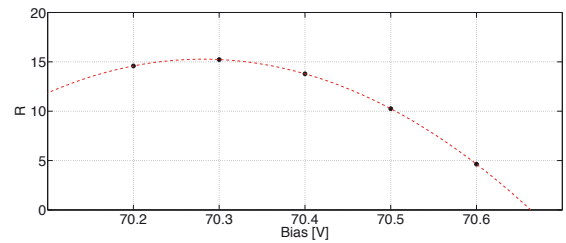


Fig. 6: Scan of the resolution power R as a function of the bias voltage at fixed temperature (25°C) and light intensity. The working point is given by a polynomial fit and equal to 70.28 V.

TABLE II: Acquisition parameters for the reference run presented in this work.

$V_{bias}$ [V]	GateWidth [ns]	Trigger frequency [kHz]	Temperature [°C]
70.3	300	100	25.0

### B. Multi-peak spectrum analysis

Spectra recorded in response to photons impacting on the sensor can be seen as a superposition of Gaussians, each

<sup>1</sup><http://www.hamamatsu.com/>.



corresponding to a well defined number of fired cells. The key point in the analysis technique is the estimation of the area underneath every peak, allowing the reconstruction of the probability density functions.

Initially, areas can be estimated by a *Pick&Play* (hereafter, P&P) procedure on the spectrum. In fact, a binned Gaussian distribution of  $N_{pk}$  events may be written as:

$$y_i = y(x_i) = y_{max} e^{-\frac{(x_i - x_0)^2}{2\sigma^2}}, \quad (15)$$

where  $y(x_i)$  is the number of events in the bin centered on  $x_i$  and  $y_{max}$  is the peak value, measured in  $x_0$ . Since  $y_{max} = N_{pk}/(\sigma\sqrt{2\pi})$ , knowing the content of the bin centered in  $x_0$  and estimating  $\sigma$  leads to  $N_{pk}$ . The standard deviation can also be calculated in a simple way by the Full Width at Half Maximum (*FWHM*), obtained searching for the position of the bins with a content equals to  $y_{max}/2$  and presuming that  $FWHM = 2.355 \times \sigma$ . Advantages and limitations of this method are quite obvious: its applicability is straightforward and essentially requires no tool beyond a Graphical User's Interface (*GUI*) for the control of the set-up; on the other hand, it can be applied only to peaks with a limited overlap and uncertainties can only be obtained by repeating the experiment. In order to overcome these limitations, a *Multi-Gaussian Fit* (MGF) procedure was implemented in MATLAB to analyze the full spectrum, according to the following work flow:

- **Initialization.** Robustness and efficiency of minimization algorithms is guaranteed by having an educated guess of the parameter values and by defining boundaries in the parameter variation, a procedure increasingly important as the number of parameters grow. Initial values are provided in an iterative procedure:
  - The user is required to identify by pointing & clicking on the spectrum the peak values and their position for 3 neighboring Gaussians, fitted to improve the estimate.
  - Initial values for every Gaussian are estimated by relying on the peak-to-peak distance from the previous step, presuming the signal from the 0-cell peak to be centered in the origin of the horizontal scale and assuming the standard deviation grows as the squared root of the number of cells.
- **Fit.** Spectra are fitted to a superposition of Gaussians with a non-linear  $\chi^2$  minimization algorithm presuming binomial errors in the content of every bin. The most robust convergence over a large number of tests and conditions have been empirically found bounding parameters to vary within 20% of the initial value for the peak position, 30% for the area and 50% for the standard deviation.

## V. RESULTS AND DISCUSSIONS.

Exemplary spectra for three light intensities were recorded and the raw data distributions are shown in Fig. 7, where the horizontal scale in ADC channels measures the integrated charge in a pre-defined gate. In the following, the analysis steps are detailed for the distribution corresponding to the highest mean photon number, hereafter identified as the *Reference Spectrum*. Remaining spectra will be used to assess the robustness of the approach and the validity of the model, with the results summarized at the end of the section.

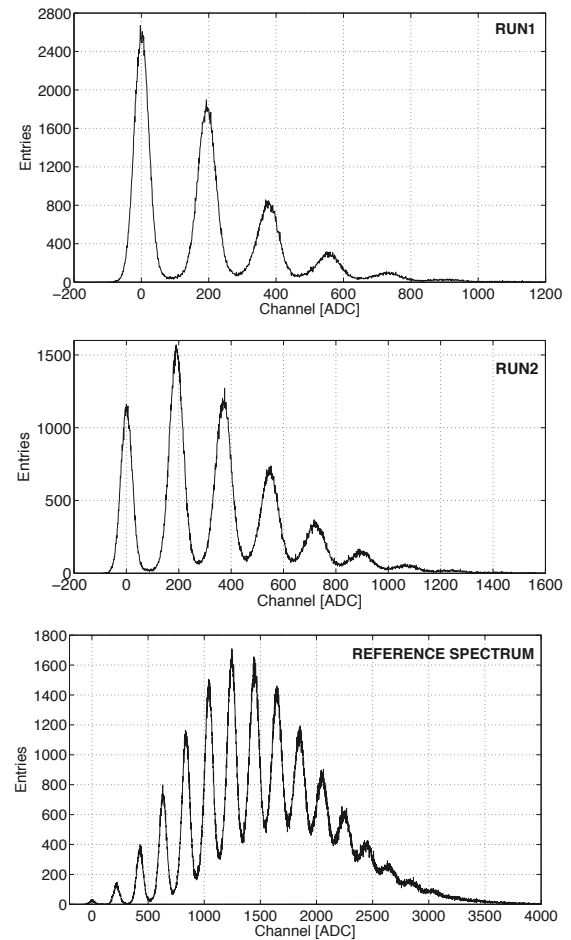


Fig. 7: Exemplary spectra. The mean number  $\mu_{MI}$  of photo-electrons is measured to be  $1.080 \pm 0.002$  (RUN1),  $1.994 \pm 0.003$  (RUN2) and  $7.81 \pm 0.01$  (Reference Spectrum).

Spectra are seen as a superposition of Gaussians, with parameters estimated according to the methods introduced in Section IV. The outcome of the procedures for the *Reference Spectrum* is reported in Table III for the P&P and the MGF procedures. For the former, uncertainties in the estimated parameters are the standard deviations from five data sets acquired in identical conditions while for the latter errors result from the fitting procedure (Fig. 8).

The characteristics of the experimental distribution can initially be studied referring to the mean number of fired cells. A *Model Independent* (MI) estimate is provided by:

$$\mu_{MI} = \frac{\overline{ADC}}{\Delta_{pp}}, \quad (16)$$

where

$$\overline{ADC} = \frac{\sum_i y_i ADC_i}{\sum_i y_i} \quad (17)$$

is the mean value of the experimental distribution (being  $y_i$  the number of events for the  $i^{th}$  bin) and  $\Delta_{pp}$  is the mean peak-to-peak distance, defining the gauge to convert values in ADC channels to number of cells.

TABLE III: Peak position, width and experimental probability of having N photo-electrons from the Pick&Play (P&P) procedure, compared to the results from the Multi-Gaussian Fit (MGF). The results are for the reference spectrum.

N	PeakPosition[ADC]		PeakWidth[ADC]		Exp. Probability	
	P&P	MGF	P&P	MGF	P&P	MGF
0	3 ± 1	2.1 ± 0.9	22 ± 1	21.7 ± 0.8	0.092 ± 0.006	0.09 ± 0.01
1	220 ± 1	220.1 ± 0.4	25 ± 1	27.3 ± 0.3	0.53 ± 0.02	0.56 ± 0.01
2	427 ± 1	428.0 ± 0.3	30 ± 1	31.5 ± 0.2	1.75 ± 0.06	1.86 ± 0.02
3	635 ± 1	633.6 ± 0.2	32 ± 1	36.0 ± 0.2	3.8 ± 0.1	4.17 ± 0.02
4	838 ± 2	837.5 ± 0.2	38 ± 1	40.5 ± 0.2	7.0 ± 0.2	7.21 ± 0.04
5	1044 ± 2	1041.3 ± 0.2	41 ± 1	44.7 ± 0.2	9.9 ± 0.2	10.30 ± 0.04
6	1247 ± 2	1243.7 ± 0.2	45 ± 1	48.2 ± 0.2	12.2 ± 0.3	12.67 ± 0.05
7	1449 ± 3	1445.6 ± 0.2	50 ± 3	51.9 ± 0.3	13.4 ± 0.8	13.43 ± 0.06
8	1650 ± 4	1645.8 ± 0.3	57 ± 2	54.8 ± 0.4	13.3 ± 0.5	12.71 ± 0.07
9	1853 ± 4	1846.4 ± 0.4	67 ± 2	59.5 ± 0.6	12.9 ± 0.4	11.2 ± 0.1
10	---	2046.5 ± 0.6	---	62.0 ± 0.9	---	8.7 ± 0.1
11	---	2245 ± 1	---	66 ± 2	---	6.6 ± 0.2
12	---	2445 ± 1	---	68 ± 2	---	4.4 ± 0.2
13	---	2632 ± 2	---	65 ± 3	---	2.4 ± 0.1

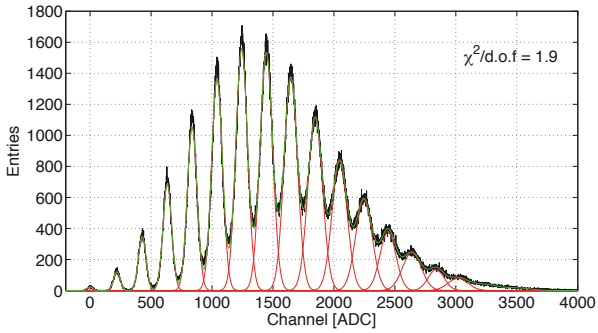


Fig. 8: Outcome of the MGF procedure. Individual Gaussians are in red, while their superposition is displayed in green. The  $\chi^2/d.o.f.$  measures the fit quality.

The value of  $\mu_{MI}$  can be compared to what is estimated presuming a pure Poissonian behaviour and referring to the probability  $P(0)$  of having no fired cell when the expected average value is  $\mu_{ZP}$ , where ZP stands for *Zero Peak*:

$$\mu_{ZP} = -\ln(P(0)) = -\ln\left(\frac{A_0}{A_{tot}}\right), \quad (18)$$

being  $A_0$  the area underneath the first peak of the spectrum and  $A_{tot}$  the total number of recorded events. Results are shown in Table IV.

TABLE IV: Estimates of the mean number of fired cells by the average value of the experimental distribution and from the probability of having none, assuming an underlying Poissonian distribution. Errors result from the uncertainties in the peak-to-peak distance and in the area of the zero-cell peak.

	$\mu_{MI}$	$\mu_{ZP}$
P&P	7.6 ± 0.3	6.99 ± 0.06
MGF	7.81 ± 0.01	7.08 ± 0.03

The P&P procedure shows a good compatibility with the hypothesis, while the MGF procedure, due to the smaller errors, presents an evident discrepancy.

The question can be further investigated considering the full distribution and comparing the experimental probability density function with the assumed model distribution by a  $\chi^2$  test, where:

$$\chi^2 = \sum_{k=0}^{N_{peaks}-1} w_k \times (A_{obs,k} - A_{model,k})^2, \quad (19)$$

being  $A_{obs,k}$  the number of events in the  $k^{th}$  peak of the distribution,  $A_{model,k}$  the corresponding number estimated from the reference model and  $w_k$  the weights accounting for the uncertainties in the content of every bin. Presuming a Poissonian distribution with mean value  $\mu_{MI}$ , the returned values of the  $\chi^2/d.o.f.$  are  $\approx 20$  for the P&P procedure and  $\approx 300$  for the MGF. The  $\chi^2/d.o.f.$  values, even assuming  $\mu$  as a free parameter, exceeds the 99% C.L. for both methods confirming that the experimental distribution may not be adequately described by a pure Poissonian model.

As a further step, the spectra were compared to the  $P \otimes G$  distribution model introduced in Section III, Eq. 10, where the actual number of fired cells results from avalanches triggered by the incoming photons and by the optical cross-talk. The optimal values of the model parameters, namely the cross-talk probability  $\epsilon_{XT}$  and the mean value  $\mu$  of the distribution of cells fired by photons, are determined by a grid search according to the following iterative procedure [20] :

- the  $\chi^2/d.o.f.$  surface, henceforth referred to as  $\Sigma$ , is sliced with planes orthogonal to the  $\epsilon_{XT}$  dimension, at values  $\tilde{\epsilon}_{XT}$  changed with constant step;
- in each slice, the minimum of the  $\Sigma(\tilde{\epsilon}_{XT}, \mu)$  curve is searched and the value  $\mu_{min,0}$  corresponding to the minimum is identified;
- the  $\Sigma(\epsilon_{XT}, \mu_{min,0})$  curve is scanned and the position  $\epsilon_{XT}^*$  of the minimum is identified by a local parabolic

fit, to overcome the limitations by the choice of the step in the grid;

- the procedure is repeated for  $\Sigma(\epsilon_{XT}^*, \mu)$  vs  $\mu$ , leading to the determination of the minimum in  $\mu^*$ .

This method leads to estimate the optimal parameters  $\mu^*$  and  $\epsilon_{XT}^*$  by the minimization of the  $\chi^2/d.o.f.$  surface for the two variables  $\mu$  and  $\epsilon_{XT}$  independently. The surface  $\Sigma$  and the  $\Sigma(\epsilon_{XT}^*, \mu)$  and  $\Sigma(\mu^*, \epsilon_{XT})$  curves are shown in Fig. 9. Uncertainties are calculated assuming a parabolic shape of the  $\chi^2/d.o.f.$  curves, leading to variances estimated by the inverse of the coefficient of the quadratic term [20], [21]. The results for the reference spectrum are  $\mu^* = 7.06 \pm 0.02$  and  $\epsilon_{XT}^* = 0.090 \pm 0.004$ .

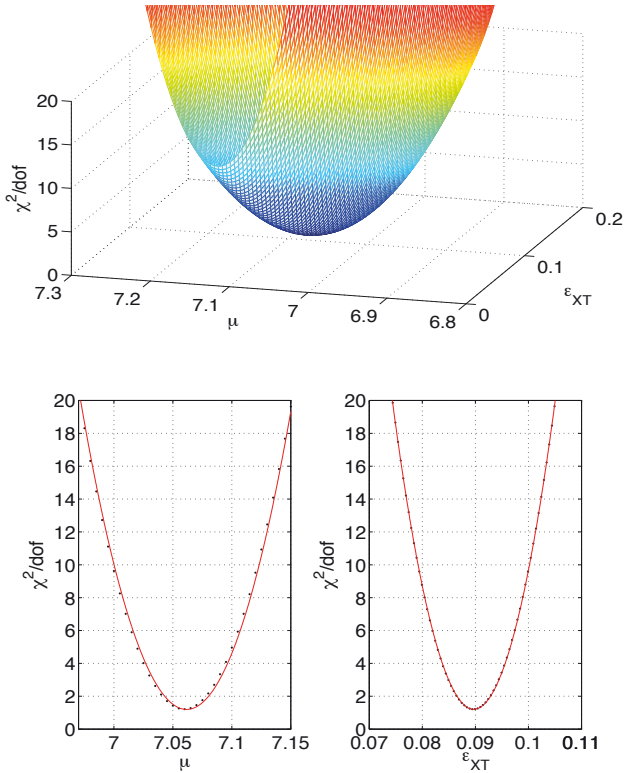


Fig. 9:  $\chi^2/d.o.f.$  surface (top panel) and parabolic behavior nearby its minimum (bottom).

In order to account for the two-parameter correlation in the calculation of the uncertainties, it is worth to referring to the *confidence region* of the joint probability distribution [22] [23]. When the parameters are estimated minimizing the  $\chi^2$  distribution, confidence levels correspond to regions defined by iso- $\chi^2$  curves. For two parameters, the region assumes an elliptic shape around the  $\Sigma$  minimum,  $\chi_{\min}^2$ . The  $\Sigma$  contour at the constant value of  $\chi_{\min}^2 + 1$  plays a crucial role due to its specific properties. In fact, the resulting ellipse contains  $\sim 38.5\%$  of the joint parameter probability distribution and

its projections represent the  $\sim 68.3\%$  of confidence interval for each parameter ( $\sigma_1$  and  $\sigma_2$ ). In addition, the correlation  $\rho$  among the parameters may be written as:

$$\rho = \frac{\sigma_1^2 - \sigma_2^2}{2\sigma_1\sigma_2} \tan 2\theta, \quad (20)$$

where  $\theta$  represents the counter-clockwise rotation angle of the ellipse. The detailed demonstration is reported in Appendix C.

In this specific case, the  $\chi_{\min}^2$  value is determined evaluating the  $\chi^2/d.o.f.$  surface at the point of coordinates  $(\mu^*, \epsilon_{XT}^*)$  while the  $\Sigma$  contour at  $\chi_{\min}^2 + 1$  is shown in Fig.10 (black crosses). The fit curve (red line) returns the value of the ellipse center  $(\mu^0, \epsilon_{XT}^0)$  (black circle). The projections of the ellipse on the  $\mu$  and  $\epsilon_{XT}$  axes are the uncertainties on the two values. The results for the reference spectrum are  $\mu^0 = 7.06 \pm 0.05$  and  $\epsilon_{XT}^0 = 0.09 \pm 0.01$ . Comparing these values with  $(\mu^*, \epsilon_{XT}^*)$  (black cross) it is possible to infer that the correlation does not affect the determination of the parameter central values while increases their standard deviation by a factor of about two. As a consequence,  $\mu^0$  and  $\epsilon_{XT}^0$  with their uncertainties are retained as the best estimate of the model parameter values.

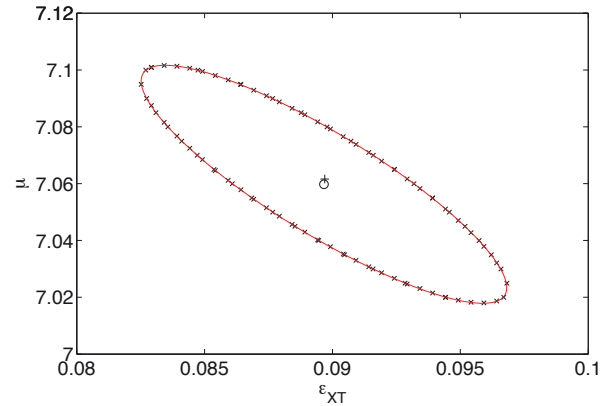


Fig. 10: The point of the  $\chi^2/d.o.f.$  surface at the constant value of  $\chi_{\min}^2 + 1$  are the black crosses, the fit curve is the red line, the center of the ellipse  $(\mu^0, \epsilon_{XT}^0)$  is represented with the black circle and the point  $(\mu^*, \epsilon_{XT}^*)$  is shown with the black cross.

The angle returned by the ellipse fit is used to calculate the correlation  $\rho$  between the two parameters through the equation (20). The result for the reference spectrum is  $\rho = -0.8$ . Then, applying the relation (11) and exploiting the full covariance matrix, the value and the uncertainty of the mean of the  $P \otimes G$  model can be obtained. For the reported spectra it results to be  $7.76 \pm 0.03$ .

The result of the fit to the data distribution with the  $P \otimes G$  probability function is displayed in Fig. 11, showing an excellent agreement between data and model.

The quality of the result is confirmed by the data reported in Table V, where the mean value of the Poissonian distribution obtained by the ellipse fit ( $\mu^0$ ) and by the *Zero Peak* are compared, together with a comparison between  $\mu_{MI}$  and  $\mu^0/(1 - \epsilon_{XT}^0)$ , the mean value of the  $P \otimes G$  distribution.



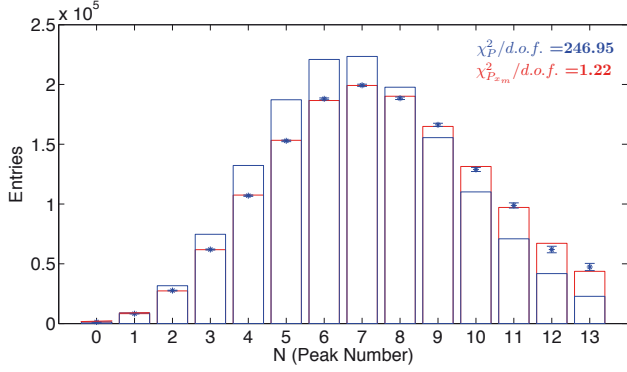


Fig. 11: Data from the reference spectrum are compared to a simple Poissonian model with mean value  $\mu_{ZP}$  (blue) and to the  $P \otimes G$  model (red), accounting for the optical cross-talk. The  $\chi^2$  value rule out the former at 99% C.L..

TABLE V: Estimates of the mean number of fired cells for  $P \otimes G$  model.

	$\mu^0$	$\mu_{ZP}$
Mean Value of the Poissonian distribution	$7.06 \pm 0.05$	$7.08 \pm 0.03$
	$\mu_{MI}$	$\mu^0/(1 - \epsilon_{XT}^0)$
Mean Number of Fired Cells	$7.81 \pm 0.01$	$7.76 \pm 0.03$

Results by the other recorded spectra are summarized in Table VI and Fig. 12 for the MGF procedure, confirming the validity of the compound Poissonian model and the need to account for detector effects to have a proper understanding of the phenomenon being investigated.

TABLE VI: Estimate of the mean number of fired cells with the  $P \otimes G$  model using the RUN1 and RUN2 data-sets. Also in this case, the  $P \otimes G$  model shows an agreement at the 99% C.L.. The measured  $\chi^2$  is 12.6 for the RUN1 and 12.0 for the RUN2 respectively.

	$\mu^0$	$\mu_{ZP}$
Mean Value of the Poissonian distribution	$0.97 \pm 0.01$	$0.985 \pm 0.002$
	$1.82 \pm 0.01$	$1.823 \pm 0.004$
	$\mu_{MI}$	$\mu^0/(1 - \epsilon_{XT}^0)$
Mean Number of Fired Cells	$1.080 \pm 0.002$	$1.08 \pm 0.01$
	$1.994 \pm 0.003$	$1.99 \pm 0.01$

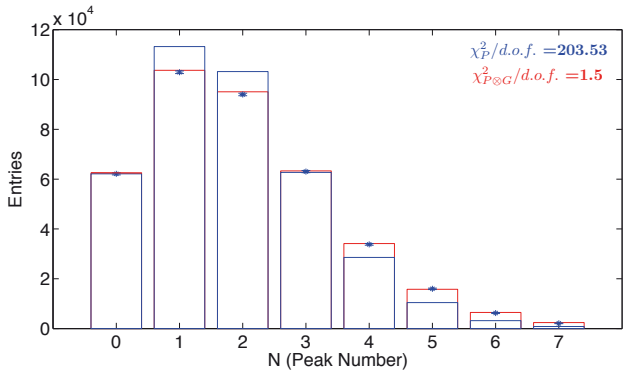
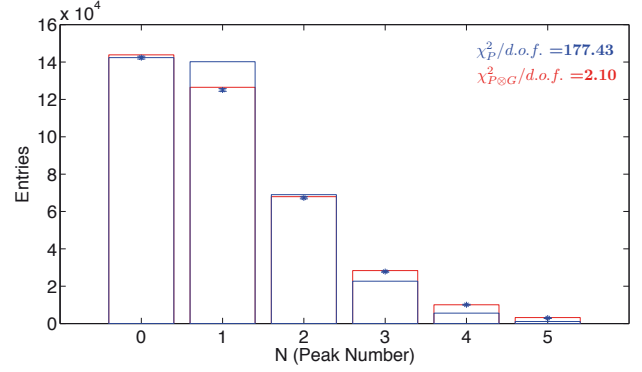


Fig. 12: Results of the MGF procedure on the low and middle intensity, RUN1 and RUN2. The pure Poissonian model with mean value  $\mu_{ZP}$  (blue) is compared to the  $P \otimes G$  model (red).

## VI. CONCLUSION

Instruments and methods for the investigation of the statistical properties of the light emitted by an incoherent source have been developed and validated. The experimental set-up is based on Silicon Photomultipliers, state-of-the art light detectors, embedded into a flexible, modular, easy-to-use kit. Methods fold the characteristics of the emitted light and the detector response, with an increasing level of refinement. The model development allows to address advanced topics in statistics and data analysis techniques, targeted to master students in Physics or Engineering.

## ACKNOWLEDGMENT

The research reported here has been developed in the framework of a Joint Development Project between CAEN S.p.A. and Università degli Studi dell'Insubria. The analysis code developed by the authors in MATLAB® is made available to interested users.

## REFERENCES

- [1] B. Dolgoshein et al., *Status report on silicon photomultiplier development and its applications*. Nucl. Instrum. Methods Phys. Res. A 563, 368376. 2006.
- [2] P. Buzhan et al., *Silicon photomultiplier and its possible applications*. Nucl. Instr. And Meth. A 504, 48-52. 2003.
- [3] D. Renker, *Geiger-mode avalanche photodiodes, history, properties and problems*, 2006, Nuclear Instruments and Methods in Physics Research A, 567, 48.
- [4] C. Piemonte, *A new Silicon Photomultiplier structure for blue light detection*, 2006, Nuclear Instruments and Methods in Physics Research A, 568, 224.
- [5] P. Eckert, H.-C. Schultz-Coulon, W. Shen, R. Stamen & A. Tadday, *Characterisation studies of silicon photomultipliers*, 2010, Nuclear Instruments and Methods in Physics Research A, 620, 217.
- [6] Y. Musienko, S. Reucroft & J. Swain, *The gain, photon detection efficiency and excess noise factor of multi-pixel Geiger-mode avalanche photodiodes*, 2006, Nuclear Instruments and Methods in Physics Research A, 567, 57.
- [7] Y. Du & F. Retière, *After-pulsing and cross-talk in multi-pixel photon counters*, 2008, Nuclear Instruments and Methods in Physics Research A, 596, 396.
- [8] P. Buzhan, B. Dolgoshein, A. Ilyin, V. Kantserov, V. Kaplin, A. Karakash, A. Pleshko, E. Popova et al., *An advanced study of silicon photomultiplier*, ICFA Instrum. Bull. **23** (2001) 28.
- [9] M. Ramilli, A. Allevi, V. Chmili & al., *Photon-number statistics with silicon photomultipliers*, 2010, Journal of the Optical Society of America B Optical Physics, 27, 852.
- [10] I. Afek, A. Natan, O. Ambar & Y. Silberberg, *Quantum state measurements using multipixel photon detectors*, 2009, Phys. Rev. A **79**, 043830.
- [11] ...
- [12] S. Vinogradov, *Analytical models of probability distribution and excess noise factor of solid state photomultiplier signals with crosstalk*, 2012, Nuclear Instruments and Methods in Physics Research A, 695, 247.
- [13] S. Vinogradov et al. *Probability distribution and noise factor of solid state photomultiplier signals with cross-talk and afterpulsing*, Nuclear Science Symposium Conference Record (NSS/MIC), 2009 IEEE.
- [14] <http://www.caentechnologies.com/csite/CaenProd.jsp?showLicence=false&parent=10&idmod=719>.
- [15] <http://www.caen.it/csite/CaenProd.jsp?parent=14&idmod=624>.
- [16] <http://www.caentechnologies.com/servlet/checkCaenManualFile?Id=7624>.
- [17] A. Vacheret, G. J. Barker, M. Dziewiecki & al., *Characterization and simulation of the response of Multi-Pixel Photon Counters to low light levels*, 2011, Nuclear Instruments and Methods in Physics Research A, 656, 69.
- [18] C. M. Sparrow, *On spectroscopic resolving power*, Astrophys. J. 44, 7686 (1916).
- [19] nnnn
- [20] L. Lyons, *Statistics For Nuclear And Particle Physicists*, Cambridge, UK: Univ. Pr. (1986).
- [21] P. R. Bevington & D. K. Robinson, *Data reduction and error analysis for the physical sciences*, 3rd ed., 2003.
- [22] W. H. Press, *Numerical Recipes in C: The Art of Scientific Computing*, Cambridge University Press; 2nd ed., 1992.
- [23] G. Cowan, *Statistical Data Analysis*, Clarendon Press, Oxford Science Publications, 1998.

## APPENDIX A

In this appendix it is demonstrated that the convolution of a Poissonian distribution of mean value  $\lambda$  (3) and a Binomial probability  $\eta$  (4) results in a Poissonian distribution of mean value  $\lambda\eta$ :

- Multiplying and dividing by  $\eta^n$  each element in the series, Eq. 5 can be written as:

$$P_{d,el} = \sum_{n=d}^{\infty} B_{d,n}(\eta) P_{n,ph}(\lambda) = \sum_{n=d}^{\infty} \frac{(\lambda\eta)^n \eta^{d-n} (1-\eta)^{n-d} e^{-\lambda}}{d!(n-d)!}.$$

- Hence, defining  $n - d = z$ :

$$\begin{aligned} P_{d,el} &= \sum_{z=0}^{\infty} (\lambda\eta)^{d+z} \left( \frac{1-\eta}{\eta} \right)^z \frac{e^{-\lambda}}{d!z!} = \\ &= \frac{(\lambda\eta)^d e^{-\lambda}}{d!} \times \sum_{z=0}^{\infty} \frac{(\lambda\eta)^z}{z!} \left( \frac{1-\eta}{\eta} \right)^z = \\ &= \frac{e^{-\lambda} (\lambda\eta)^d}{d!} \times \sum_{z=0}^{\infty} \frac{(\lambda - \lambda\eta)^z}{z!}. \end{aligned}$$

- The series actually corresponds to the Taylor expansion of  $e^{\lambda - \lambda\eta}$ , so that:

$$P_{d,el} = \sum_{n=d}^{\infty} B_{d,n}(\eta) P_{n,ph}(\lambda) = \frac{e^{-\lambda\eta} (\lambda\eta)^d}{d!}$$

## APPENDIX B

This appendix is dedicated to the demonstration of the relations for the probability density function (10), the mean value and variance (11) of the total fired cell number  $m$  assuming that every primary events can generate a unique infinite chain of secondary pulses.

This purpose is pursued by applying the probability generating function definition and properties.

For a discrete random variable  $\phi$ , the generating function is defined as:

$$\tilde{\Phi}(s) = \sum_{i=0}^{\infty} P(\phi = i) \times s^i.$$

The probability distribution function, the mean and the variance of the random variable  $\phi$  can be calculated as:

$$\Phi(\phi = m) = \frac{1}{m!} \times \left. \frac{d^m \Phi}{ds^m} \right|_0 \quad (21)$$

$$\bar{m}_\Phi = \Phi(1) \quad (22)$$

$$\sigma_\Phi^2 = \Phi(1)'' + \Phi(1)' - [\Phi(1)']^2. \quad (23)$$

The random variable considered here is the total number of detected pulses,  $m$ . Because it is defined by a sum of discrete random variables, its generating function is the composition of the pure Poisson distribution generating function:

$$\tilde{P}(s) = e^{\mu(s-1)}$$

and of the geometric distribution generating function:

$$\begin{aligned} \tilde{G}(s) &= \sum_{i=1}^{\infty} P(g = i - 1) \times s^i \\ &= \sum_{i=1}^{\infty} \epsilon_{XT}^{i-1} \times (1 - \epsilon_{XT}) \times s^i \\ &= \frac{(1 - \epsilon_{XT})s}{1 - \epsilon_{XT}s}. \end{aligned}$$

Finally, the analytical expression of the generating function for the total number of fired cells result to be:

$$\begin{aligned} \tilde{P} \circ \tilde{G} &= \tilde{P}(\tilde{G}(s)) \\ &= e^{\mu(\tilde{G}(s)-1)} \\ &= e^{\mu\left(\frac{s-1}{1-\epsilon_{XT}s}\right)}. \end{aligned}$$

Using the relation (21) it is possible to derive the probabilities to detect an arbitrary number of total pulses. For 0, 1 and 2 events the result is:

$$P \otimes G(0) = e^{-\mu},$$

$$P \otimes G(1) = e^{-\mu} \mu (1 - \epsilon_{XT}),$$

$$P \otimes G(2) = e^{-\mu} \left[ \mu(1 - \epsilon_{XT})\epsilon_{XT} + \frac{\mu^2(1 - \epsilon_{XT})^2}{2} \right].$$

An analysis of these expressions lead to the compact and general formula reported in (10), which refers to the compound Poisson distribution and is valid for  $m=0, 1, 2, \dots$ . In addition, applying the properties (22) and (23) at  $\tilde{P} \circ \tilde{G}$ , it is possible to obtain the mean value and the variance of the distribution of the total number of fired cells, as expressed by the relations in (11).

#### APPENDIX C: THE COVARIANCE ELLIPSE

In this appendix the confidence region of two variables is demonstrated to assume the shape of an ellipse. Moreover, the relation between the parameters describing the ellipse, the standard deviation of the variables and their correlation is established.

The joint probability density of two variables  $x^T = [x_1, x_2]$  gaussian distributed may be written as:

$$P(x) = k \cdot \exp\left\{-\frac{1}{2}(x - \mu)^T C^{-1}(x - \mu)\right\}, \quad (24)$$

where  $k$  is a normalization constant,  $\mu^T = [\mu_1, \mu_2]$  is the vector of the mean values of  $x$  and  $C$  is the covariance matrix:

$$C = E\{(x - \mu)(x - \mu)^T\} = \begin{bmatrix} \sigma_1^2 & \sigma_{12} \\ \sigma_{21} & \sigma_2^2 \end{bmatrix}.$$

The diagonal elements of  $C$  are the variances of the variables  $x_i$  and the off-diagonal elements represent their covariance, which can be expressed as:

$$\sigma_{12} = \rho \sigma_1 \sigma_2,$$

where  $\rho$  is the correlation coefficient.

Curves of constant probability are determined by requiring the exponent of the equation (24) to be constant:

$$(x - \mu)^T C^{-1}(x - \mu) = c \quad (25)$$

$$\frac{(x_1 - \mu_1)^2}{\sigma_1^2} - 2\rho \frac{(x_1 - \mu_1)}{\sigma_1} \frac{(x_2 - \mu_2)}{\sigma_2} + \frac{(x_2 - \mu_2)^2}{\sigma_2^2} = c',$$

where  $c' = c(1 - \rho^2)$ . This equation represents an ellipse with the center located at  $(\mu_1, \mu_2)$  and the semi-axes placed at an angle  $\theta$  with respect to the  $x_1, x_2$  axes.

As shown in the following, the equation (25) can be rewritten as a sum of squares of two stochastically independent variables, which results to be  $\chi^2$  distributed with two degrees of freedom:

$$\frac{\xi_1^2}{a^2} + \frac{\xi_2^2}{b^2} = \chi^2. \quad (26)$$

This relation describes an ellipse centered in the origin of the reference system and with the semi-axes of length  $a, b$  parallel to the  $\xi_1, \xi_2$  axes.

As a first step, the origin of the reference system is translated in the center of the ellipse, resulting in equation:

$$\tilde{x}^T C^{-1} \tilde{x} = c, \quad (27)$$

where  $\tilde{x} = x - \mu$ .

As a second step, axes are rotated in order to coincide with the  $(\xi_1, \xi_2)$  reference system by the transformation:

$$\tilde{x} = Q^T \xi,$$

where

$$Q = \begin{bmatrix} \cos \theta & \sin \theta \\ -\sin \theta & \cos \theta \end{bmatrix}.$$



As a consequence, equation (27) is turned to the form

$$\xi^T Q C^{-1} Q^T \xi = c,$$

corresponding to the equation (26) as long as

$$Q C^{-1} Q^T = \begin{bmatrix} \frac{1}{a^2} & 0 \\ 0 & \frac{1}{b^2} \end{bmatrix},$$

or, equivalently,

$$Q C Q^T = \begin{bmatrix} a^2 & 0 \\ 0 & b^2 \end{bmatrix}.$$

The vector of the mean values and the covariance matrix of  $\xi$  results to be:

$$\begin{aligned} \mu_\xi &= E\{\xi\} = Q E\{x\} = Q \mu \\ C_\xi &= E\{(\xi - \mu_\xi)(\xi - \mu_\xi)^T\} \\ &= Q E\{(x - \mu)(x - \mu)^T\} Q^T \\ &= Q C Q^T \end{aligned} \quad (28)$$

So it can be noticed that the eigenvalues of the covariance matrix  $C_\xi$  correspond to the squared semi-axes of the canonical ellipse (26).

Because of the symmetry of the covariance matrix,  $C$  can be diagonalized exploiting its decomposition in eigenvalues and eigenvectors:

$$C = U \Lambda U^T,$$

where  $\Lambda$  is the diagonal matrix of eigenvalues and  $U$  is the rotation matrix constituted by eigenvectors. Comparing this formula with the expression (28) and using the properties of the rotation matrix ( $Q Q^T = Q^T Q = I$ ,  $\det Q = 1$ ) it can be inferred that:

$$U = Q^T \quad \Lambda = C_\xi.$$

As a consequence, the eigenvalues of  $C$  can be obtained through the quadratic equation:

$$\det(C - \lambda I) = 0,$$

whose solutions are:

$$\lambda_{1,2} = \frac{1}{2} \left[ (\sigma_1^2 + \sigma_2^2) \pm \sqrt{(\sigma_1^2 + \sigma_2^2)^2 - 4\sigma_1^2\sigma_2^2(1 - \rho)} \right].$$

The lengths of the ellipse semi-axes result to be the square root of the eigenvalues multiplied by the two degrees of freedom  $\chi^2$  value:

$$a = \sqrt{\chi^2 \lambda_1} \quad b = \sqrt{\chi^2 \lambda_2}. \quad (29)$$

The eigenvectors of  $C$  can be found with the following equation:

$$(C - \lambda_i I) u_i = 0, \quad \text{with } i = 1, 2.$$

For  $i = 1$ :

$$\begin{bmatrix} \sigma_1^2 - \lambda_1 & \rho\sigma_1\sigma_2 \\ \rho\sigma_1\sigma_2 & \sigma_2^2 - \lambda_1 \end{bmatrix} \begin{bmatrix} u_{1,1} \\ u_{1,2} \end{bmatrix} = 0,$$

and the solution is:

$$u_1 = \alpha_1 \begin{bmatrix} -\rho\sigma_1\sigma_2 \\ \sigma_1^2 - \lambda_1 \end{bmatrix},$$

where  $\alpha_1$  is a normalization constant. In the case of  $i = 2$ :

$$\begin{bmatrix} \sigma_1^2 - \lambda_2 & \rho\sigma_1\sigma_2 \\ \rho\sigma_1\sigma_2 & \sigma_2^2 - \lambda_2 \end{bmatrix} \begin{bmatrix} u_{2,1} \\ u_{2,2} \end{bmatrix} = 0,$$

and the solution is:

$$u_2 = \alpha_2 \begin{bmatrix} \sigma_2^2 - \lambda_2 \\ -\rho\sigma_1\sigma_2 \end{bmatrix},$$

where  $\alpha_2$  is the normalization constant. Using the eigenvalues definition, it can be proved that  $\sigma_2^2 - \lambda_2 = -(\sigma_1^2 - \lambda_1)$ . As a result, the  $U$  matrix turns out to be equal to  $Q^T$ , with  $\cos \theta = -\rho\sigma_1\sigma_2$  and  $\sin \theta = \sigma_1^2 - \lambda_1$ . From these identities it is possible to calculate the angle  $\theta$  between the ellipse axis, which lies on  $\xi_i$ , and the  $x_i$  axis:

$$\tan \theta = -\frac{\sigma_1^2 - \lambda_1}{\rho\sigma_1\sigma_2}.$$

As  $\theta$  belongs to the range  $[-\pi/2, \pi/2]$  and the above expression is quite complex, it is more convenient to estimate the  $\tan 2\theta$ :

$$\tan 2\theta = \frac{2 \tan \theta_1}{1 - \tan^2 \theta_1} = \frac{2\rho\sigma_1\sigma_2}{\sigma_1^2 - \sigma_2^2}. \quad (30)$$

The angle  $\theta$  measures the rotation which brings the  $(x_1, x_2)$  coordinate system in the  $(\xi_1, \xi_2)$  reference system, which represent the rotation undergone by the ellipse. The rotation matrix  $Q$  has been completely determined and the ellipse has been entirely defined.

The covariance ellipse of the bivariate normal distribution assumes a particular importance when  $\chi^2 = 1$  and its features can be analyzed in two extreme cases:

- if the variables are not correlated ( $\rho = 0$ ), then  $\theta = 0$ ,  $a = \sigma_1$  and  $b = \sigma_2$ , which means that the ellipse axes are parallel to  $x_i$  and equal to the variable standard deviations,
- if the correlation is maximum ( $\rho = \pm 1$ ), then the ellipse degenerates into a straight line of length  $a = \sqrt{\sigma_1^2 + \sigma_2^2}$  (in fact  $b = 0$ ).

In all the intermediate cases the ellipse is inscribed in a rectangle of center  $(\mu_1, \mu_2)$  and sides  $2\sigma_1$  and  $2\sigma_2$ . The projections on the  $x_i$  axes of the four intersection points between the ellipse and the rectangle represent the 68% confidence interval for the parameter centered in the mean value  $\mu_i$ .

All these characteristics of the covariance ellipse can be demonstrated exploiting the conic equations. The general quadratic equation:

$$Ax_1^2 + Bx_1x_2 + Cx_2^2 + Dx_1 + Ex_2 + F = 0 \quad (31)$$

represents the canonical ellipse if  $B = 0$  and  $AC > 0$ . It is always possible to find a new coordinate system, rotated by an angle  $\theta$  with respect to the  $x_i$  axes, in which the equation does not involve the mixed variable product. Calling  $\xi_i$  the new set of axis, the  $x_i$  variables can be expressed as:

$$x_1 = \xi_1 \cos \theta - \xi_2 \sin \theta \quad x_2 = \xi_1 \sin \theta + \xi_2 \cos \theta.$$

Substituting these relations in (31) and collecting the similar terms a new equation in  $\xi_i$  can be obtained:

$$\begin{aligned} & \xi_1^2(A \cos^2 \theta + B \cos \theta \sin \theta + C \sin^2 \theta) + \\ & \xi_1 \xi_2(-2A \cos \theta \sin \theta + B(\cos^2 \theta - \sin^2 \theta) + 2C \sin \theta \cos \theta) + \\ & \xi_2^2(A \sin^2 \theta - B \cos \theta \sin \theta + C \cos^2 \theta) + \\ & \xi_1(D \cos \theta + E \sin \theta) + \xi_2(-D \sin \theta + E \cos \theta) + F = 0. \end{aligned} \quad (32)$$

In order to eliminate the  $\xi_1 \xi_2$  term, the angle  $\theta$  has to satisfy:

$$-2A \cos \theta \sin \theta + B(\cos^2 \theta - \sin^2 \theta) + 2C \sin \theta \cos \theta = 0.$$

Simplifying the equation:

$$\begin{aligned} 2(A - C) \cos \theta \sin \theta &= B(\cos^2 \theta - \sin^2 \theta) \\ \frac{2 \sin \theta \cos \theta}{\cos^2 \theta - \sin^2 \theta} &= \frac{B}{A - C} \\ \tan 2\theta &= \frac{B}{A - C} \end{aligned} \quad (33)$$

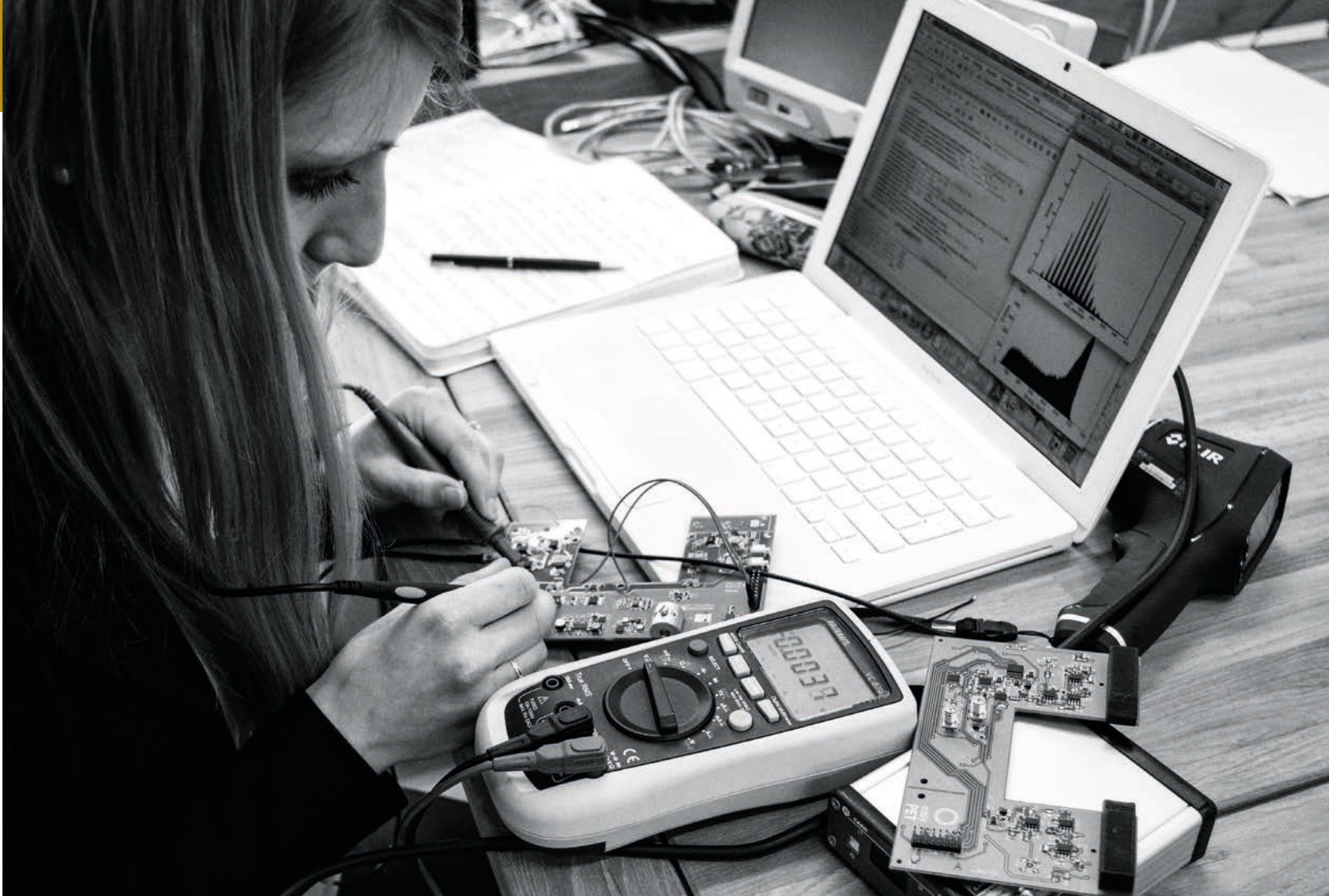
In the specific case corresponding to equation (25),

$$A = \frac{1}{\sigma_1^2} \quad B = -\frac{2\rho}{\sigma_1\sigma_2} \quad C = \frac{1}{\sigma_2^2}.$$

As a consequence the expression (33) assume the form of the relation (30). Finally, the coefficients of the second order variables in equation (32) have to be interpreted as the inverse square of the semi-axes lengths. Replacing the definition of  $A$ ,  $B$  and  $C$  and solving for  $a$  and  $b$  gives:

$$\begin{aligned} a &= \sqrt{\frac{\sigma_1^2 \sigma_2^2 (1 - \rho^2)}{\sigma_2^2 \cos^2 \theta - 2\rho \sigma_1 \sigma_2 \cos \theta \sin \theta + \sigma_1^2 \sin^2 \theta}} \\ b &= \sqrt{\frac{\sigma_1^2 \sigma_2^2 (1 - \rho^2)}{\sigma_2^2 \sin^2 \theta - 2\rho \sigma_1 \sigma_2 \cos \theta \sin \theta + \sigma_1^2 \cos^2 \theta}}. \end{aligned}$$

Expressing  $\theta$  as a function of  $\rho$  and  $\sigma_i$  it is possible to obtain for the semi-axes the same definition as found previously in equation (29).



## D.2 A simple and robust method to study after-pulses in Silicon Photomultipliers

ED3235

### Equipment

SP5600E - Educational Photon Kit and a Timing Unit

Model	SP5600	DT5720A	SP5601	SP5650A	DT993
Description	Power Supply and Amplification Unit	Desktop Digitizer 250 MS/s	LED Driver	Sensor Holder for SP5600 with SiPM	Dual Timer
					
	p. 93	p. 93	p. 94	p. 94	

### Ordering Options

Equipment	
Code	Description
WK5600XEAAAA	SP5600E - Educational Photon Kit
WDT993XAAAAA	DT993 - Dual Timer Desktop
or the all inclusive Premium Version	
WK5600XANAAA	SP5600AN - Educational Kit - Premium Version
WDT993XAAAAA	DT993 - Dual Timer Desktop



# A simple and robust method to study after-pulses in Silicon Photomultipliers

M. Caccia, R. Santoro, G. A. Stanizzi

**Abstract**—The after-pulsing probability in Silicon Photomultipliers and its time constant are obtained measuring the mean number of photo-electrons in a variable time window following a light pulse. The method, experimentally simple and statistically robust due to the use of the Central Limit Theorem, has been applied to an HAMAMATSU MPPC S10362-11-100C.

**Keywords**—Silicon Photo-Multipliers, after-pulses, Photon Statistics

## I. INTRODUCTION

Silicon Photomultipliers (SiPM) are state-of-the-art detectors of light consisting of a matrix of P-N junctions with a common output, with a density of cells up to  $\approx 10^4/\text{mm}^2$ . Each diode is operated in a limited Geiger-Muller regime in order to achieve gains at the level of  $\approx 10^6$  and to guarantee an extremely high homogeneity in the cell-to-cell response. Subject to the high electric field in the depletion zone, initial charge carriers generated by an absorbed photon or by thermal effects trigger an exponential charge multiplication by impact ionization. When the current spike across the quenching resistor induces a drop in the voltage across the junction, the avalanche is stopped. SiPM can be seen as a collection of binary cells, providing altogether an information about the intensity of the incoming light by counting the number of fired cells [1] - [4].

SiPM feature an unprecedented photon number resolving capability and offer relevant advantages due to the low operating voltage, the immunity to magnetic field, ruggedness and the design flexibility due to the Silicon Technology. However, they also suffer from drawbacks related to a significant temperature dependence of the gain and a high rate of spurious hits. The latter is due to thermally generated carriers (Dark Counts, DC), Optical Cross-Talk (OCT) and after-pulsing. The OCT is linked to photons generated during a primary avalanche, triggering simultaneous secondaries [3], [5]. The OCT is affected by the sensor design [3], [6] - [8] and strongly depends on the bias voltage. After-pulses are associated to the late release of a charge carrier that has been produced in the original avalanche and trapped by an impurity [3]. After-pulsing is essentially dependent on the sensor technology [3], [6], [8].

Dark Counts, Optical Cross-Talk and after-pulsing occur stochastically and introduce fluctuations in the multiplication process that contribute to deteriorate the resolution in both

photon counting and spectrometry. Moreover, after-pulsing may be critical in photon correlation experiments [9] - [11].

The after-pulsing effect has been investigated by various authors, relying on the time correlation of neighbouring pulses [12] - [14]. A simple and statistically robust method is proposed here, based on the sensor current integration and the use of the Central Limit Theorem to estimate the mean number of pulses in a variable time window.

## II. MATERIALS AND METHODS

After-pulses can be seen as an excess of fired cells in a time window following the signal due to a light pulse (Figure 1), where the excess is calculated with respect to Dark Counts occasionally appearing. A statistical analysis of the excess, varying the gate length, is expected to lead to a measurement of the after-pulsing probability and of its time constant.

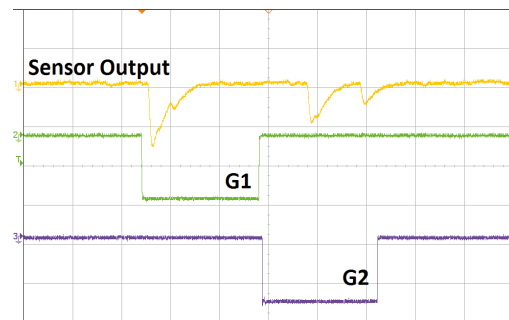


Fig. 1: The figure shows the response of the SiPM to a light burst, synchronised with the leading edge of the gate  $G_1$ . Pulses in the  $G_2$  gate may be due to both random Dark Counts and after-pulses. The exemplary event shown here features as well an after-pulse occurring during the recovery time of the sensor. The rate of Dark Counts is measured switching off the LED.

### A. Experimental setup

The block diagram of the experimental set-up is shown in Figure 2. A master clock is synchronising the light pulser illuminating the SiPM and the data acquisition, integrating the signal pulses in a variable duration gate  $G_2$  delayed with respect to the light pulse. Results reported here were obtained with the following specific system:

- An ultra-fast LED source (SP5601 - CAEN), emitting  $\approx 5 \text{ ns}$  long light pulses at  $405 \text{ nm}$ , with intensities in the 1-2000 photon range.

M. Caccia, R. Santoro, G. A. Stanizzi are with the Dipartimento di Scienza e Alta Tecnologia, Università degli Studi dell'Insubria, 22100, Como, Italy.

- The SP5600 - CAEN power supply and amplification unit, housing an Hamamatsu MPPC S10362-11-100C.
- A charge digitisation unit, either based on the CAEN - DT5720A waveform digitizer or on the CAEN - V792N QDC.
- A Dual-Timer (N93B - CAEN) to generate the integration gate.

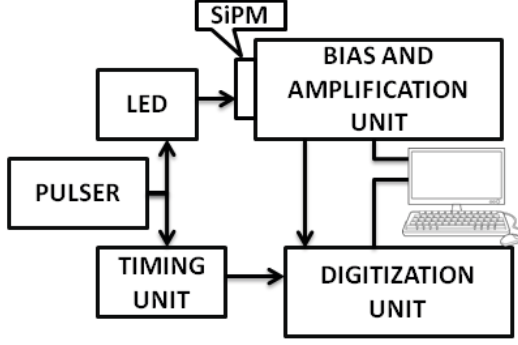


Fig. 2: Block diagram of the experimental setup for the after-pulsing characterization.

### B. Experimental procedure

The experimental procedure starts by defining two gates, synchronized to the light pulse (see Figure 1). The first gate  $G_1$  encompasses the time development of the signal due to a light pulse. The de-trapping of charge carriers within  $G_1$  originates avalanches piled-up with the signal from the light pulse and the probability for this to occur is inferred by studying the excess of pulses in a second variable gate  $G_2$ , following  $G_1$ . The estimation of the mean number of fired cells in  $G_2$  is obtained by the analysis of the spectrum of the released charge, provided integrating the sensor output current. Exemplary spectra for  $G_2 = 400 \text{ ns}$  are shown in Figure 3, with the LED switched ON and OFF. The peak positions identify the value of the digitized charge for the different number of avalanches while the peak areas measure the corresponding probability.

The spectra clearly show evidence of two statistics characterized by a different mean value. In order to obtain a quantitative information, the data were analysed as follows:

- The average charge  $\bar{Q}_N$  by a sequence of  $N$  events was retained as the main observable. According to the Central Limit Theorem,  $\bar{Q}_N$  is expected to be Gaussian distributed, with the advantage of an easy and robust way to estimate its value and to measure its uncertainty. The value of  $N$  was determined studying the evolution of the  $\bar{Q}_N$  distribution vs.  $N$  and fixing its value at 200, when it was shown to be asymptotically gaussian (Figure 4).
- In order to turn  $\bar{Q}_N$  into a number of fired cells, a multi-photon spectrum was recorded illuminating the sensor within  $G_1$ . The reference spectrum is shown in Figure 5.

This can be fit with a sum of gaussians [15] to find the average peak-to-peak distance  $\bar{\Delta}_{pp}$  which provides the conversion factor from ADC channels to number of cells.

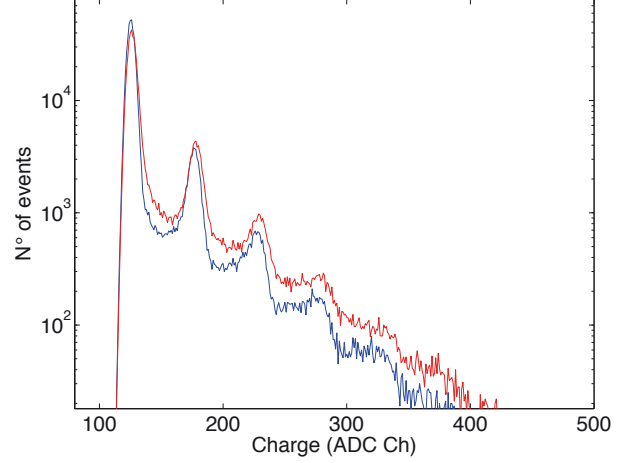


Fig. 3: Spectra of the charge collected in  $G_2$ , recorded without illuminating the sensor (blue) and after a light burst (red) pulsed  $500 \text{ ns}$  before the gate opening. Spectra were normalised to the same number of events.

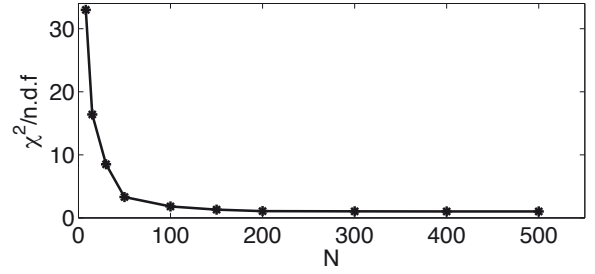


Fig. 4: The  $\bar{Q}_N$  distribution was tested against the hypothesis of being Gaussian. The plot shows the  $\chi^2/n.d.f.$  vs.  $N$  of the fit.

The spectra of  $\bar{Q}_N$  are shown in Figure 6, where the shift for the illuminated sensor is very clear. Eventually, the quantity

$$\Delta_{QQ}(G_2) = \frac{\langle \bar{Q}_N(\text{light ON}, G_2) \rangle - \langle \bar{Q}_N(\text{light OFF}, G_2) \rangle}{\bar{\Delta}_{pp}} \quad (1)$$

measures the excess of avalanches due to after pulses associated to the light burst with respect to Dark Counts.

The procedure is iterated increasing  $G_2$  till when  $\Delta_{QQ}(G_2)$  achieves a constant value, indicating that the after-pulsing phenomenon is exhausted.

In order to cope with possible temperature changes during the experiment, for every value of  $G_2$ , a multi-photon spectrum is recorded to have an actual value of  $\bar{\Delta}_{pp}$ .

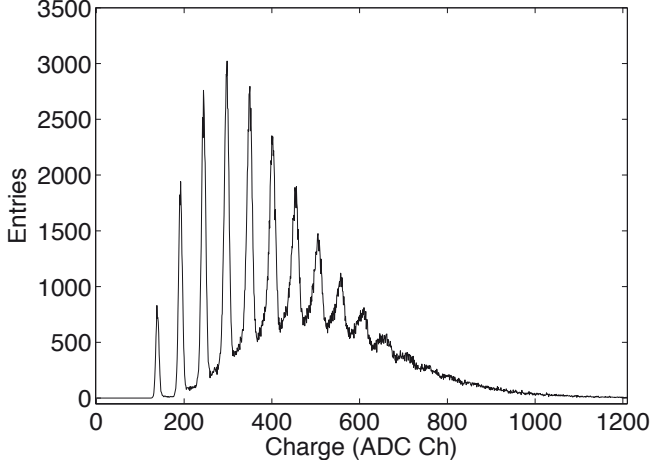


Fig. 5: The distribution of the detected photons used to calibrate the charge in photo-electrons.

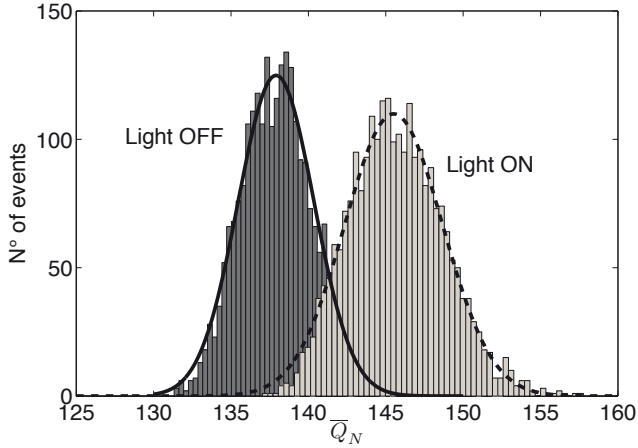


Fig. 6: Exemplary distribution of  $\bar{Q}_N$  for  $G_2 = 400 ns$ , having the LED switched ON and OFF.

### III. RESULTS

The procedure has been initially qualified measuring the Dark Count Rate (DCR) by the calculation of  $\langle \bar{Q}_N \rangle$ . The trend of  $\langle \bar{Q}_N(\text{light OFF}) \rangle / \bar{\Delta}_{pp}$  vs. time is shown in Figure 7, where the straight line fit corresponds to a slope  $m = 593 \pm 5 kHz$ . The average number of photo-electrons is actually affected by the OCT and  $\langle \bar{Q}_N \rangle / \bar{\Delta}_{pp} = n_{p.e.} \times (1 + \epsilon)$ , where  $\epsilon = (22 \pm 1)\%$  is the measured Cross-Talk probability and  $n_{p.e.}$  is the number of primary avalanches. As a consequence, the DCR may be calculated as  $\frac{m}{1+\epsilon} = 486 \pm 8 kHz$ , in fair agreement with the value of  $480 \pm 4 kHz$  by a direct count of the pulses above the 0.5 photo-electron threshold.

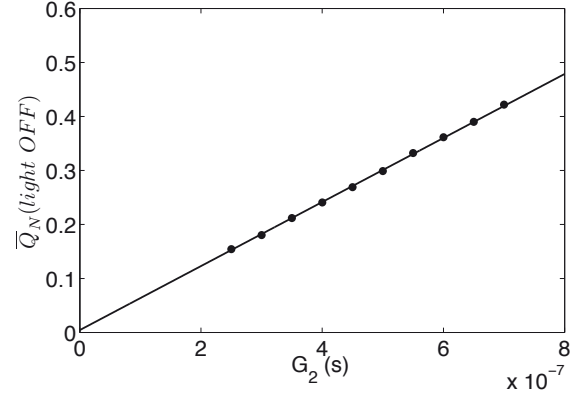


Fig. 7:  $\bar{Q}_N(\text{light OFF}) / \bar{\Delta}_{pp}$  as a function of  $G_2$  (s).

Concerning after-pulses, once the de-trapping of the charge carriers is assumed to have an exponential time dependence, the probability density function may be written as:

$$y(t) = \frac{P}{\tau} e^{-\frac{t}{\tau}}, \quad (2)$$

where  $P$  is the probability for a single avalanche to originate an after-pulse and  $\tau$  is the characteristic time constant of the phenomenon. The quantity  $\Delta_{QQ}(G_2)$  corresponds to the cumulative distribution function in the integration gate  $G_2$ , since:

$$\Delta_{QQ}(G_2) = \int_{G_1}^{G_1+G_2} \frac{N \times P}{\tau} e^{-\frac{t}{\tau}} dt = a(1 - e^{-\frac{G_2}{\tau}}), \quad (3)$$

where  $N$  is the mean number of photo-electrons generated by the light burst and  $a = N \times P e^{-\frac{G_1}{\tau}}$  is the asymptotic value of  $\Delta_{QQ}(G_2)$ .

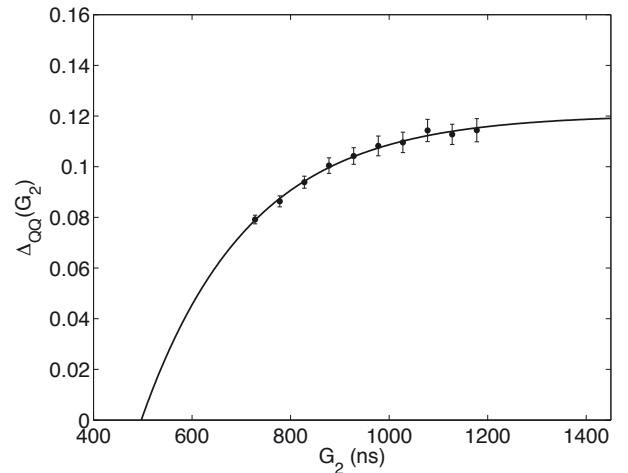


Fig. 8:  $\Delta_{QQ}(G_2)$  vs.  $G_2$ . Data are fitted by equation 3, with a  $\chi^2/n.d.f. = 0.94$



The data resulting by a  $G_2$  scan are shown in Figure 8. A fit to equation (3) yields a value of  $\tau = 217.5 \pm 5.9$  ns and  $a = 0.1206 \pm 0.0010$  photo electrons (p.e.). Since N was measured to be  $6.1 \pm 0.1$  p.e., this is resulting in an after-pulsing probability of  $(19.44 \pm 1.38)\%$  in fair agreement with data found in the Hamamatsu datasheet [16] and in reference [9], [12], reporting values between 17% and 22%.

#### IV. CONCLUSIONS

A method for the characterisation of the after-pulses based on the analysis of the charge distribution in a variable time window has been proposed and qualified. Its advantages are the simplicity and the robustness. Its main limitation is the intrinsic impossibility to probe the after-pulsing components characterised by a short time constant.

#### REFERENCES

- [1] B. Dolgoshein et al., *Status report on silicon photomultiplier development and its applications*. Nuclear Instruments and Methods in Physics Research A 563, 368376. 2006.
- [2] P. Buzhan et al., *Silicon photomultiplier and its possible applications*. Nuclear Instruments and Methods in Physics Research A 504, 48-52. 2003.
- [3] D. Renker, *Geiger-mode avalanche photodiodes, history, properties and problems*. Nuclear Instruments and Methods in Physics Research A 567, 48. 2006.
- [4] C. Piemonte, *A new Silicon Photomultiplier structure for blue light detection*. Nuclear Instruments and Methods in Physics Research A 568, 224. 2006.
- [5] A. L. Lacaita, *On the Bremsstrahlung Origin of Hot-Carrier-Induced Photons in Silicon Devices*. IEEE Trans. Electron Devices, 40, 57782. 1993.
- [6] T. Nagano et al., *Timing Resolution Improvement of MPPC for TOF-PET Imaging*. 10.1109/NSSMIC.2012.6551376. IEEE 2012
- [7] P. Eckert, *Study of the response and photon-counting resolution of silicon photomultipliers using a generic simulation framework*. arXiv:1206.4154v1. 2012
- [8] R. Pagano, *Silicon Photomultiplier: Technology Improvement and Performance*. International Journal on Advances in Systems and Measurements, vol 6 n. 1-2, 124-136. 2013.
- [9] T. Niggemann et al., *Status of the silicon photomultiplier telescope FAMOUS for the fluorescence detection of UHECRs*. Proceeding of 33rd International Cosmic Ray Conference. 143.107.180.38/indico/confAuthorIndex.py?confId=0. 2013.
- [10] P. Schuck, *Protein Interactions: Biophysical Approaches for the Study of Complex Reversible Systems*. 27-30. Springer, 2007.
- [11] T. Toyama et al., *Novel photo multiplier tubes for the Cherenkov Telescope array project*. Proceeding of 33rd International Cosmic Ray Conference. 143.107.180.38/indico/confAuthorIndex.py?confId=0. 2013.
- [12] P. Eckert, H.-C. Schultz-Coulon, W. Shen, R. Stamen & A. Tadday, *Characterisation studies of silicon photomultipliers*. Nuclear Instruments and Methods in Physics Research A 620, 217. 2010.
- [13] Y. Du, F. Retière, *After-pulsing and cross-talk in multi-pixel photon counters*. Nuclear Instruments and Methods in Physics Research A 596, 396-401. 2008.
- [14] C. Piemonte et al., *Development of an automatic procedure for the characterization of silicon photomultipliers*. 978-1-4673-2030-6. IEEE 2012.
- [15] M. Caccia et al., *An Educational Kit Based on a Modular Silicon Photomultiplier System*. arXiv:1308.3622. 2013.
- [16] [hamamatsu.com/eu/en/product/category/3100/4004/4113/index.html](http://hamamatsu.com/eu/en/product/category/3100/4004/4113/index.html)



### D.3 Background removal procedure based on the SNIP algorithm for $\gamma$ -ray spectroscopy with the CAEN Educational Kit

ED3163

## Equipment

SP5600C - Educational Gamma Kit

Model	SP5600	DT5720A	SP5606	A315	SP5607
Description	Power Supply and Amplification Unit	Desktop Digitizer 250 MS/s	Mini-Spectrometer	Splitter	Absorption tool
					
	p. 93	p. 93	p. 95	p. 95	p. 96

## Requirements

Gamma radioactive source 



Data analysis code developed in MATLAB is available.

### Related Experiment

B.1.3

B.1.4

B.3.1

### Ordering Options

Equipment	
Code	Description
WK5600XCAAAA	SP5600C - Educational Gamma Kit
or the all inclusive Premium Version	
WK5600XANAAA	SP5600AN - Educational Kit - Premium Version

# Background removal procedure based on the SNIP algorithm for $\gamma$ -ray spectroscopy with the CAEN Educational Kit.

Massimo Caccia, Amedeo Ebolese, Matteo Maspero, Romualdo Santoro

*Dipartimento di Scienza e Alta Tecnologia,*

*Universita' degli Studi dell'Insubria, 22100, Como, Italy*

Marco Locatelli, Maura Pieracci, Carlo Tintori

*CAEN S.p.A., 55049, Viareggio, Italy*

**Abstract**—In gamma spectra the energy, the intensity and the number of resolved photo peaks depend on the detector resolution and the background from physics processes. A widely used method for subtracting the background under a photo-peak is provided by the Sensitive Nonlinear Iterative Peak (SNIP) algorithm. This paper reports a validation procedure of the SNIP algorithm, based on the invariance of the photo-peak area for different background levels.

**Index Terms**—Silicon Photo Multipliers, gamma ray spectroscopy

## I. INTRODUCTION

**G**AMMA-RAY spectroscopy is relevant in basic and applied fields of science and technology, from nuclear to medical physics, from archaeometry [1], [2] to homeland security [3], [4].

In recorded  $\gamma$ -spectra of radioactive samples the number of resolved photo-peaks and the measurement of their energy and intensity is affected by the detector resolution and by background physics processes. In general, the characterization of the photo-peaks implies a robust estimation of the underlying background. Several approaches have been proposed, going from a simple estimate by an analysis of the side bands of the peaks to a spectrum fit with an analytical description of the background.

A flexible and widely used method is provided by the Sensitive Nonlinear Iterative Peak (SNIP) algorithm [5]–[7]. This paper presents a validation procedure of the SNIP algorithm based on the invariance of the photo-peak area when the underlying background changes.

## II. BACKGROUND SUBTRACTION IN $\gamma$ -SPECTRA

For energies of  $\gamma$  below the pair production, the interaction with the detector is dominated by Compton scattering and photo-absorption. Exemplary theoretical and experimental spectra are shown in Fig. 1. The Compton continuum is due to the recoiling electrons with energy

$$E_e = E_0 \times \left( \frac{\frac{E_0}{mc^2}(1 - \cos\theta)}{1 + \frac{E_0}{mc^2}(1 - \cos\theta)} \right),$$

where  $E_0$  is the incoming  $\gamma$ -ray energy,  $\theta$  is the scattering angle and  $mc^2$  is the electron rest-mass. The experimental spectrum results by a smearing of the underlying physics distribution [8] [9], implying a photo-absorption peak broadening possibly contaminated by the edge of the Compton spectrum and referred as background in the following.

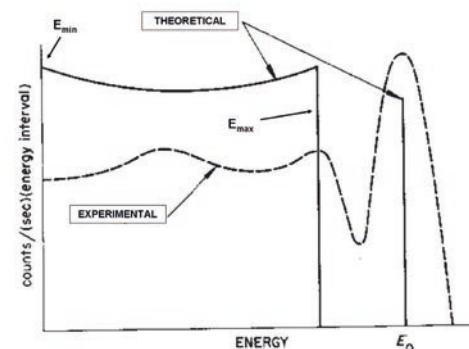


**Fig. 1:** Theoretical energy distribution for Compton and photoelectric interaction (continuous line) and experimental pulse-height distribution in a scintillation detector [8].

The photo-peaks are the signature of a spectrum. Their analysis conveys relevant information about the radioactive sample and the experimental apparatus:

- the peak energies are distinctive of the decaying nuclei in the sample;
- the area of peaks measure the relative concentrations of isotopes;
- the linearity of the system is provided by the spectra for a set of known  $\gamma$  emitters;
- the width of the peaks represents the electronics plus detector resolution. Its dependence against the energy accounts for the poissonian fluctuations in the signal and the detector response.

The SNIP algorithm has been introduced with the aim to separate useless information (i.e.: background, noise and detector artifacts) from useful information contained in the

Corresponding  
m.locatelli@caen.it,

Authors: massimo.caccia@uninsubria.it,



peak.

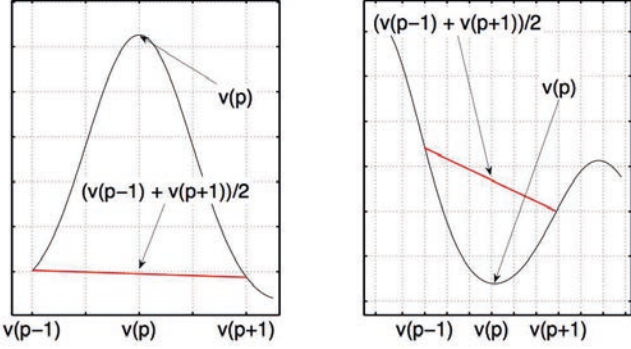


**Fig. 2:** Illustration of the SNIP algorithm applied to the peak region (left plot) and to a valley of the spectrum (right plot). Figure adapted from [7].

The core procedure of the SNIP [7] requires a pre-processing step, where the count  $y(i)$  in channel  $i - th$  is transformed according to:

$$y(i) \mapsto v(i) = \log(\log(\sqrt{y(i) + 1} + 1) + 1).$$

The square-root operator enhances small peaks while the double log operator was introduced to cope with complex spectra with relative intensities over several orders of magnitude.

The background under the peak is evaluated in an iterative way. For the  $M-th$  iteration, the content of the transformed bin  $v_M(i)$  is compared to the mean of the values at distance equals to  $\pm M$  and the updated spectrum is evaluated as:

$$v_{M+1}(i) = \min \left\{ v_M(i), \frac{v_M(i - M) + v_M(i + M)}{2} \right\}.$$

In proximity of peaks, as long as the distance is comparable to the peak width, the updated spectrum will result by the shape of the side bands. On the other hand, valleys will be essentially unchanged (see Fig. 2). An exemplary illustration of the outcome of the procedure is shown in Fig. 3, where the raw spectrum, the background estimated with SNIP and the spectrum with the subtracted background are overimposed. Fig. 3 clearly shows that the peak side wings fluctuate around zero as expected after a correct background subtraction.

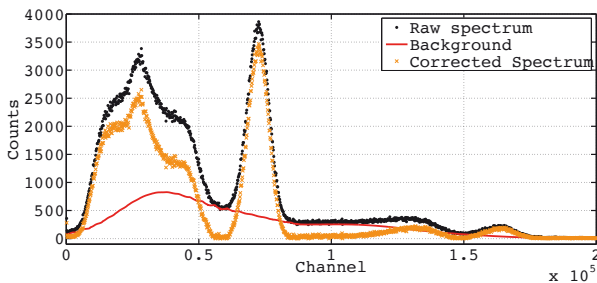


**Fig. 3:** Typical  $^{22}\text{Na}$  gamma spectrum. The raw data are shown in black, the estimated background in red and the spectrum with the subtracted background in brown.

The main advantage of the SNIP algorithm is the capability to cope with a large variety of background shapes. Its potential weakness is in the absence of a built-in convergence criterion. In this specific application, the iterative procedure is stopped as long as the estimated background is monotonically changing in the peak region. As a complementary condition, essentially applied for low background spectra where the statistical fluctuations are dominating, the procedure is stopped as long as the background drops below 5% of the total area underneath the peak.

### III. EXPERIMENTAL SET-UP

The experimental set-up is based on the CAEN Silicon PhotoMultiplier Educational Kit [10], a modular system for undergraduate experiments in nuclear science, photonics and statistics.



**Fig. 4:** The CAEN educational kit full package.

The kit, shown in Fig. 4, include two  $\gamma$  spectrometry heads housing:

- a  $3 \times 3 \text{ mm}^2$  Hamamatsu MPPC S10362-33-100C with 100 cells and breakdown voltage of 68.5V, optically coupled with  $3 \times 3 \times 15 \text{ mm}^3$  LYSO/BGO/CsI crystals;
- a  $6 \times 6 \text{ mm}^2$  SensL MicroSM-60035-X13 (18980 cells, breakdown voltage 27.35V), optically coupled with  $3 \times 3 \times 30 \text{ mm}^3$  CsI scintillating crystal.

The analog signal generated in the SiPM is amplified by the CAEN SP5600 PSAU Power Supply and Amplification Unit [11] and sampled at 250 MS/s over a 12 bit dynamic range by the CAEN DT5720A Desktop Digitizer [12]. The DT5720A embeds an FPGA for on-board data processing, e.g. baseline calculation and charge integration. The system is controlled by a LabView based Graphical Users Interface and USB interfaced to a computer.

The proposed experiments are based on the use of the head equipped with the  $6 \times 6 \text{ mm}^2$  SensL SiPM.

### IV. SNIP ALGORITHM VALIDATION

The validation of the convergence criteria for the SNIP algorithm is based on the assumption that the information in the photo-peak shall be preserved as the underlying background changes. This was established by processing  $^{22}\text{Na}$  spectra

for different biasing voltages of the SiPM used to detect the scintillation light from the CsI crystal. Data were recorded for  $^{22}\text{Na}$  since the interaction of the two  $\gamma$ -rays by the positron annihilation results in a spectrum featuring a continuous and significant background to the left and right hand side of the 511 keV photo-peak.

Twelve spectra were acquired in the bias voltage range 29.8 – 31.1 V. A subset is shown in Fig. 5 displaying both raw and background subtracted data. As the over-voltage is raised, the gain of the system is expected to increase together with the photon detection efficiency (PDE), the optical cross-talk and the dark count rate (DCR) [13]–[18]. As a consequence, spectra are expected to change, featuring a shift in the peak position due to the gain change and a width increase associated to the PDE variation and to a different smearing function because of the DCR and the cross-talk.

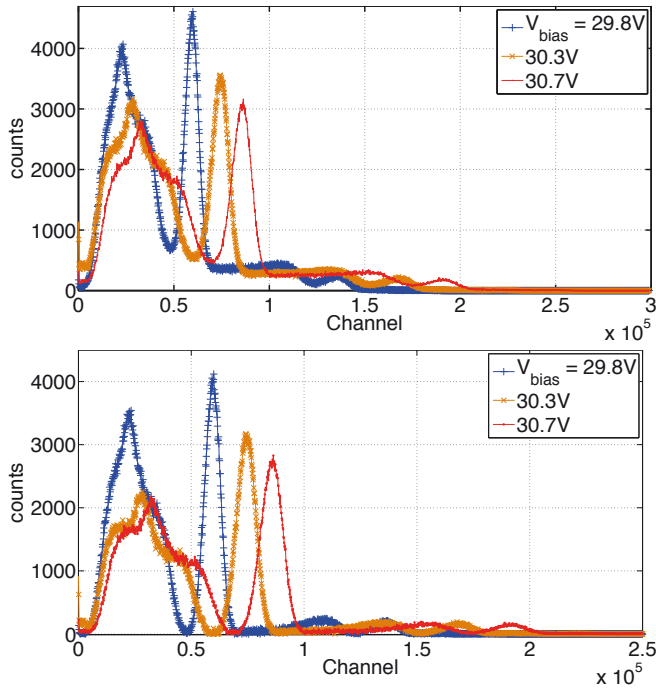


**Fig. 5:** Measured  $^{22}\text{Na}$  gamma spectra for different bias voltages (upper panel). The SNIP processed spectra for the same subset of data are shown in the bottom panel.

After the background subtraction by SNIP algorithm, the 511 keV peak was fitted with a gaussian function. The values of the area for the different biasing conditions are presented in Fig. 6, following a normalization to the total number of events for energies higher than the back-scattering peak.

The reported errors account for the poissonian fluctuations ( $\sim 0.2\%$ ) and the effect of the background subtraction ( $\sim 1\%$ ). They correspond to the standard deviation of the values for a set of ten spectra recorded in identical conditions.

Effects due to the convergence criteria of the SNIP algorithm were estimated stopping the procedure one step beyond and behind the iteration corresponding to the convergence step.

The distribution of experimental areas is statistically compliant with the hypothesis of a constant value confirming that

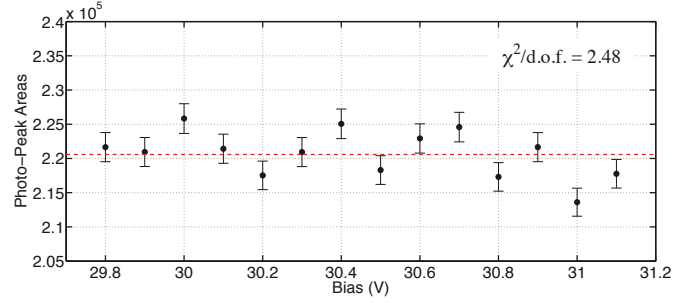


**Fig. 6:** Values of the photo-peak areas for different biasing conditions.

the SNIP background subtraction routine is not introducing any systematic errors.

## V. MEASUREMENTS

The SNIP processed spectra from a series of sources used in educational labs (Tab. I, [19]) were used to calibrate the system response and check its linearity. Results up to the 835 keV from  $^{54}\text{Mn}$  are shown in Fig. 7. The linearity of the system can be assessed, and results are shown in Fig. 7, with no indication of saturation.

**TABLE I:** Relevant characteristics of the used gamma isotopes.

Isotope Name	Symbol	Peak Energy (MeV)
Cadmium-109	Cd-109	0.022, 0.025, 0.088
Cobalt-57	Co-57	0.122, 0.136
Sodium-22	Na-22	0.511 (1.275)
Cesium-137	Cs-137	0.662
Manganese-54	Mn-54	0.835

Spectra were also used to verify the energy dependence of the system resolution, where a  $dE/E \propto 1/\sqrt{E}$  trend can be assumed by the poissonian fluctuations in the number of scintillation photons. Data are reported in Fig. 8.

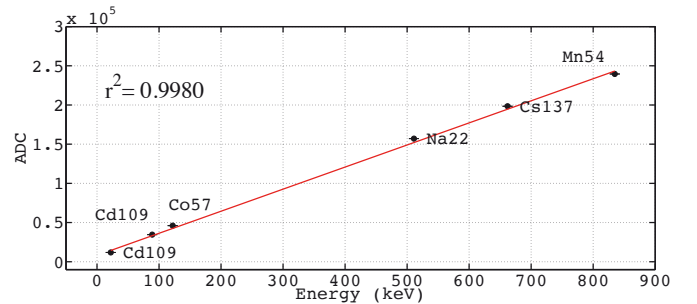


**Fig. 7:** Energy calibration.

The power law fit  $f(E) \propto E^{-b}$  gives a value of  $b = 0.57 \pm 0.03$ , in agreement with the expectations. It is worth mentioning that the resolution at the  $^{137}\text{Cs}$  peak is less than 9%, at the level of the standard educational devices.

## VI. CONCLUSIONS

The flexibility and the potential of the SiPM kit have been confirmed considering its configuration for gamma spectrometry. Basic measurements proving its linearity and assessing

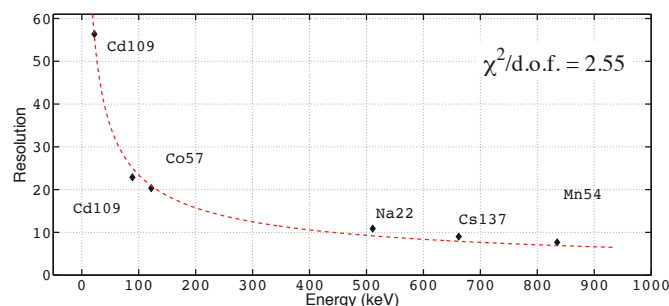


Fig. 8: Power law fit of data after the SNIP background subtraction.

its energy resolution have been performed. A MATLAB implementation of the SNIP background subtraction algorithm has been validated, providing altogether a valuable platform for entry-level experiments in gamma spectrometry tailored for undergraduate students in Physics.

#### REFERENCES

- [1] M. S. Shackley, *Gamma Rays, X-Rays and Stone Tools: Some Recent Advances in Archaeological Geochemistry*, Journal of Archaeological Science, Volume 25, Issue 3, 1998;
- [2] M. Moussa, *Gamma-ray spectrometry: a new tool for exploring archaeological sites; a case study from East Sinai, Egypt*, Journal of Applied Geophysics, Volume 48, Issue 3, 2001;
- [3] Aage, H., Orsbech, U., *Search for lost or orphan sources based on NaI gamma spectrometry*, Appl. Radiat. Isot. 58, 103113 (2003);
- [4] Ely, J., Kouzes, R., Schweppe, J., Siciliano, E., Strachan, D., Weier, D., *The use of energy windowing to discriminate SNM from NORM in radiation portal monitors*, Nucl. Instrum. Methods A 560, 373387 (2006);
- [5] Ryan, C. G. and Clayton, E. and Griffin, W. L. and Sie, S. H. and Cousens, D. R., *SNIP, a statistics-sensitive background treatment for the quantitative analysis of PIXE spectra in geoscience applications*;
- [6] Ene, A., Badica, T., Olariu, A., Popescu, I. V., & Besliu, C. 2001, *Nuclear Instruments and Methods in Physics Research B*, 179, 126;
- [7] Morháč, M. and Kliman, J. and Matoušek, V. and Veselský, M. and Turzo, I., *Background elimination methods for multidimensional coincidence  $\gamma$ -ray spectra*;
- [8] G. F. Knoll, *Radiation Detection and Measurement*, John Wiley & Sons (2000);
- [9] Adrian C. Melissinos and Jim Napolitano, *Experiments in Modern Physics, Second Edition*, Academic Press 2003;
- [10] <http://www.caen.it/jsp/Template2/CaenProd.jsp?parent=61&idmod=719>;
- [11] <http://www.caentechnologies.com/csite/CaenProd.jsp?showLicence=false&parent=10&idmod=719>;
- [12] <http://www.caen.it/csite/CaenProd.jsp?parent=14&idmod=624>;
- [13] D. Renker, *Geiger-mode avalanche photodiodes, history, properties and problems*, 2006, Nuclear Instruments and Methods in Physics Research A, 567, 48.
- [14] P. Eckert, H.-C. Schultz-Coulon, W. Shen, R. Stamen & A. Tadday, *Characterisation studies of silicon photomultipliers*, 2010, Nuclear Instruments and Methods in Physics Research A, 620, 217.
- [15] Y. Musienko, S. Reucroft & J. Swain, *The gain, photon detection efficiency and excess noise factor of multi-pixel Geiger-mode avalanche photodiodes*, 2006, Nuclear Instruments and Methods in Physics Research A, 567, 57.
- [16] Y. Du & F. Retière, *After-pulsing and cross-talk in multi-pixel photon counters*, 2008, Nuclear Instruments and Methods in Physics Research A, 596, 396.
- [17] M. Ramilli, A. Allevi, V. Chmill & al., *Photon-number statistics with silicon photomultipliers*, 2010, Journal of the Optical Society of America B Optical Physics, 27, 852;
- [18] Caccia, M. and Chmill, V. and Ebolese, A. and Martemiyarov, A. and Risigo, F. and Santoro, R. and Locatelli, M. and Pieracci, M. and Tintori, C., *An Educational Kit Based on a Modular Silicon Photomultiplier System*, 2013arXiv1308.3622C;
- [19] [http://www.pasco.com/prodCatalog/SN/SN-7949\\_gamma-sources-set-of-8/#overviewTab](http://www.pasco.com/prodCatalog/SN/SN-7949_gamma-sources-set-of-8/#overviewTab).



# PRODUCTS

This section is dedicated to a short description of the advanced instrumentations developed by CAEN and used to perform the experiments proposed in this Handbook.

The devices are put together to form educational kits, suitable to a specified application in Nuclear and Modern Physics fields. Moreover three educational kits, “Educational Gamma Kit”, “Educational Beta Kit” and “Educational Photon Kit”, are included in a “Educational Kit – Premium Version” that allows to perform almost entirely the Handbook experiments.

The “Emulation Kit” allows to perform a series of lab experiments related to gamma spectroscopy with no radioactive source and detector, but simulating the signals produced by interaction of particle with the detecting unit.

The “EasyPET” is the only not modular system. It is a user friendly and portable PET system that allows to perform nuclear imaging experiments.

All the experimental setups are provided by a complete software suite for remote control of the system and data analysis.

The complete list of Physics Experiments and the concerning CAEN Educational Systems is reported in the following table.



# Choose Your Educational Kit!

Section	Subsection	Experiment
A. Particle Detector Characterization	A1. Silicon Photomultiplier (SiPM)	A.1.1 SiPM Characterization
		A.1.2 Dependence of the SiPM Properties on the Bias Voltage
		A.1.3 Temperature Effects on SiPM Properties
B. Nuclear Physics and Radioactivity	B.1 $\gamma$ Spectroscopy	B.1.1 Detecting $\gamma$ -Radiation
		B.1.2 Poisson and Gaussian Distributions
		B.1.3 Energy Resolution
		B.1.4 System Calibration: Linearity and Resolution
		B.1.5 A Comparison of Different Scintillating Crystals: Light Yield, Decay Time and Resolution
		B.1.6 $\gamma$ -Radiation Absorption
		B.1.7 Photonuclear cross-section/Compton Scattering cross-section
	B.2 $\beta$ Spectroscopy	B.2.1 Response of a Plastic Scintillating Tile
		B.2.2 $\beta$ Spectroscopy
		B.2.3 $\beta$ -Radiation: Transmission through Matter
		B.2.4 $\beta$ -Radiation as a Method to Measure Paper Sheet Grammage and Thin Layer Thickness
	B.3 Nuclear Imaging - PET	B.3.1. Basic Measurements: $\gamma$ Spectroscopy and System Linearity <sup>(1)</sup>
		B.3.2. Positron Annihilation Detection <sup>(1)</sup>
		B.3.3. Two-dimensional Reconstruction of a Radioactive Source
		B.3.4. Spatial Resolution
C. Particle Physics	C.1 Cosmic Rays	C.1.1 Muons Detection
		C.1.2 Muons Vertical Flux on Horizontal Detector
	C.2 Photons	C.2.1 Quantum Nature of Light
		C.2.2 Hands-on Photon Counting Statistics
D. Advanced Statistics based on Silicon Photomultiplier Detectors	D.1 An Educational Kit Based on a Modular SiPM System	
	D.2 A simple and robust method to study after-pulses in Silicon Photomultipliers <sup>(2)</sup>	
	D.3 Background removal procedure based on the SNIP algorithm for $\gamma$ -ray spectroscopy	

The table is a simple guide to associate each physics experiment to the kit used to perform it.








For all Physics Application fields, identified in "Section" column, one or more topics are associated as shown in "subsection" column. A series of applications linked to each topic and listed in "Experiment" column is allowed by using the modular kit.

The conclusive matrix of the table allows to associate the equipments to the experiments. Each column is connected to one of the modular kits presented for educational purpose. The checked cells identify the experiments allowed by the chosen kit.

<sup>(1)</sup> DT5720A is necessary to perform the experiment. The digitizer is already included in the other educational kits.

<sup>(2)</sup> DT993 Dual Timer is also necessary to perform this experiment.

								EQUIPMENTS
								SP5600C - Educational Gamma Kit
								SP5600D - Educational Beta Kit
								SP5600E - Educational Photon Kit
								SP5600AN - Educational Kit - Premium Version
								SP5600EMU - Emulation Kit
								SP5700 - EasyPET
								SP5701 - EasyPET Kit
pp.								
10	-	-	✓	✓	-	-		
12	-	-	✓	✓	-	-		
14	-	-	✓	✓	-	-		
18	✓	-	-	✓	-	-		
20	✓	-	-	✓	✓	-		
22	✓	-	-	✓	✓	-		
24	✓	-	-	✓	✓	-		
26	✓	-	-	✓	-	-		
28	✓	-	-	✓	-	-		
30	✓	-	-	✓	✓	-		
34	-	✓	-	✓	-	-		
36	-	✓	-	✓	-	-		
38	-	✓	-	✓	-	-		
40	-	✓	-	✓	-	-		
44	-	-	-	-	-		✓	
46	-	-	-	-	-		✓	
48	-	-	-	-	-	✓	✓	
50	-	-	-	-	-	✓	✓	
54	-	✓	-	✓	-	-		
56	-	✓	-	✓	-	-		
60	-	-	✓	✓	-	-		
62	-	-	✓	✓	-	-		
66	-	-	✓	✓	-	-		
79	-	-	✓	✓	-	-		
84	✓	-	-	✓	-	-		

Ordering Options		
Kit Model	Code	Description
	WK5600XCAAAA	SP5600C - Educational Gamma Kit
	WK5600XDAAAA	SP5600D - Educational Beta Kit
	WK5600XEAAAA	SP5600E - Educational Photon Kit
	WK5600XANAAA	SP5600AN - Educational Kit - Premium Version
	WK5600XEMUAA	SP5600EMU - Emulation Kit
	WSP5700XAAAA	SP5700 - EasyPET
	WK5701XAAAAA	SP5701 - EasyPET Kit




# Content of the Modular Kits

## SP5600C - Educational Gamma Kit

Model	SP5600	DT5720A	A315	SP5606	SP5607
Description	Power Supply and Amplification Unit	Desktop Digitizer 250 MS/s	Splitter	Mini-Spectrometer	Absorption tool
					
	p. 93	p. 93	p. 95	p. 95	p. 96

## SP5600D - Educational Beta Kit

Model	SP5600	DT5720A	SP5608
Description	Power Supply and Amplification Unit	Desktop Digitizer 250 MS/s	Scintillating tile
			
	p. 93	p. 93	p. 96



## SP5600E - Educational Photon Kit

Model	SP5600	DT5720A	SP5601	SP5650C
Description	Power Supply and Amplification Unit	Desktop Digitizer 250 MS/s	LED Driver	Sensor Holder for SP5600 with SiPM
				
	p. 93	p. 93	p. 94	p. 94


## SP5600AN - Educational Kit - Premium Version

Model	SP5600	DT5720A	A315	SP5606	SP5607	SP5601	SP5650C	SP5608
Description	Power Supply and Amplification Unit	Desktop Digitizer 250 MS/s	Splitter	Mini-Spectrometer	Absorption tool	LED Driver	Sensor Holder for SP5600 with SiPM	Scintillating tile
								
	p. 93	p. 93	p. 95	p. 95	p. 96	p. 94	p. 94	p. 96



## SP5600EMU - Emulation Kit

Model	DT4800	DT5770
Description	Digital Detector Emulator	Desktop Multi-Channel Analyzer
		
	p. 97	p. 97

## SP5700 - EasyPET

Model	SP5700
Description	EasyPET
	
	p. 98

## SP5701 - EasyPET Kit

Model	SP5700	DT5770
Description	EasyPET	Desktop Multi-Channel Analyzer
		
	p. 98	p. 97

# SP5600

## Power Supply and Amplification Unit

The SP5600 is a General purpose Power Supply and Amplification Unit, integrating up to two SiPMs in a mother & daughter architecture allowing for easy mounting and replacement of the sensors. The basic configuration features two channels with independent gain control up to 50 dB and provides the bias voltage (up to 100 V) to the sensors with gain stabilization. Each channel can provide a digital output generated by the fast leading edge discriminators. A timing coincidence of the two channels is also available.

- Variable amplification gain (up to 50 dB)
- Low noise, not to spoil the sensor performances for small signals
- Wideband, to comply with the fast sensor response
- Fast leading edge discriminator and time coincidence
- Provides the bias for the sensors with gain stabilization
- USB 2.0 interface
- Mechanical structure with an embedded SiPM 1 x 1 mm<sup>2</sup>
- Dimension: 154 x 50 x 70 mm<sup>3</sup> (WxHxD)
- User Friendly Control Software with all-in-a Window Graphical Interface (together for SP5600 and DT5720A)



### Ordering Options

Code	Description
WSP5600XAAA	SP5600 - 2 Channels General Purpose Amplifier

# DT5720A

## Desktop Digitizer

The DT5720A is a CAEN Desktop Waveform digitizer housing 2 channels 12 bit 250 MS/s ADC with a dedicated charge integrating firmware (DPP-PSD) for real time pulse processing.

- 2 Channel 12 bit 250 MS/s Digitizer
- Digital Pulse Processing for Charge Integration DPP-PSD
- Best suited for PMT and SiPM/MPPC readout at low and high rates
- Mid-High speed signals (Typ: output of PMT/SiPM)
- Good timing resolution with fast signals (rise time < 100 ns)
- Optical Link and USB 2.0 interfaces
- Dimension: 154 x 50 x 164 mm<sup>3</sup> (WxHxD)
- User Friendly Control Software with all-in-a Window Graphical Interface (together for SP5600 and DT5720A)



### Ordering Options

Code	Description
WDT5720AXAAA	DT5720A - 2 Ch. 12 bit 250 MS/s Digitizer: 1.25MS/ch, C4, SE

# SP5601

## LED Driver

The SP5601 is an ultra-fast LED Driver with pulse width at ns level, tunable intensity and frequency, that provides a low-cost tool for the detector characterization. The LED pulse generation can be triggered by an internal oscillator or by an external pulser.

- Pulse width: 8 ns
- LED color: violet (400 nm) 1500 mcd
- Pulse generator: internal/external
- Optical output connectors: FC
- Optical fiber included
- Dimension: 79 x 42 x 102 mm<sup>3</sup> (WxHxD)



Ordering Options

Code	Description
WSP5601XAAAA	SP5601 - Led Driver for SiPM development kit

# SP5650C

## Sensor Holder with SiPM

The SP5650C is a sensor holder provided in the Educational Photon kit. The holder hosts a 1.3 x 1.3 mm<sup>2</sup> Silicon Photo-Multipliers; moreover, a probe inside the holders senses temperature variations, thus allowing the user to compensate for possible gain instability. The SP5650C is made of a mechanical structure providing a FC fiber connector and a PCB where the SiPM is soldered. Bias voltage for the SiPM and temperature probe output are provided through a 10 pin female socket, while the analog output connector is MCX.

- Size 20 mm (diameter) x 6 mm (height)
- Analog Out Connector RADIAL: R113425000 (MCX MALE)
- Bias Connector M22-7140542 Female Vertical Socket
- Embedded Hamamatsu MPPC S13360- 1350CS:
  - 1.3 x 1.3 mm<sup>2</sup> Active Area
  - 667 Number of pixel
  - 50 µm Pixel Pitch



Ordering Options

Code	Description
WSP5650XCAAA	SP5650C - Sensor Holder for SP5600 with HAMAMATSU 1.3x1.3mm <sup>2</sup>



# SP5606

## Mini-Spectrometer

SP5606 is mini-spectrometer for gamma ray detection. The spectrometer is composed of a mechanical structure that houses a scintillating crystal, coupled to a dedicated SiPM. Three different crystals are available: CsI, LYSO and BGO. The spectrometer is equipped with a bottom support to allows an easy connection to the SP5600 via the splitter A315, to avoid saturation effects.

- Mechanical structure for optimal SiPM to crystal coupling
- Scintillating Crystals: CsI, LYSO, BGO (6 x 6 x 15 mm<sup>3</sup> )
- One SiPM embedded 6 x 6 mm<sup>2</sup>



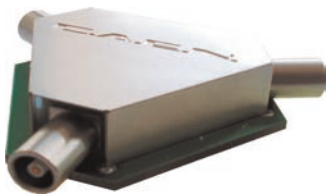
Ordering Options

Code	Description
WSP5606XAAAA	SP5606 - Mini Spectrometer with 6x6 sensor coupled to three scintillating crystals.

# A315

## Splitter

The Mod. A315 splits one input on two output signals. All the connectors are LEMO female type. The splitter is adapted for 50 Ohm lines. The device is completely passive (no power supply is required); the amplitude on each output is one half of that on the input.



Ordering Options

Code	Description
WA315XAAAAAA	A315 - Splitter

# SP5607

## Absorption Tool

The Gamma absorption tool allows to perform gamma attenuation measurements. It is a modular tool and its design allows an easy connection to the SP5606 bottom support. It is composed of:

- Spacers: one 4mm thick, five 10 mm thick;
- Aluminum Absorbers: one 4 mm thick, five 10 mm thick;
- PMMA Absorbers: one 4 mm thick, five 10 mm thick.



Ordering Options

Code	Description
WSP5607XAAAA	SP5607 - Absorption Tool for Gamma Applications

# SP5608

## Scintillating Tile

The SP5608 is a support with a embedded plastic scintillating tile, directly coupled to a SiPM . The tile, with a sensitive volume of 47 x 47 x 10 mm<sup>3</sup>, is the ideal tool for tests with beta emitting isotopes and cosmic rays. The support structure allows to use the SP5608 stand-alone or to use two tile modules to build a cosmic telescope. A special source holder allows to perform beta attenuation measurements in a thin thickness material due to 2mm distance from the scintillating tile. It is provided by a paper and aluminum sheets

- Sensitive volume: 47 x 47 x 10 mm<sup>3</sup>
- Scintillator: polystyrene
- Directly coupled to a SiPM 6 x 6 mm<sup>2</sup>
- 20 Paper and Aluminum sheets



Ordering Options

Code	Description
WSP5608XAAAA	SP5608 - Scintillating Tile

# DT4800

## Micro Digital Detector Emulator

The DT4800, called Micro Digital Detector Emulator, is the most compact and cost effective model of the Detector Emulators family. It is available only in a one channel version and it is particularly suited for simple emulation needs and educational purposes. The unit features one analog output and one digital input. As a Pulser it can generate exponential decay signals with programmable Rise Time and Fall Time up to a rate of 1 Mcps. The rate can be fixed or it can follow a Poissonian distribution. In Emulation mode the unit can reproduce signals from a real energy spectrum that can be uploaded in the form of CSV or ANSI N42.42 files. A database of nuclides is provided to generate specific emission lines and Gaussian noise can be added. An user friendly control software is provided with the unit.

- Pulser/Emulator operating modes
- Real Energy spectrum emulation
- Time distribution emulation (Poissonian)
- Noise emulation
- Continuous pre-amplifier emulation
- Nuclides database
- Emulation and Detection Educational Software
- Digital Detector Emulator Software



Digital Detector Emulator Software

### Ordering Options

Code	Description
WDT4800XAAAA	DT4800 – Micro Digital Detector Emulator

# DT5770

## Digital Multi Channel Analyzer

The DT5770 is a compact portable Digital MCA for Gamma spectroscopy. It is suited for high energy resolution semiconductor detectors, like HPGe and Silicon Drift Detector, connected to a Charge Sensitive Preamplifier. The unit can also properly operate directly connected to a PMT with inorganic scintillators (e.g. NaI or CsI scintillators), provided exponential pulse shape and decay time above 200 ns. It integrates analog front-end with programmable gain and possible AC coupling.

- Compact portable 16k Digital MCA
- Suited for high resolution Gamma Spectroscopy
- Support continuous and pulsed reset preamplifiers
- Software selectable coarse and fine gain
- DB9 connector for preamplifier power supply
- Features Pulse Height Analysis firmware for energy calculation
- Different acquisition modes available: PHA and signal inspector for an easy setup and signal monitoring
- USB and Ethernet communication interfaces

Three control software allow to manage the acquisition and perform basic spectrum analysis:

- Emulation and Detection Educational Software
- EasyPET Control Software
- MC<sup>2</sup>Analyzer Software



MC<sup>2</sup> Analyzer Software      Emulation and Detection Educational Software      EasyPET Control Software

### Ordering Options

Code	Description
WDT5770AXAAA	DT5770 – Digital MCA - 1 LVPS $\pm 12V/100mA$ $\pm 24V/50mA$



# SP5700

## EasyPET



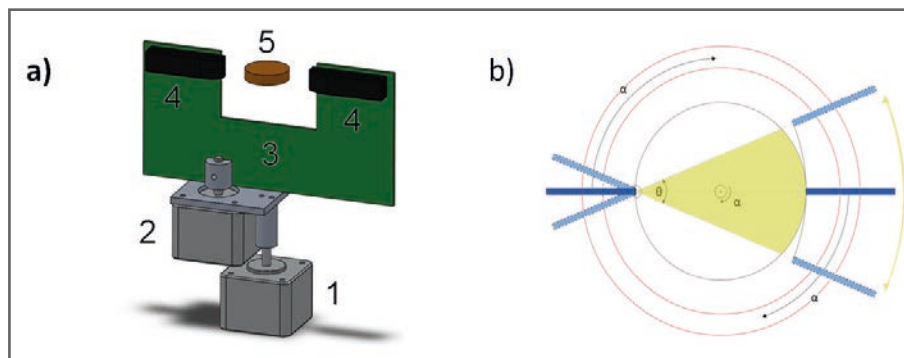
EasyPET is a simple, user friendly and portable didactic PET system developed for high-level education, which allows exploring the physical and technological principles of the conventional human PET scanners, using the same basic detectors of state-of-the-art systems. The Positron Emission Tomography (PET) scanner is the state-of-the-art medical imaging system, capable of providing detailed functional information of physiological processes inside the human body. Functional imaging has a great impact in cancer diagnostics, monitoring of therapy effects and cancer drug development. The underlying principle to PET systems is the detection of high energy radiation emitted from a chemical marker, a molecule labelled with a radioisotope, administered to a patient. The radioisotope emits positrons which, after annihilating with atomic electrons, result in the isotropic emission of two photons back to back with an energy of 511 keV. The two photons are detected by a ring of detectors, which allows a pair of them to detect two back to back photons in any direction.

The simplicity of EasyPET derives from the innovative characteristics of the system and its acquisition method<sup>3</sup>. EasyPET comprehends only two detector modules that move together and execute two types of independent movements, around two rotation axes,

<sup>3</sup>Patent pending, Universidade de Aveiro.

a) The EasyPET component layout:  
1 - bottom motor, 2 - top motor, 3 - U-shaped PCB, 4 - pair of detector modules, 5 - radioactive source;

b) Top-view schematics of the EasyPET image acquisition method with two axes of rotation.  $\alpha$  represents the angle step of the bottom motor rotation, while  $\theta$  represents the scanning angle of the top stepper motor. The two axes are used to move one pair of scintillation detectors (blue rectangles) so as to acquire lines of response covering a cylindrical field of view between the detectors.



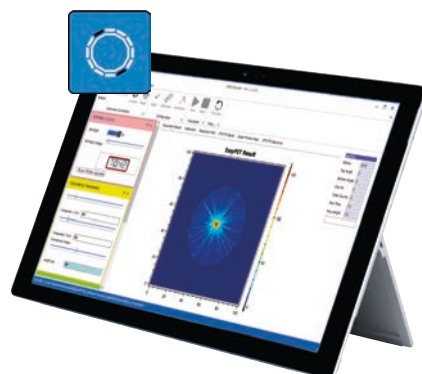
The bottom motor (1) has a fixed axis, whose position defines the center of the field of view. The bottom motor supports and performs a complete rotation of a second motor, in predefined steps of amplitude  $\alpha$ . The axis of the top motor (2) is thus always positioned within a circumference of radius equal to the distance between the two axes. The top motor, in its turn, supports and moves a U shaped printed circuit board (3), where a pair of aligned and collinear detector modules (4) is mounted, performing a symmetric scan of range  $\theta$  around the center, for each position of the bottom motor. In this way, EasyPET can reconstruct an image of a radioactive source (5) placed anywhere within a cylindrical field of view between the pair of detectors. The diameter of the field of view is defined by the amplitude of  $\theta$ , the range of the top motor scan.

The EasyPET operation principle is simple: the two small detector cells, each composed of a small scintillator crystal coupled to a silicon photomultiplier (SiPM), develop a signal when they detect a photon emitted by the source. A fast electronic readout system allows detecting coincident events resulting from the same decay process: if the signals from each detector are higher than a reference signal and occur within a specific time validation window, they are considered a coincidence event. For each scanning position, the number of coincidences is counted and an image of the accumulated lines of response is reconstructed in real-time.

EasyPET reduces the number of detectors required for the acquisition of a PET image to the minimum, while at the same time it eliminates the parallax error and the need for determination of depth of interaction in the crystals (DOI), thus allowing the obtainment of high-resolution PET images in all the field of view.

Main EasyPET components:

- Two detectors, each composed of a LYSO scintillator crystal optically coupled to a SiPM;
- Printed Circuit Board (PCB) equipped with electronics used for SiPMs supply voltage, signal readout and coincidence detection;
- Two stepper motors;
- Microcontroller unit responsible for controlling EasyPET parameters, driving the stepper motors and communicating with the computer;
- Holder for radioactive source;
- EasyPET Control Software.



EasyPET Control Software

### Ordering Options

Code	Description
WSP5700XAAAA	SP5700 - EasyPET

# Sales Network

CAEN is proud to have served many customers and research labs world wide.

CAEN continues to supply its equipment to physics research centers and industrial market offering world wide sales and support.

Our products appeal to a wide range of customers including engineers, scientists and technical professionals who all trust them to help achieve their goals faster and more effectively.

CAEN is sure to have the equipment suited to your need, and we will back it up with the best service and support in the industry.

***Call today your closest representatives!***



## Italy and CERN

### CAEN SpA

#### Corporate Headquarters

Via Vetraria 11  
55049 - Viareggio • Italy  
Phone +39.0584.388.398  
Fax +39.0584.388.959  
info@caen.it  
www.caen.it

## USA and Canada

### CAEN Technologies, Inc.

1140 Bay Street - Suite 2C  
Staten Island, NY 10305 • USA  
Phone +1.718.981.0401  
Fax +1.718.556.9185  
info@caentechnologies.com  
www.caentechnologies.com

## Germany

### CAEN GmbH

Klingenstraße 108  
D-42651 Solingen • Germany  
Phone +49 (0)212.254.4077  
Fax +49 (0)212.25.44079  
Mobile +49 (0)151.16.548.484  
info@caen-de.com  
www.caen-de.com

**For a full and updated list of our Resellers and Distributors please visit our website at the following link:**

**[www.caen.it/salesnetwork](http://www.caen.it/salesnetwork)**

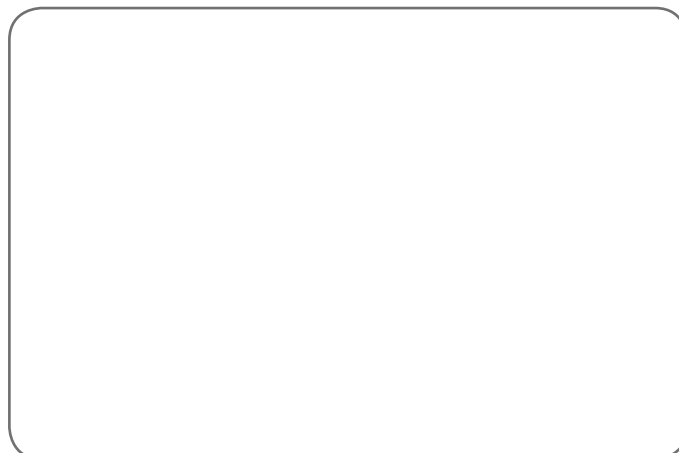




Image Credits:

Icons made by Freepik from [www.flaticon.com](http://www.flaticon.com)

Pag. 8, 9, 16, 17, 32, 52, 53, 58, 59, 64, 66 Credit: © Massimiliano Antonello

CAEN S.p.A. has publishing rights for all images reproduced in "CAEN Educational Handbook except when indicated.

This catalog, or parts thereof, may not be reproduced in any form or by any means without written permission from CAEN S.p.A.

**CAEN S.p.A.**

Via Vetraia 11  
55049 - Viareggio  
Italy  
Phone +39.0584.388.398  
Fax +39.0584.388.959  
[info@caen.it](mailto:info@caen.it)  
[www.caen.it](http://www.caen.it)

**CAEN GmbH**

Klingenstraße 108  
D-42651 Solingen - Germany  
Phone +49 (0)212.254.4077  
Fax +49 (0)212.25.44079  
Mobile +49 (0)151.16.548.484  
[info@caen-de.com](mailto:info@caen-de.com)  
[www.caen-de.com](http://www.caen-de.com)

**CAEN Technologies, Inc.**

1140 Bay Street - Suite 2C  
Staten Island, NY 10305  
USA  
Phone +1.718.981.0401  
Fax +1.718.556.9185  
[info@caentechnologies.com](mailto:info@caentechnologies.com)  
[www.caentechnologies.com](http://www.caentechnologies.com)

